PLANAR NEAR-FIELD MEASUREMENT TECHNIQUES ON HIGH PERFORMANCE ARRAYS. PART I. ERROR ANALYSIS FOR NONSCANNING BEAM PATTERNS

Arthur D. Yaghjian

National Bureau of Standards

Prepared for:

Air Force Avionics Laboratory

July 1975

DISCLAIMER NOTICE

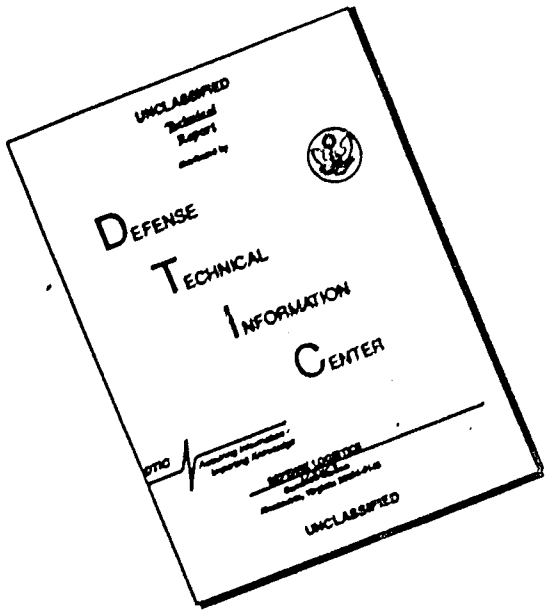

THIS DOCUMENT IS BEST QUALITY AVAILABLE. THE COPY FURNISHED TO DTIC CONTAINED A SIGNIFICANT NUMBER OF PAGES WHICH DO NOT REPRODUCE LEGIBLY.

258109
AFAL-TR-75-67

PLANAR NEAR-FIELD MEASUREMENT TECHNIQUES ON HIGH PERFORMANCE ARRAYS - PART I: ERROR ANALYSIS FOR NONSCANNING BEAM PATTERNS

NATIONAL BUREAU OF STANDARDS

JULY 1975

TECHNICAL REPORT AFAL-TR-75-67
FINAL REPORT FOR PERIOD JULY 1973 – JULY 1974

Prepared for
AIR FORCE AVIONICS LABORATORY
AIR FORCE WRIGHT AERONAUTICAL LABORATORIES
Air Force Systems Command
Wright-Patterson Air Force Base, Ohio 45433

AIR FORCE SYSTEMS COMMAND
United States Air Force

NOTICE

When Government drawings, specifications, or other data are used for any purpose other than in connection with a definitely related Government procurement operation, the United States Government thereby incurs no responsibility nor any obligation whatsoever; and the fact that the government may have formulated, furnished, or in any way supplied the said drawings, specifications, or other data, is not to be regarded by implication or otherwise as in any manner licensing the holder or any other person or corporation, or conveying any rights or permission to manufacture, use, or sell any patented invention that may in any way be related thereto.

This report has been reviewed by the Information Office (OI) and is releasable to the National Technical Information Service (NTIS). At NTIS, it will be available to the general public, including foreign nations. This technical report has been reviewed and is approved for publication. Publication of this report does not constitute Air Force approval of the findings or conclusions. It is a publication for the exchange and stimulation of ideas.

W. Russell Boario

W. RUSSELL BOARIO, Acting Chief
Microwave Technology Branch
Electronic Technology Division

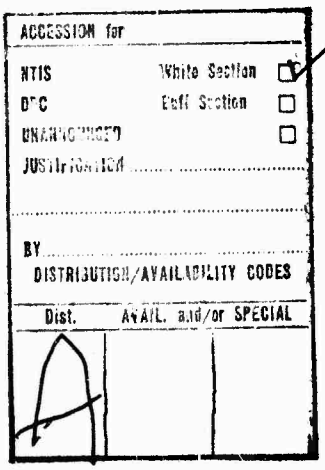

Copies of this report should not be returned unless return is required by security considerations, contractual obligations, or notice on a specific document.

UNCLASSIFIED

SECURITY CLASSIFICATION OF THIS PAGE (When Data Entered)

REPORT DOCUMENTATION PAGE		READ INSTRUCTIONS BEFORE COMPLETING FORM
1. REPORT NUMBER AFAL-TR-75-67	2. GOVT ACCESSION NO.	3. RECIPIENT'S CATALOG NUMBER
4. TITLE (and Subtitle) Planar Near-Field Measurement Techniques on High Performance Arrays -- Part I: Error Analysis for Nonscanning Beam Patterns		5. TYPE OF REPORT & PERICD COVERED Final 7/73-7/74 6. PERFORMING ORG. REPORT NUMBER
7. AUTHOR(s) Arthur D. Yaghjian		8. CONTRACT OR GRANT NUMBER(s) F33615-73-M-6001
9. PERFORMING ORGANIZATION NAME AND ADDRESS Electromagnetics Division Institute for Basic Standards National Bureau of Standards Boulder, Colorado 80302		10. PROGRAM ELEMENT, PROJECT, TASK AREA & WORK UNIT NUMBERS Program Element 62204F Project 20020404
11. CONTROLLING OFFICE NAME AND ADDRESS Air Force Avionics Laboratory Air Force Systems Command Wright-Patterson Air Force Base, OH 45433		12. REPORT DATE July 1975 13. NUMBER OF PAGES 120
14. MONITORING AGENCY NAME & ADDRESS(if different from Controlling Office)		15. SECURITY CLASS. (of this report) Unclassified 15a. DECLASSIFICATION/DOWNGRADING SCHEDULE

16. DISTRIBUTION STATEMENT (of this Report)

Approved for public release; distribution unlimited.

17. DISTRIBUTION STATEMENT (of the abstract entered in Block 20, if different from Report)

18. SUPPLEMENTARY NOTES

This report has been prepared under delivery order contractual arrangement for the Air Force Avionics Laboratory

19. KEY WORDS (Continue on reverse side if necessary and identify by block number)

Antennas; error analysis; far-field pattern; near-field measurements; planar scanning; plane-wave spectrum.

20. ABSTRACT (Continue on reverse side if necessary and identify by block number)

General expressions are derived for estimating the errors in the sum or difference far-field pattern of electrically large aperture antennas which are measured by the planar near-field scanning technique. Upper bounds are determined for the far-field errors produced by 1) the nonzero fields outside the finite scan area, 2) the inaccuracies in the positioning of the probe, 3) the distortion and nonlinearities of the instrumentation which measures the amplitude and phase of the probe output, and 4) the multiple reflections.

DD FORM 1 JAN 73 1473 EDITION OF 1 NOV 65 IS OBSOLETE

AIR FORCE - [illegible] - 1975

SECURITY CLASSIFICATION OF THIS PAGE (When Data Entered)

20. Abstract

Computational errors, uncertainties in the receiving characteristics of the probe, and errors involved with measuring the input power to the test antenna are briefly discussed.

FOREWORD

The research in this report, which represents Part I of an extensive analysis and computer simulation to determine the errors associated with planar near-field measurements, was performed in the Electromagnetics Division of the National Bureau of Standards, Boulder, Colorado. The research was generated as part of an ongoing program sponsored by the Air Force Avionics Laboratory, Air Force Systems Command, Wright-Patterson Air Force Base, Ohio under contract number F33615-73-M-6001, to develop the measurement techniques and accuracy requirements for the planar near-field scanning of airborne phased-array antennas.

The forthcoming Part II of the error study emphasizes antennas with beams which steer electronically. The initial computer simulation was reported in the NBS Internal Report 74-380. The extension of the error analysis to broadbeam antennas is described in the NBS Internal Report 75-815. A summary of the major results and conclusions of this report can be found in Section IV.

The author is grateful to Allen C. Newell for his invaluable consultation throughout the preparation of this report. Much appreciation is extended to John W. Greene and Douglas P. Kremer for the information they provided about the NBS near-field scanning facilities. Mark T. Ma and Carl F. Stubenrauch of the Department of Commerce, and Kenneth Grimm of the Air Force Avionics Laboratory contributed many helpful suggestions in reviewing the report. Many thanks also go to Janet R. Jasa for carefully and patiently typing the manuscript.

CONTENTS

LIST OF FIGURES AND TABLES

LIST OF FIGURES AND TABLES (continued)

I. Introduction

The planar near-field scanning method has been used to measure with high accuracy the electromagnetic fields of microwave antennas. High accuracy is possible primarily because so few restrictive approximations are involved in the formulation and application of the near-field techniques. Moreover, the far-field errors associated with each approximation can be estimated because the approximations themselves can be expressed in convenient mathematical form. This report essentially derives and evaluates some of these mathematical expressions under the given laboratory conditions to determine quantitatively the accuracy with which the far-field of antennas can be measured by the planar near-field scanning method.

The error analysis was undertaken for two main reasons. One, it was desired to find general upper-bound expressions for the limits of accuracy in computing far-fields from planar near-field measurements without resorting to direct far-field comparisons. It has long been the feeling of those involved with the near-field measurement techniques at the NBS that these techniques were often more accurate than measurements taken on conventional "far-field" ranges with a standard antenna. Thus comparisons with patterns measured on conventional far-field ranges would not give a reliable evaluation of the near-field techniques which do not have to cope with proximity corrections, ground reflections, or the calibration of standard far-field antennas. Two, the upper-bound expressions could be used to stipulate design criteria for the construction of new near-field scanning facilities. This meant that the upper-bounds for the accuracy in a given far-field parameter should be expressed in terms of measured near-field data and/or the computed far-field, the frequency and dimensions of the antenna-probe system, the variation in the positioning of the scanner, and the precision of the instrumentation which measures the probe output. The design engineer could then compute from the upper-bound expressions the near-field tolerances required to insure a given far-field accuracy for the range in size and frequency of the antennas he was considering.

There have been two major computer studies performed in the past to estimate the errors involved with planar near-field scanning

measurements [11,16]. Rodrigue, Joy and Burns [16] have introduced position and instrumentation errors into a hypothetical near-field distribution in order to compute their effects on the far-field. Newell and Crawford [11,17] performed a similar analysis with measured near-field data which included an estimate of errors involved with truncating the scan plane. A major drawback of the computer studies, as well as direct far-field comparisons, is that they apply to particular antennas and their results do not necessarily represent upper-bounds to errors which will hold for large general classes of antennas. It should be emphasized, however, that the computer studies are an extremely useful aid in giving direction to the general analysis and checking its results.

This report does not attempt to estimate the accuracy of the extrapolation technique for measuring the gain of antennas [22]. An error analysis involving the extrapolation technique has been performed recently by Kanda [23].

If we assume that the antennas under consideration are linear, of finite extent, and operating in a single mode at fixed frequency and amplitude, and that Maxwell's equations for free space describe the region in which the antenna is situated, the only approximations involved in formulating and applying the planar scanning method are:

1) The fields outside the finite scan area are zero.
2) The scanner is aligned and positioned with infinite precision.
3) The instrumentation introduces no distortion and measures the amplitude and phase of the probe output with perfect accuracy.
4) Multiple reflections between the test antenna and "probe" antenna are zero.
5) Computation errors in "deconvoluting" the measured near-field data to get the far-field are nil.

Errors caused by uncertainties in the receiving characteristics of the probe, and errors involved with measuring the input power to the test antenna are discussed in Section IV, which, incidently, contains a summary of the major results and conclusions of this report.

The far-field errors introduced by the computations (approximation 5) are so much smaller than the combined errors in the far-field caused by a finite scan area, positioning, instrumentation, and multiple reflections (approximations 1-4) that they are of little consequence. With the help of the sampling theorem, Fast Fourier Transform, and computers accurate to many places, the necessary deconvolution of the measured data can be performed with insignificant error.[1]

The amplitude of the near-field multiple reflections (approximation 4) can be estimated in practice by changing the distance between the probe and test antennas. Any periodic variations in the amplitude of the received signal repeating about every $\lambda/2$ (λ = wavelength) would be caused primarily by the multiple reflections. In Section III.C the effects on the far-field of multiple reflections are discussed and estimated analytically. Although they cannot be eliminated completely, multiple reflections can be reduced by using efficient absorber material, by decreasing the size of the probe, or by increasing the distance between the probe and test antenna. Also, it is likely that the effect of multiple reflections on the far-field can be reduced by averaging the far-field patterns obtained by scanning on a number of near-field planes which are separated by a small fraction of a wavelength.

Far-field errors caused by the errors in the scanner positioning and instrumentation (approximations 2 and 3) are determined from a common set of equations. These equations are derived and evaluated in Section III.B for both systematic and random near-field

---

[1]Without the advantage of the FFT, typically the computer would add 20,000 terms to calculate the variable which yields the far-field. Even if we make the absurd hypothesis that every round-off error adds in the same direction, a computer of 10-place accuracy adding 20,000 numbers would retain more than 5-place accuracy (.001%) for the sum. Of course, in practice the FFT algorithm vastly reduces the number of necessary computations.

There is also the approximation associated with applying the sampling theorem, which assumes that the output of the probe is the Fourier transform of a band-limited function. For a separation distance between test antenna and probe of more than a few wavelengths, this can be shown to be an extremely good approximation which introduces negligible errors into the far-field.

errors. "Position errors" may be reduced by scanning along both vertical and horizontal lines and appropriately averaging the two sets of measurements. "Instrumentation errors" can be reduced if the distortion and nonlinearities of the receivers can be determined and included as part of the computer program that deconvolutes the near-field data.

The first portion of the error analysis (Section III.A) is devoted to determining the maximum far-field errors introduced by neglecting the fields outside the scan area. As part of the analysis, asymptotic expressions are derived for the near-field in front of large aperture radiators.

All errors are assumed small enough so that the individual contribution to the far-field error from each source of near-field error can be estimated independently and then combined to give the total far-field error. We shall find that all the individual errors in the far-field combine linearly except for the on-axis sum pattern, position and instrumentation phase errors which combine quadratically (see footnote 12).

II. Relationship of Errors in Gain Function, Sidelobe Level, Polarization Ratio, and Beamwidth to the Far-Field Error in Electric Field

Let $\bar{E}(\bar{r})$ denote the electric field (to within the limits of error) of an antenna radiating into free-space and $\pm \Delta\bar{E}(\bar{r})$ the limits of error involved with the measurement of $\bar{E}(\bar{r})$ ($e^{-i\omega t}$ time dependence has been suppressed). The magnitude of the fractional error $\eta(\bar{r})$ in the electric field amplitude can be defined for small errors as,

$$\eta(\bar{r}) = \left| \frac{|\bar{E}\pm\Delta\bar{E}| - |\bar{E}|}{|\bar{E}|} \right| \leq \frac{|\Delta\bar{E}(\bar{r})|}{|\bar{E}(\bar{r})|}. \qquad (1)$$

(Henceforth, the < sign will be omitted when eq. (1) or similar expressions are used.) The Hermitian amplitude $|\bar{E}| \equiv \sqrt{\bar{E}\cdot\bar{E}^*}$ (the asterisk * denotes the complex conjugate) is related to the power S radiated per unit area in the far-field or any other locally

plane-wave field in free-space by $S = \sqrt{\epsilon_o/\mu_o}|\bar{E}|^2$. From the values of $\eta(\bar{r})$ as r approaches infinity and the approximate amplitude of the far-field $|\bar{E}(\bar{r})|_{r\to\infty}$, all other errors in far-field quantities can be found. Four such quantities of interest are the gain function, the sidelobe level, the polarization ratio, and the half-power beamwidth. Of course, these four are not always the only far-field quantities of interest, but they will be used as typical examples to demonstrate how the error in any far-field quantity can be related easily to $\eta(\bar{r})$ and $|\bar{E}(\bar{r})|_{r\to\infty}$. (In eqs. (2)-(5) below, where the error in these four quantities is derived, the subscript "$r\to\infty$" is understood, but not shown explicitly.)

The error η_G in the gain function $G(\bar{r})$, which is proportional to the square of the far-field amplitude, may be written immediately as (for small $|\Delta\bar{E}|/|\bar{E}|$, so that $|\Delta\bar{E}|^2$ terms can be neglected)

$$\eta_G = \left\{\frac{|\bar{E} \pm \Delta\bar{E}|^2 - |\bar{E}|^2}{|\bar{E}|^2}\right\} G = \pm 2 \frac{|\Delta\bar{E}|}{|\bar{E}|} G \qquad (2a)$$

$$= \pm 2\eta(\bar{r})G(\bar{r}),$$

or in decibels

$$\eta_G^{dB} \equiv 10 \log\left(\frac{|\bar{E} \pm \Delta\bar{E}|^2}{|\bar{E}|^2}\right) = 20 \log(1\pm\eta(\bar{r})). \qquad (2b)$$

For small errors, $\eta << 1$, and

$$\boxed{\eta_G^{dB} = \pm 8.7\, \eta(\bar{r}).} \qquad (2c)$$

The sidelobe level, when meaningful, is usually stated in decibels and is defined as the ratio of the maximum far-field intensity of the largest sidelobe to the maximum far-field intensity of the main beam [1]. The error η_s in sidelobe level SL is

$$\eta_s = \frac{|\bar{E}_{side} \pm \Delta\bar{E}_{side}|^2}{|\bar{E}_{max} \pm \Delta\bar{E}_{max}|^2} - \frac{|\bar{E}_{side}|^2}{|\bar{E}_{max}|^2}.$$

For $SL = |\bar{E}_{side}|^2/|\bar{E}_{max}|^2$, and small $\eta(\bar{r})$,

$$\eta_s = \pm 2[\eta(\bar{r}_s) + \eta(\bar{r}_o)]SL, \qquad (3a)$$

with $\eta(\bar{r}_s)$ and $\eta(\bar{r}_o)$ denoting the values of η at the sidelobe maximum and main beam maximum respectively. In most cases $\eta(\bar{r}_s)$ will be much larger than $\eta(\bar{r}_o)$ so that

$$\eta_s = \pm 2\eta(\bar{r}_s)SL. \tag{3b}$$

In decibels

$$\eta_s^{dB} = 20\left\{\log \frac{|\bar{E}_{side} \pm \Delta\bar{E}_{side}|}{|\bar{E}_{max} \pm \Delta\bar{E}_{max}|} - \log \frac{|\bar{E}_{side}|}{|\bar{E}_{max}|}\right\},$$

or for small η, and $\eta(\bar{r}_s) >> \eta(\bar{r}_o)$,

$$\boxed{\eta_s^{dB} = \pm\ 8.7\ \eta(\bar{r}_s),} \tag{3c}$$

i.e., as we might expect, simply the error in the gain of the sidelobe itself.

The polarization ratio of the electric field is defined as the ratio of the minor to major axis of its polarization ellipse [1]. The maximum error in the polarization ratio at a point in the far-field occurs when the error $\Delta\bar{E}$ is linearly polarized in phase with the component of $\bar{E}$ along the minor axis. Thus the maximum error η_p in polarization ratio is simply

$$\eta_p = \pm \frac{|\Delta\bar{E}|}{|\bar{E}_{major}|}.$$

Since the smallest possible value of $|\bar{E}_{major}|$ is $\sqrt{1/2}\ |\bar{E}|$ (circular polarization), the maximum possible error η_p may be written as

$$\boxed{\eta_p = \pm\sqrt{2}\ \frac{|\Delta\bar{E}|}{|\bar{E}|} = \pm\sqrt{2}\eta(\bar{r}).} \tag{4}$$

For antennas which have small cross polarization, the factor of $\sqrt{2}$ in eq. (4) is removed. Also footnote 11 should be remembered when applying eq. (4) to instrumentation amplitude errors.

The half-power beamwidth is defined for a plane containing the line along the maximum intensity of the beam. It is simply "the angle between the two directions in which the radiation intensity is one half the maximum value of the beam" [1]. If we know $\bar{E}(\bar{r})$

and $\Delta\bar{E}(\bar{r})$ in the far-field we can determine the maximum errors in measuring the beamwidth. In figure 1, $|\bar{E}|^2$ and $|\bar{E} \pm \Delta\bar{E}|^2 = |\bar{E}|^2 \pm 2|\bar{E}||\Delta\bar{E}|$ (neglecting $|\Delta\bar{E}|^2$ terms, as usual) are plotted for the main beam of an arbitrary test antenna. The beamwidth is $\theta_1+\theta_2$. From figure 1, we see that the error in θ_1 is

$$\Delta\theta_1 = \pm \frac{2|\Delta\bar{E}(\theta_1)||\bar{E}(\theta_1)|}{\tan\alpha} = \frac{\pm\,|\Delta\bar{E}(\theta_1)||\bar{E}(\theta_1)|}{|\bar{E}(\theta_1)|\,\dfrac{d|\bar{E}(\theta_1)|}{d\theta}} = \frac{\pm\eta(\theta_1)|\bar{E}(\theta_1)|}{\dfrac{d|\bar{E}(\theta_1)|}{d\theta}} \text{ radians.}$$

Similarly the error in $\Delta\theta_2$ is

$$\Delta\theta_2 = \frac{\pm\,\eta(\theta_2)\;|\bar{E}(\theta_2)|}{\dfrac{d|\bar{E}(\theta_2)|}{d\theta}} \text{ radians.}$$

The total fractional error η_B in beamwidth may be written

$$\boxed{\eta_B = \pm \frac{\Delta\theta_1 + \Delta\theta_2}{\theta_1 + \theta_2}\,,} \tag{5a}$$

or, for symmetrical beams ($\theta = \theta_1 = \theta_2$), simply

$$\boxed{\eta_B = \frac{\pm\Delta\theta}{\theta} = \frac{\pm\eta(\theta)\;|\bar{E}(\theta)|}{\theta\,\dfrac{d|\bar{E}(\theta)|}{d\theta}}\,.} \tag{5b}$$

For large circular or square apertures of uniform amplitude and phase distribution, $|\bar{E}(\theta)|/\left[\theta\frac{d|\bar{E}(\theta)|}{d\theta}\right]$ can be shown to approximately equal 1, and η_B becomes simply,

$$\boxed{\eta_B = \pm\eta(\theta)} \tag{5c}$$

As expected, eqs. (2)-(5) verify that a knowledge of $|\bar{E}(\bar{r})|$ and $\eta(\bar{r})$ as $r \to \infty$ (as mentioned above, the "$r \to \infty$" is suppressed in eqs. (2)-(5)) is all that is required to determine the errors in the gain function, sidelobe level, polarization ratio, and beamwidth. If desired, errors in other far-field parameters can equally well be expressed in terms of $|\bar{E}(\bar{r})|$ and $\eta(\bar{r})$. The far-field $|\bar{E}|_{r\to\infty}$ may be computed from the measured near-field data or estimated analytically. Thus, the problem of finding the far-field errors reduces to the problem of evaluating $\eta(\bar{r})$ of eq. (1) in the far-field.

III. Error Analysis

A. Finite Scan Errors

The purpose of the present section is to estimate the maximum errors in the far-field introduced by scanning in the near-field over a plane of finite area. "Finite" is the key word. In principle, the planar scan method requires that the output of the probe be recorded over an infinite plane in front of the test antenna. In practice, of course, only a finite area of the plane is scanned and the fields outside that finite area are set equal to zero. The scan area is usually, but not necessarily, rectangular with the boundaries commonly chosen where the output of the probe antenna is down 30 or 40 dB or more from its maximum. For many microwave antennas such a scan area turns out to be about two or three times the aperture area of the antenna. The present analysis will be restricted to electrically large (average width/wavelength > 10 will do) aperture-type antennas, usually but not necessarily operating at microwave frequencies. The phase will be assumed fairly uniform across the aperture with the amplitude of the field either uniform or reaching a maximum near the center of the aperture and convexly tapered toward the edge to reduce the sidelobe radiation [2].[2] Near-field, centerline, amplitude and phase data for the sum pattern of a typical antenna measured at NBS can be seen in figure 9d. Reflectors, large horns, and broadside arrays are probably the most common examples of the test antennas under consideration. The results of this finite scan part of the error analysis apply to antennas with their boresight direction steered at an arbitrary angle with respect to the scan plane.

[2] Initially we are assuming the antenna is operating in a sum mode or pattern. For finite scan errors it will be shown that difference patterns need not be considered separately since they are formed by the superposition of two sum patterns with wavefronts slightly skewed to create a "null" in the boresight direction. For position and instrumentation errors, however, Section III.B along with Appendix B shows that sum and difference patterns must be considered separately, at least when determining far-field errors near the boresight direction.

The approach which is used to estimate the finite scan errors involves finding an upper-bound to the appropriate integral of the fields outside the finite scan area. Physical optics and the geometrical theory of diffraction are used to show that the fields outside the scan area are determined chiefly by edge diffracted fields of the antenna. For each antenna these edge diffracted fields are different. However, they all can be expressed in a general form (eq. (19)) which allows upper-bound expressions (eqs. (32) and (36)) to be found by evaluating the integral outside the scan area in terms of the probe output on the edge of the scan area. Outside the "solid angle" formed by the edge of the aperture and edge of the scan area, the evaluation of the integral can be done by the method as stationary phase to show that in this region the far-fields computed from the near-field data cannot be relied upon with any confidence. Well within the solid angle the integral evaluation can be performed through integration by parts to yield an upper-bound expression for finite scan errors from both centerline data scans (eq. (32)) and full scans (eq. (36) or (32)).

1. Mathematical Formulation of the Problem

Suppose we want to determine the radiation pattern of a given antenna of aperture area A bounded by the curve C, as in figure 2. The task is accomplished experimentally by recording the output of an arbitrary but known probe antenna (for two orientations, in general) as the probe scans in front of the radiating test antenna on a plane of area A' bounded by C'. The z-axis will always be chosen perpendicular to the scan plane with origin 0 in the antenna aperture. The scan plane, however, may not always be chosen parallel to the aperture plane. For beams steered off-axis, larger scan areas may be required if the scan plane does not lie perpendicular (approximately)to the boresight direction.

After taking a double Fourier transform of the probe output in each orientation, the radiating characteristics ($\overline{S}_{1o}(\overline{K})$) of the test antenna are found simply by solving simultaneously the two resulting linear equations. In particular, if the probe were a perfect dipole,

the output of the probe would be proportional to the electric field at the dipole in the direction of the dipole moment. The expression for $\bar{S}_{1o}(\bar{K})$ (defined with respect to the reference plane z=0, and the transverse part of the propagation vector denoted by $\bar{K}$) then becomes [3]

$$\bar{S}_{1o}(\bar{K}) = \frac{1}{4\pi^2 a_o} e^{-i\gamma d} \int_{A'} \bar{E}_t(\bar{P},d) e^{-i\bar{K}\cdot\bar{P}} \, d\bar{P}, \qquad (6)$$

($e^{-i\omega t}$ time dependence)

where $\bar{E}_t(\bar{P},d)$ is the electric field, i.e., the output of the dipole probe in two mutually perpendicular orientations, transverse to the z-axis at the point $(\bar{P},d)$ in the scan plane A'. (The equation of the A' plane is z = d.) The amplitude of the input mode to the test antenna is designated by a_o, and the variable γ is defined by $\gamma = (k^2-K^2)^{\frac{1}{2}}$ ($k = \omega/c = \frac{2\pi}{\lambda}$), where the radical is chosen to keep γ positive real or imaginary.[3a,b]

For the sake of simplifying the theory we will assume a perfect electric dipole as the probe. The dipole gives information about the electric field only at a point. All physically realizable probes respond to a weighted average of the field near the probe. Thus it is expected that the errors in the computed far-field introduced by omitting a part of the infinite scan plane are as great or greater for a perfect dipole than for any other probe antenna, and that the following conclusions and resulting upper bound expressions (32) and (36) hold for arbitrary probes. Also, at this point in the error

---

[3a] The sampling theorem shows that to obtain the far-field pattern the double integral in eq. (6) can essentially be replaced by a double summation over points in A' separated by about $\lambda/2$ or less. Thus, in practice, data need be taken only at a finite number of discrete points for eq. (6) to be evaluated. However, for most of the error analysis we prefer (somewhat arbitrarily) the integral representation of $\bar{S}_{1o}$ to the summation.

[3b] Strictly speaking, the Fourier transform in eq. (6) and eqs. (7), (10), and (11) below may not converge to a unique value as the scan area approaches infinity because $\bar{E}_t(\bar{P},d)$ has a 1/P dependence in a lossless medium as $P\to\infty$, and thus gives rise to a rapidly oscillating part in the transform as $P\to\infty$. Usually this oscillatory term can be ignored with impunity because it vanishes upon integration when taking the inverse transform. However, it does determine the limiting value of the finite scan errors (see footnote 9).

analysis any uncertainty in the receiving characteristics (S'_{01}) of the measuring probe are ignored.

For eq. (6) to represent $\bar{S}_{1o}(\bar{K})$ exactly, the probe scan and subsequent integration would have to be performed over the infinite plane. Thus the error ($\Delta\bar{S}_{1o}$) produced in $\bar{S}_{1o}$ by a scan of finite area may be written formally as

$$\Delta\bar{S}_{1o} = \frac{1}{4\pi^2 a_o} e^{-i\gamma d} \int_{A'_c} \bar{E}_t(\bar{P},d) e^{-i\bar{K}\cdot\bar{P}}\, d\bar{P}, \tag{7}$$

where A'_c is the infinite area outside or complementary to A'. The far-fields can be found from $\bar{S}_{1o}(\bar{K})$ by taking the inverse double Fourier transform of eq. (6) and evaluating the resulting expression by the method of stationary phase for double integrals. So doing yields [3]

$$\bar{E}_t(\bar{r}) = -2\pi a_o ik \cos\theta\, \bar{S}_{1o}(k\bar{R}/r)\, \frac{e^{ikr}}{r} \tag{8}$$
$$r \to \infty$$

and from eq. (8)

$$\Delta\bar{E}_t(\bar{r}) = -2\pi a_o ik \cos\theta \Delta\bar{S}_{1o}(k\bar{R}/r)\, \frac{e^{ikr}}{r}. \tag{9}$$
$$r \to \infty \quad (\cos\theta = z/r,\ z>0)$$

Substitution of $\bar{S}_{1o}$ and $\Delta\bar{S}_{1o}$ from eqs. (6) and (7) into eqs. (8) and (9), respectively, produces expressions for the far-electric-field and its error in terms of the near-field data:

$$\bar{E}_t(\bar{r}) = -\frac{ik\cos\theta}{2\pi r} e^{ik(r-d\cos\theta)} \int_{A'} \bar{E}_t(\bar{P},d) e^{-i\frac{k}{r}\bar{R}\cdot\bar{P}}\, d\bar{P} \tag{10}$$
$$r \to \infty$$

$$\Delta\bar{E}_t(\bar{r}) = -\frac{ik\cos\theta}{2\pi r} e^{ik(r-d\cos\theta)} \int_{A'_c} \bar{E}_t(\bar{P},d) e^{-i\frac{k}{r}\bar{R}\cdot\bar{P}}\, d\bar{P}. \tag{11}$$
$$r \to \infty$$

(For a dipole probe, $\bar{E}_t(\bar{P},d)$ and the output of the probe are identical.) Equations (10) and (11) express mathematically the well-known

"Fourier optics" result that the far-field amplitude is proportional to the spatial Fourier transform of the near-field times $\cos\theta$. Division of eq. (10) by eq. (11) results in the fractional error η_t in the transverse part of the far-electric-field

$$\eta_t(\bar{r}) = \frac{|\Delta\bar{E}_t(\bar{r})|}{|\bar{E}_t(\bar{r})|} = \frac{\left|\int_{A'_c} \bar{E}_t(\bar{P},d)\, e^{-i\frac{k}{r}\bar{R}\cdot\bar{P}}\, d\bar{P}\right|}{\left|\int_{A'} \bar{E}_t(\bar{P},d)\, e^{-i\frac{k}{r}\bar{R}\cdot\bar{P}}\, d\bar{P}\right|}, \tag{12a}$$

or simply

$$\eta_t(\bar{r}) = \frac{\cos\theta\left|\int_{A'_c} \bar{E}_t(\bar{P},d)\, e^{-i\frac{k}{r}\,\bar{R}\cdot\bar{P}}\, d\bar{P}\right|}{\lambda r|\bar{E}_t(\bar{r})|_{r\to\infty}}. \tag{12b}$$

Of course, the fractional error η in the total far-electric-field is not necessarily η_t except on the z-axis. However we can find η in terms of η_t by a simple argument. In the far-field $|\bar{E}_t(\bar{r})|$ differs from $|\bar{E}(\bar{r})|$ at most by a factor $\cos\theta$, i.e.

$$|\bar{E}(\bar{r})|\cos\theta \leq |\bar{E}_t(\bar{r})| \leq |\bar{E}(\bar{r})|. \tag{12c}$$

Similarly,

$$|\Delta\bar{E}|\cos\theta \leq |\Delta\bar{E}_t| \leq |\Delta\bar{E}|. \tag{12d}$$

Consequently η is greater than η_t by at most a factor $\frac{1}{\cos\theta}$, and from eqs. (12) we can express the maximum possible η in the far-field as

$$\eta(\bar{r}) = \frac{|\Delta\bar{E}|}{|\bar{E}|} = \frac{\left|\int_{A'_c} \bar{E}_t(\bar{P},d)\, e^{-i\frac{k}{r}\,\bar{R}\cdot\bar{P}}\, d\bar{P}\right|}{\lambda r|\bar{E}(\bar{r})|_{r\to\infty}}. \tag{13}$$

For the denominator of eq. (13) we can use the far-field estimated analytically or computed from the measured near-field data. Thus, the problem of finding η reduces to that of estimating $\bar{E}_t(\bar{P},d)$ on A'_c, i.e., on the area outside the finite scan plane.

2. The Fields of Electrically Large Aperture Antennas

If the behavior of the electric field $\bar{E}_t(\bar{P},d)$ were known in the area A_c', the integral of eq. (13),

$$I = \int_{A_c'} \bar{E}_t(\bar{P},d) e^{-\frac{ik}{r}\bar{R}\cdot\bar{P}} \, d\bar{P}, \tag{14}$$

could be evaluated and the far-field errors could be found immediately from eqs. (1)-(5). Even asymptotic methods cannot be applied to eq. (14) until the behavior of $\bar{E}_t(\bar{P},d)$ is determined. Fortunately, the electric field outside the aperture of electrically large aperture antennas can be determined analytically from the electric field distribution across the aperture. In fact, it will be shown shortly that just the electric field at the edge of the aperture distribution is required.

As a first step in finding the electric field $\bar{E}_t(\bar{P},d)$ to use in eq. (14), consider the aperture antenna drawn schematically in figure 3. (The boundary or rim of the antenna is assumed to lie in a plane with $\hat{e}_z$ here chosen perpendicular to the plane. These restrictions are relaxed later.) It is well-known [4] that the electric field everywhere to the right of the infinite plane A_∞ can be expressed in terms of an integral of the electric field over A_∞,

$$\bar{E}(\bar{r}) = -\frac{1}{2\pi} \int_{A_\infty} [\hat{e}_z \times \bar{E}_t(\bar{R}')] \times \nabla G(\bar{r},\bar{R}') \, d\bar{R}', \tag{15}$$

where

$$G = \frac{e^{ik|\bar{r}-\bar{R}'|}}{|\bar{r}-\bar{R}'|},$$

and $\bar{E}_t(\bar{R}')$ is the transverse electric field on the plane A_∞ emanating from sources to the left of A_∞ (e.g., electric fields from a feed located to the right of A_∞ would not be included in $\bar{E}_t(\bar{R}')$, except, of course, indirectly as reflected fields from the antenna).

For an aperture antenna, whether it be a reflector, large horn, or broadside array, the components of the electric field $\bar{E}_t(\bar{R}')$ are

slowly varying in phase[4] and amplitude across the aperture, except possibly right near the edge. The amplitude often tapers toward the edge of the aperture and drops abruptly (in a distance less than a wavelength) to zero or near zero beyond the edge. Thus the limits of integration in eq. (15) reduces to the aperture area A or at most a couple of wavelengths beyond A. Also, since eq. (14) requires only the transverse component of $\bar{E}_t(\bar{r})$, we can ignore the z-components of eq. (15) and write

$$\bar{E}_t(\bar{r}) = -\frac{1}{2\pi}\frac{\partial}{\partial z}\int_A \bar{E}_t(\bar{R}')G(\bar{r},\bar{R}')\,d\bar{R}'. \qquad (16)$$

For electrically large apertures, eq. (16) can be evaluated asymptotically. Before doing this a couple of remarks are in order.

The first has to do with neglecting the fields outside the aperture area A when in reality there may be scattering from the edge of the antenna aperture. In those cases it may seem unreasonable to neglect, initially, the fields beyond the aperture area A as part of the procedure to calculate the fields beyond the scan area A'. The "canonical" problems that can be solved exactly, such as scattering by an infinite wedge or elliptical disk, indicate, however, that at short wavelengths the scattered fields are caused predominantly by high intensity fields within a wavelength or so of the edge, and indeed the fields more than this distance beyond the edge may be neglected [5]. Of course, this assumption has been confirmed by experiment and constitutes the basic postulate of the geometrical theory of diffraction [6]. In terms of the radiation from large aperture antennas, it means simply that the fields everywhere to the right of the aperture plane depend solely upon the fields within and near the edge of the aperture, even when appreciable scattering from the edges is present.

The second remark concerns antennas that have part of their feeding mechanism mounted to the right of the aperture plane--as in the case of reflector antennas. As mentioned above, the direct radiation from the feed must not be included as part of $\bar{E}_t(\bar{R}')$ for eq. (16) to be correct. However, scattering from feed mounts

[4]For electrically steered arrays the planes of "uniform" phase may be skewed with respect to the aperture plane. This situation is considered at the end of the section.

(including the feed itself) of the fields reflected by the antenna are not taken into account by eq. (16). Although the mount scattered fields can be ignored if they are small compared to the fields scattered from the aperture edge, there is no reason to believe this will always be the case even in the region A_c'. Fortunately, the results of the geometrical theory of diffraction (GTD) can also be used to determine the behavior of the fields diffracted from the mounting in front of the aperture as well as from any sharp edges at the boundary of the aperture [6]. Moreover, we shall find that the final expression (eqs. (32) and (36)) for the far-field error does not require an explicit estimation of either the mount or edge diffracted fields. Of course, for many antennas such as horns and arrays there are no obstructions in front of the aperture.

For the moment we shall ignore the problems of the exact nature of the edge diffraction and diffraction from feed mounts and return to evaluate eq. (16) for a smoothly tapered amplitude within A and zero outside A. For apertures which are many wavelengths across, the double integral (16) can be expanded in an asymptotic series. The first three terms in the series for integrals like eq. (16) have been derived by Van Kampen [7]. Keller, Lewis and Seckler [8] apply Van Kampen's results to eq. (16) specifically. The final expression has been confirmed by the present author using an approach different from Van Kampen's. In the shadow region, i.e., the entire half space $z > 0$ excluding the cylindrical volume formed by the projection of the aperture area A along the z-axis, the electric field in eq. (16) is approximated by

$$\bar{E}_t(\bar{r}) = \sum_m \frac{1}{2\pi}\sqrt{\frac{\lambda}{Dm}}\left(\frac{a_m}{a_m+D_m \sin\theta_m}\right)^{\frac{1}{2}} \frac{\cos\theta_m \, \bar{E}_{tm}}{\sin\theta_m} e^{i\left(kD_m+\frac{\pi}{4}\right)}. \qquad (17)$$

The variables in eq. (17) are defined with the help of figure 4. The distance from the point $\bar{r}$ to the edge of an aperture with a smooth boundary has at least one relative maximum and one relative minimum. The subscript m simply refers to the mth relative extremum point on the edge of the aperture. D_m is the distance from $\bar{r}$ to the mth relative extremum, a_m is the radius of curvature of the edge (in

the plane of the aperture) at the mth relative extremum, θ_m is the angle between D_m and the z-direction, and $\bar{E}_{tm}$ is the value of the transverse electric field at the edge of the aperture excluding the fields diffracted from the edge. The radius of curvature a_m is taken positive if the distance D_m is a relative minimum and negative if a relative maximum. The radical $\left[\frac{a_m}{a_m+D_m\sin\theta_m}\right]^{1/2}$ is taken positive if real and negative if imaginary. Of course, all subscripted quantities are, in general, functions of position $\bar{r}$.

Actually, in order for expression (17) to remain valid, θ_m must be greater than a few λ/ℓ^{ave} ($\ell^{ave} \equiv \sqrt{A}$), and D_m no closer than a couple of wavelengths λ from the edge. This latter restriction says simply that eq. (17) does not describe the reactive fields. The former restriction can be understood physically by dividing the aperture into Fresnel zones for the direction θ_m. For θ_m greater than a few λ/ℓ^{ave} there are enough Fresnel zones (even for the far-field) to assure that the main contribution to the fields in the shadow region are from the fields near the edge of the aperture rather than from the fields well within the aperture.[5]

The expression (17) does not necessarily account correctly for scattering from edges that may be present on the boundary or rim of the antenna. The necessary modification of eq. (17), for example, when scattering from sharp conducting edges occurs can be extracted from Kellers GTD [6]. Kouyoumjian [9a] has written Keller's results in a form similar to eq. (17). The GTD expression differs from eq. (17) only in that the factor $\cos\theta_m \bar{E}_{tm}$ is replaced by

$$\bar{E}^{\parallel}_{tm}\, g_{\parallel}(\theta_m) + \bar{E}^{\perp}_{tm}\, g_{\perp}(\theta_m), \qquad (18)$$

where $\bar{E}^{\parallel}_{tm}$ and $\bar{E}^{\perp}_{tm}$ are the transverse components of the incident electric field parallel and perpendicular to the edge of the aperture. The factors $g_{\parallel}$ and $g_{\perp}$ can be found from either reference [6a] or [9a], but it is not necessary to know them explicitly for our purposes. Moreover, scattering from other than sharp conducting edges can also be handled by changing appropriately the factors $g_{\parallel}$ and $g_{\perp}$ in eq. (18).

[5] Note that in a similar manner it can be argued that the far-fields for θ less than a couple λ/ℓ^{max} (ℓ^{max} = maximum width of aperture) are determined mainly by the near-fields well within the boundary of the aperture.

Thus it is seen from eqs. (17) and (18) that regardless of the nature of the scattering from the edges, the fields in the shadow zone appear to emanate from points along the edge of the aperture. For our purposes it proves convenient to write simply the one equation valid for the scattered field in the shadow zone

$$\bar{E}_t(\bar{r}) = \sum_m \bar{F}_{tm}(\bar{r}) e^{ikD_m}. \tag{19}$$

$\bar{F}_{tm}$ is defined by comparing eq. (19) with eqs. (17) and (18). The essential property of $\bar{F}_{tm}(\bar{r})$, which allows the asymptotic evaluation of eq. (14), is that unlike e^{ikD_m} it varies slowly with $\bar{r}$. In fact, for the error analysis it turns out that this is the only property of $\bar{F}_{tm}(\bar{r})$ that is required. Never is it necessary to evaluate $\bar{F}_{tm}(\bar{r})$ explicitly, although for reasons of general interest it has been evaluated in Appendix A for the circular aperture of uniform distribution. Results from Appendix A are also used in Section III.B.1.

Before carrying out the integration of eq. (14) it should be mentioned that eqs. (17) and (18) are not valid for large D_m if the radius of curvature a_m approaches infinity. For example, the expressions would be modified if the aperture were rectangular. However, the modifications occur in $\bar{F}_{tm}(\bar{r})$ but not e^{ikD_m}. Thus, eq. (19) remains valid for all shaped apertures even when part of the edge is a straight line or has infinite radius of curvature.

Also if the edge of the aperture has points where the radius of curvature is much smaller than a wavelength (e.g., the corners of a rectangular aperture), these corners and tips contribute to the field. For large apertures at least it can be shown [5-9] that their contribution is usually much smaller (higher order in λ/ℓ^{ave}) than the edge fields of eq. (19), and thus can usually be neglected for the purpose of evaluating eq. (14). However, even if they cannot be neglected, the fields from corners and tips can be expressed in the same form as eq. (19).

Electronically steered aperture antennas (broadside phased arrays) are also covered by eq. (19) with the appropriate modifications of $\bar{F}_{tm}$ (see, for example, reference [8] which deals with an arbitrary phase of the field across the aperture). When the axis of the main beam is steered away from the perpendicular to the aper-

ture, the region of validity of eq. (19) changes to the entire half space in the direction of the new axis, excluding the projection of the aperture along that axis, i.e., eq. (19) is still valid in the shadow zone regardless of what direction the beam is steered.

Eq. (19) also applies to antennas operating in a difference pattern where the on-axis field drops to a sharp minimum. As in the case of the sum pattern, the fields in the shadow zone are determined by whatever value of electric field impinges upon the edge of the aperture. And again the variation in electric field separates into a rapidly oscillating part e^{ikD_m} and a slowly varying part $\bar{F}_{tm}$.

Eq. (17) (or (17) modified by (18)) represents the first term in an asymptotic expansion of the electric field. The higher order terms are assumed so much smaller than the first that they are neglected. However, if the electric field at the edge of the aperture becomes too small, the second term in the asymptotic expansion must be included.[6] Even then, for reasonably smooth aperture distributions, this second term also has the form of eq. (19) but with $\bar{F}_{tm}$ depending on the derivative of the electric field at the edge rather than the field itself. This "slope diffraction coefficient" has been derived for the GTD by Hwang and Kouyoumjian [9b].

In brief, eq. (19) describes the electric field in the shadow zone of nearly all large aperture antennas including electronically steered arrays, antennas excited in a difference pattern, and antennas with aperture distributions that taper to zero at the edge.

3. Evaluation of $\eta(\bar{r})$

The evaluation of the integral in eq. (14) and subsequently $\eta(\bar{r})$ in eq. (13) is accomplished by first substituting the electric field from eq. (19) into eq. (14),

$$\bar{I} = \sum_m \int_0^{2\pi} \int_{D_m'}^{\infty} \bar{F}_{tm}(\bar{P},d) e^{ik[D_m - p\sin\theta\cos(\phi-\phi_p)]} \, p \, dp \, d\phi_p . \qquad (20)$$

The vectors $\bar{P}$ and $\bar{r}$ have been written in cylindrical (p,ϕ_p) and spherical coordinates (r,θ,ϕ), respectively, defined explicitly in

[6] The fields at the edge of the aperture would have to be quite small for the second term to be significant. For example, an expansion of eq. (16) for a cosine distribution on a circular aperture of radius "a" shows that the second term would be required only after the edge taper became less than about 20 log $\lambda/4a$ (e.g., if $a/\lambda = 10$, 20 log $\lambda/4a = -32$ dB).

figure 5. (The z-axis is chosen to intersect the scan area perpendicularly at a point somewhat centrally located.) D_m' denotes the distance D_m when $\bar{P}$ is on the boundary C' of the scan area, which is always assumed to be outside the aperture boundary C.

Eq. (20) is amenable to the method of stationary phase for double integrals. The critical points of the first kind of $[D_m - p \sin\theta \cos(\phi-\phi_p)]$ occur at

$$\frac{\partial D_m}{\partial \phi_p} = p \sin\theta \sin(\phi-\phi_p) \tag{21a}$$

$$\frac{\partial D_m}{\partial p} = \sin\theta \cos(\phi-\phi_p). \tag{21b}$$

Consider the derivative $\frac{\partial D_m}{\partial p}$, which can be interpreted physically by referring to figure 5. Let the vector $\bar{P}_m$ be the perpendicular projection of the line D_m such that

$$p_m = \sqrt{p^2-\ell_m^2}.$$

Then

$$\frac{\partial D_m}{\partial p} = \frac{\partial D_m}{\partial p_m}\frac{\partial p_m}{\partial p} = \frac{p-\ell_m \frac{\partial \ell_m}{\partial p}}{p_m} \cos\gamma_m,$$

where γ_m is the angle between $\bar{P}_m$ and D_m. Ordinarily, the scan areas are appreciably larger than the aperture area so that

$$\frac{p-\ell_m \frac{\partial \ell_m}{\partial p}}{p_m} \simeq 1$$

and (21b) may be written

$$\cos\gamma_m = \sin\theta \cos(\phi-\phi_p). \tag{22}$$

Similarly, it can be argued that $\frac{\partial D_m}{\partial \phi_p}$ is much less than p for scan areas appreciably larger than the aperture area. Thus for θ not too small eq. (21a) implies the critical point must be near $\phi_p = \phi$. Now $\cos\gamma_m$ has a minimum value greater than zero because γ_m never reaches 90°. The minimum value of $\cos\gamma_m$ occurs at the maximum value of

$\gamma_m = \gamma_{max}$ or on the boundary of the scan area near ϕ. This maximum value is important because eq. (22) reveals that there are no critical points near the angle ϕ for $\theta < 90 - \gamma_{max}(\phi)$.

For $\theta > 90 - \gamma_{max}$ critical points exist at

$$\phi \simeq \phi_p$$

$$\theta \simeq 90 - \gamma_m = \theta_m,$$

and eq. (20) can be evaluated immediately by the method of stationary phase for double integrals [10]. Such a procedure yields after some rearrangement

$$\bar{I} = \sum_m \frac{\bar{F}_{tm} \lambda D_m}{\cos\theta} e^{ik(d \cos\theta \mp \bar{x}_m \sin\theta)} \tag{23}$$

Actually, eq. (23) was derived using the approximation $D_m \simeq \sqrt{(p \pm x_m)^2 + d^2}$ and $\frac{1}{p} \frac{\partial x_m}{\partial \phi_p} << 1$, where x_m and d are defined in figure 5. The above approximations simplify the mathematics but do not alter by a great amount the amplitude of the final expression (nor the following conclusions).

The implications of eq. (23) prove to be quite significant because it shows that for $\theta > 90 - \gamma_{max}(\phi)$ the magnitude of the integral $\bar{I}$ is of the same order as the amplitude of the electric field itself with each term multiplied by $\lambda D_m / \cos\theta$. By referring back to eqs. (12) and (13) we see that this result implies the following:

> In the region outside of the envelope, which is formed by the rays running from the edge of the aperture through the boundary of the scan area, the fractional error $\eta(\bar{r})$ is on the order of unity. Thus, outside the envelope the far-fields computed from a planar scan in the near-field cannot be relied upon with any confidence.

Moreover, diffraction from feed mounts, if present, does not affect the above conclusion, because the radiation scattered by the feed mounts grazes the boundary of the scan area at a wider angle than the radiation from the edge of the aperture.

The conclusion says, essentially, that the planar scan technique does not give information about the fields outside the solid

angle formed by the edge of the aperture antenna and the boundary of the scan area. (We use the term "solid angle" loosely since it will not be a solid angle in the strict mathematical sense unless the extension of its sides meet at a single point.) As an example consider a circular reflector antenna of radius "a" scanned in the near-field on a larger concentric circular area of radius $a\sqrt{2}$. Suppose the scan area were a distance d = a in front of the aperture. Then, as shown in figure 6, the above results reveal immediately that the data from the near-field scan would not contain reliable information about the fields outside the angle $\theta_m = 22.5°$.

Newell and Crawford [11] reached the same conclusion from experimental data taken on scan planes at different distances in front of the same microwave antenna. It appears from the above analysis that their conclusion is a general result which holds for all electrically large aperture radiators.

It should be emphasized that the above results were derived for the sum and difference pattern of electrically large aperture antennas and for a scan area that extends well beyond the main near-field beam region. Also the main near-field beam has been assumed to be characterized by planes of fairly uniform phase. The above conclusion would not necessarily apply, for instance, to broadbeam horns with dimensions on the order of a wavelength or less, to beams steered nearly to the edge of the scan area and scan areas just covering the main near-field beam, to apertures on a finite ground plane, to defocussed antennas, or to electrically large aperture antennas with a diverging or converging lens placed within or directly in front of the aperture. Fortunately, special situations and classes of antennas such as these can often be analyzed separately within the framework of the preceding analysis and results. The special cases mentioned above are discussed in the following paragraph.

Specifically, an analysis similar to the preceding shows that the encircled conclusion applies to the latter three classes of antennas (the defocussed antennas and antennas with a ground plane or lens), provided the scan area extends well beyond the edge of the antenna, the ground plane or lens, and provided the edge of the ground

plane or lens is used as the base perimeter for the solid angle when the edge of the ground plane or lens extends appreciably beyond the edge of the aperture and significant scattering occurs at these edges. Also, it can be shown [20] that the encircled conclusion applies to broadbeam horns if the center of the horn is taken as the base of the solid angle instead of the perimeter of the horn. (For scan areas much larger than the aperture of the horn, there is little difference in size between these two solid angles.) Similarly, for antennas with their mainbeam steered close to the edge of the scan area it may be more accurate to choose a point nearer the center of the aperture rather than the edge to determine the side of the solid angle near the direction of the main beam. Again it makes little difference for large scan areas. In general, when the scan area is close to the boundary of the main beam, the base of the solid angle outside of which the computed far-field pattern is unreliable tends to shift from the perimeter of the aperture (ground plane or lens) toward the center. Often the increase in solid angle is slight, however.

In brief, the above encircled conclusion (in its stated or slightly modified forms just explained) applies to a very large variety of antennas, including electrically large aperture antennas operating in a sum or difference pattern (with or without beam steering, defocussing, a finite ground plane, or modifying lens) and broadbeam horns.

Next we want to evaluate $\bar{I}$ of eq. (20) for points within the solid angle formed by the edges of the antenna and scan area. Within this solid angle the integrand contains no critical points of the first kind. Consequently, the p integration can be done by parts to yield

$$\bar{I} = \frac{\lambda}{2\pi i}\sum_m \int_c^{2\pi} \frac{\bar{F}_{tm}(p',\phi_p)p'\, e^{ik[D_m'-p'\sin\theta\,\cos(\phi-\phi_p)]}}{[\cos\gamma_m'-\sin\theta\,\cos(\phi-\phi_p)]}\, d\phi_p, \qquad (24)$$

where again $\cos\gamma_m'$ has replaced $\frac{\partial D_m'}{\partial p'}$, and the primes refer to points on the boundary of the scan area. It should be noted that eq. (24) represents the first term in an asymptotic expansion of eq. (20),

and when $\cos\gamma_m'$ gets too small eq. (24) no longer represents a good approximation to eq. (20). We can get an idea of the largest permissible γ_m' by realizing that the result (24), if valid, must be much smaller in amplitude than the amplitude of the integrand of eq. (20) multiplied by the change in distance p as D_m changes from D_m' to $D_m' + \lambda/2$. A little mathematics shows that this condition is always satisfied if $\cos\gamma_m'$ is greater than about $\sqrt{\frac{\lambda}{d'}}$, where d' is the perpendicular distance from the edge of the aperture to the scan plane. However, when used to find an upper bound expression for $|\bar{I}|$ (see eq. (28) below), eq. (24) remains valid for γ_m' right up to 90°.

Eq. (24) has been derived under the condition that the fields emanate or at least appear to emanate from points on the edge of the antenna aperture. If the fields are also scattered from the feed mounts, eq. (24) must include these fields as well. The $\cos\gamma_m'$ associated with these mount scattered fields will always be equal to or greater than that of the edge diffracted fields--since the fields scattered by feed mounts make larger angles with the plane of the scan area at its boundary than the edge diffracted fields. Thus, the integration by parts remains valid (as an upper bound expression within the solid angle formed by the edges of the aperture and scan area), and eq. (24) holds even when there exists appreciable radiation scattered from feed mounts in front of the antenna.

For angles near the z-axis ($\sin\theta \ll \cos\gamma_m$) eq. (24) becomes

$$\bar{I} = \frac{\lambda}{2\pi i} \int_0^{2\pi} \left(\sum_m \frac{\bar{F}_{tm} e^{ikD_m'}}{\cos\gamma_m'} \right) p' e^{-ikp' \sin\theta \cos(\phi - \phi_p)} \, d\phi_p . \qquad (25)$$

Upon taking the amplitude of eq. (25) we find

$$|\bar{I}| \leq \frac{\lambda}{2\pi} \int_0^{2\pi} \left| \sum_m \frac{\bar{F}_{tm} e^{ikD_m'}}{\cos\gamma_m'} \right| p' \, d\phi_p . \qquad (26)$$

For scan areas whose boundary is well outside the edge of the aperture, $\cos\gamma_m' \simeq 1$. For scan areas with boundaries somewhat close to the edge of the aperture, the term (in the summation over m) which corresponds to the minimum D_m' (maximum γ_m') predominates (assuming

fairly uniform illumination around the edge of the aperture), so that

$$\sum_m \frac{\bar{F}_{tm} e^{ikD'_m}}{\cos\gamma'_m} \simeq \frac{1}{\cos\gamma_{max}} \sum_m \bar{F}_{tm} e^{ikD'_m}.$$

In either case, we see from eq. (19) that

$$\left| \sum_m \frac{\bar{F}_{tm} e^{ikD'_m}}{\cos\gamma'_m} \right| \simeq \frac{|\bar{E}_t(p',\phi_p)|}{\cos\gamma_{max}},$$

where $E_t(p',\phi_p)$ is the electric field at the boundary of the scan area. Eq. (26) can now be written

$$|\bar{I}| \leq \frac{\lambda}{2\pi \cos\gamma_{max}} \int_0^{2\pi} |\bar{E}_t(p',\phi_p)| p' \, d\phi_p, \tag{27}$$

or

$$|\bar{I}| \leq \frac{\lambda L_{max}}{2 \cos\gamma_{max}} \left| \bar{E}_t^{'max} \right|, \tag{28}$$

with $|\bar{E}_t^{'max}|$ denoting the maximum amplitude of the transverse electric field found on the boundary C' of the scan area, and L^{max} is the maximum width of the scan area. If the output of the measuring probe at the limits of the scan area is down at least X dB from its maximum output, then eq. (28) may be rewritten

$$|\bar{I}| \leq \frac{\lambda L^{max} 10^{-\frac{X}{20}}}{2 \cos\gamma_{max}} E_{to}, \tag{29}$$

where E_{to} represents the highest amplitude of the transverse electric field found on the scan area.[7,8] Equation (29) combines with eqs. (13) and (14) to yield an upper bound expression for the error η in

[7]For an arbitrary probe (i.e., not necessarily a dipole probe) E_{to} represents the highest output amplitude of the probe on the scan area and X the largest output amplitude of the probe at the edge of the scan area measured in dB down.

[8]The maximum electric field on the scan area in the near-field ($z << A/\lambda$) of an electrically large aperture is very nearly equal to the maximum electric field on the aperture itself.

the far-field produced by neglecting the fields outside the finite scan area:

$$\eta(\bar{r}) \leq \frac{\lambda L^{max} 10^{-\frac{X}{20}} g(\bar{r})}{2 \cos\gamma_{max} \left| \int_{A_o} \frac{\bar{E}_t}{\bar{E}_{to}} da \right|}, \tag{30a}$$

where $g(\bar{r})$ is the ratio of the amplitude of the maximum far-electric-field to the far-electric-field in the given direction $\bar{r}$. In other words, itisthe inverse of the normalized far-field pattern. Use has been made of eq. (10) which shows that for sum patterns

$$\lambda r |\bar{E}_o|_{r\to\infty} \simeq \left| \int_{A_o} \bar{E}_t \, da \right|, \tag{30b}$$

where $|\bar{E}_o|_{r\to\infty}$ is the amplitude of the maximum far-field, and the integration is performed in the near-field over the area A_o, that part of the beam which has nearly uniform phase. Since we are in the near-field, $A_o \simeq A \cos\theta_o$, where A is the aperture area. (The factor $\cos\theta_o$ accounts for the reduction in effective aperture area for beams which are steered off-axis electronically through an angle θ_o.)

Because $|\bar{E}_t|/E_o \leq 1$, where E_o is the highest amplitude of electric field on the scan area, and $E_{to} \simeq E_o \cos\theta_o$, we can write

$$\frac{1}{\left| \int_{A_o} \frac{\bar{E}_t}{\bar{E}_{to}} da \right|} = \alpha \cos\theta_o / A_o = \alpha / A, \tag{31}$$

where the factor α is greater than its minimum value of 1.0 (for apertures of uniform amplitude and phase) but less than 5 for most tapered aperture distributions found in practice. For example, the tapered distributions found in Table IX of [13] have a maximum α of 4.0. Newell [17] has found that the factor we have called α has not been greater than about 2 A/A_e for any microwave antenna he has measured. Since the effective area A_e (see [12] for a definition of effective area) is less than the aperture area A and greater than .5A for most aperture antennas [13], the experience of Newell

also indicates that α is less than 4 or 5 for nearly all electrically large aperture antennas found in practice.

Equation (31) combines with eq. (30a) to give the final expression for $\eta(\bar{r})$

$$\eta(\bar{r}) \leq \frac{\alpha \lambda L^{max} 10^{-\frac{X}{20}} g(\bar{r})}{2 A \cos\gamma_{max}}, \tag{32}$$

where

A = area of the antenna aperture.

λ = wavelength.

L^{max} = maximum width of the scan area.

γ_{max} = maximum acute angle between the plane of the scan area and any line connecting the edges of the aperture and scan area.

X = the largest amplitude of the probe output at the edge of the scan area, measured in dB down from the maximum amplitude of probe output in the scan plane.

α = a "taper" factor--equal to a minimum of 1.0 (for apertures of uniform amplitude and phase) and less than 5 for most tapered distributions found in practice. (See eq. (31) for the precise definition of α.)

$g(\bar{r})$ = ratio of the amplitude of the maximum far-electric-field to the far-electric-field at the given direction $\bar{r}$, i.e., the inverse of the normalized far-field pattern. ($g(\bar{r}) = 1$ for the center of the main beam, or beams if a difference pattern.)

(If desired the errors in the gain function sidelobe level, polarization ratio, and beamwidth may be calculated from eqs. (2)-(5) once η and the far-field pattern is known.)

Equation (32) has been derived for antennas operating in a sum pattern. But since a difference pattern can be divided into two, approximately equal, sum patterns with wavefronts slightly skewed, eq. (32) holds for difference patterns as well. (For a difference pattern one should still use the taper factor α of the constituent sum patterns.)

In summary, eq. (32) applies to either sum or difference patterns of all electrically large aperture antennas (including antennas

with their boresight direction steered away from the axis perpendicular to the scan area) within a solid angle ($\sin\theta << \cos\gamma_{max}$) about the axis perpendicular to the scan area. Again, it has been assumed that the scan area extends well beyond a main near-field beam which is characterized by planes of fairly uniform phase. It can be shown that eq. (32) and eq. (36) below apply even to defocussed antennas, apertures in a finite ground plane, and to antennas with a diverging or converging lens, provided the angle γ_{max} is chosen in accord with the second paragraph preceding that of eq. (24). The condition ($\sin\theta << \cos\gamma_{max}$) can be made more specific by returning to eqs. (24) and (25). For all practical purposes, eq. (25) follows from eq. (24) if

$$\boxed{\sin\theta < \frac{1}{2}\cos\gamma_{max} = \frac{1}{2}\sin\theta_{max} \qquad (\theta_{max} = 90 - \gamma_{max}).} \tag{33}$$

For example, if γ_{max} were 45°, condition (33) becomes $\theta < 20°$, which is a large enough angle to include many side lobes of most microwave antennas (assuming their boresight direction at $\theta = 0$). Roughly speaking, eq. (32) represents a valid upper bound within the region $\theta < \frac{1}{2}\theta_{max}$.

As an upper bound, eq. (32) remains valid for γ_{max} right up to 90°. However, from the discussion immediately following eq. (24), it is unlikely that eq. (32) would remain small enough to be very useful when

$$\boxed{\cos\gamma_{max} < \sqrt{\frac{\lambda}{d_{min}}},} \tag{34}$$

where d_{min} refers to the minimum perpendicular distance from the edge of the aperture to the scan plane.

The error η given by eq. (32) can be compared with the results of the empirical error analysis performed by Newell and Crawford [11]. They took "centerline" data on a near-field scan plane 25 cm in front of a circular, fixed-beam "constrained lens" array, which was 80 cm in diameter (see figure 9). The centerline was 213 cm long.

Assuming a rectangularly separable field pattern, they first used the 213 cm centerline data to compute the far-field pattern. Successively, more and more of the 213 cm distance was deleted and

the corresponding far-field pattern computed. In that way they could get an idea of the errors involved in scanning on a near-field plane of finite area.

The envelope of their near-field centerline amplitude is reproduced in figure 7a. The on-axis gain change computed by Newell and Crawford by deleting distances from the scan line is reproduced by the dashed line in figure 8a. The solid lines in figure 8a represent the maximum envelope of on-axis gain change calculated from eqs. (32) and (2c) of the present report. The values of X and L^{max} (see eq. (32)) were taken from figure 7a. The value of α was estimated from eq. (31) and figure 7a to be about 3. The remaining parameters needed to calculate η from eq. (32) are contained in reference [11]:

$$\gamma_{max} = \tan^{-1}\left(\frac{d}{\left[\frac{L^{max}}{2} - a\right]}\right)$$

$$\lambda = 3.26 \text{ cm}$$

$$A = \pi a^2$$

$$a = 40 \text{ cm}$$

$$d = 25 \text{ cm}$$

$$g(\bar{r}) = 1.$$

Figure 8a confirms the result that the fractional error η of eq. (32) represents a reasonable upper bound. In the region $L^{max}/2a > 1.7$ ($\gamma_{max} < 42°$) the upper-bound error from eq. (32) is no more than double the error estimated by computer "deconvolution" of the near-field data. The upper bound error grows inordinately large, however, for $L^{max}/2a$ much less than about 1.2 ($\gamma_{max} > 75°$), as eq. (34) predicts.

Figure 8b shows the same comparison as that made in figure 8a but for a 46 cm (18 in) reflector antenna operating at 60 GHz (λ = .5 cm). (The envelope of the amplitude for a centerline scan of this antenna is shown in figure 7b. The value of α is about 2.) The dashed line in figure 8b represents the on-axis gain change which Newell [17] computed by deleting distances from the centerline scan length taken 43.18 cm in front of the aperture. The agreement between his computations and the upper bound solid curve calculated from eq. (32) is even closer than for that of the constrained lens

antenna (figure 8a). The upper bound error is no more than double the computed error for $L^{max}/2a > 1.05$ ($\gamma_{max} < 88°$) which is very close to the value of $\gamma_{max} < 84°$ predicted for the range of usefulness by eq. (34).

It appears from this somewhat limited experimental evidence with centerline data that the simple formula (32) provides a useful upper bound error at least for scan areas with $\cos\gamma_{max} > \sqrt{\frac{\lambda}{d_{min}}}$. It should be noted, however, that centerline data do not account for changes in phase of the field around the perimeter of the scan area, and thus would predict larger finite scan errors in most cases than the complete 2-dimensional scan data. An upper bound expression of smaller magnitude generally than eq. (32) that takes the phase changes into account can be derived by returning to eq. (24). Under the condition of eq. (33), eq. (24) becomes

$$|\bar{I}| \leq \frac{\lambda}{2\pi \cos\gamma_{max}} \left| \int_0^{2\pi} \bar{E}_t(p',\phi_p) e^{-ikp'\sin\theta \cos(\phi-\phi_p)} p' \, d\phi_p \right|. \quad (35)$$

Again $\bar{E}_t(p',\phi_p)$ refers to the transverse electric field, i.e., output of the dipole probe, at the boundary of the scan area. Substitution of eq. (35) into eq. (13) yields the fractional error $\eta(\bar{r})$ in the far-field for $\theta \leq \frac{1}{2}\theta_{max} = \frac{1}{2}(90 - \gamma_{max})$,

$$\boxed{\eta(\bar{r}) \leq \frac{\left| \int_0^{2\pi} \bar{E}_t(p',\phi_p) e^{-ikp'\sin\theta \cos(\phi-\phi_p)} p' \, d\phi_p \right|}{2\pi r \, |\bar{E}(\bar{r})|_{r\to\infty} \cos\gamma_{max}}.} \quad (36)$$

The far-field pattern $r|\bar{E}(\bar{r})|_{r\to\infty}$ in eq. (36) can be approximated analytically by $\frac{AE_{to}}{\alpha\lambda g(\bar{r})}$ or found by deconvoluting the measured near-field data. The field $\bar{E}_t(p',\phi_p)$ at the boundary of the scan area can be taken from the measured near-field data. Thus, in practice both the numerator and denominator of eq. (36) can be determined straightforwardly. Although eq. (36) involves more computations than eq. (32) even for the on-axis value for which $\theta=0$, it could be computed by a simple routine added to the program which deconvolutes the near-field data, since $\bar{E}_t(p',\phi_p)$ represents merely the output of the

probe on the perimeter of the scan area. In cases where the antenna pattern is assumed separable in xy coordinates and only centerline data is taken, eq. (36) cannot be applied but eq. (32) still can.[9]

In Table 1 are listed the errors calculated from eq. (32) for some of the far-field parameters of a typical X-band antenna operating in a sum and difference pattern. The finite scan errors are proportional to wavelength, so changing the wavelength while holding the other antenna dimension the same merely changes the values in Table 2 proportionately. Of course, such an isolated change is rather unrealistic.

B. Position and Instrumentation Errors

To determine the radiating fields of an unknown antenna by scanning on a near-field plane with a given probe, the output $b_o'(\bar{P})$ of the probe must be recorded throughout the scan area A' (see footnote 3a). In principle, the data points should lie in a plane and the position of the probe should be recorded exactly as it scans from point to point. And, ideally, the instrumentation used to measure the phase and amplitude of b_o' should do so with perfect accuracy.

Obviously, in practice, neither the position of the probe nor the phase and amplitude of the probe output b_o' can be measured exactly. Regardless of how small the uncertainties in the measurement of $b_o'(\bar{P})$ they will introduce errors into the calculated far-field. It is the purpose of this section to derive general expressions which estimate the magnitude of the errors in the far-field produced by the inaccuracies in measuring the position and output of the probe in the near-field.

Specifically, we want to evaluate $\Delta\bar{E}$ in the far-field so that the fractional error $\eta(\bar{r})$ of eq. (1) can be determined. (In Section

[9] It is interesting to note that η in both eqs. (32) and (36) does not approach zero but simply an insignificantly small number as the scan boundary approaches infinity. This limiting value of η represents the contribution of the oscillatory part of the Fourier transform mentioned in footnote 3b. Consequently, once the edges of the scan area reach the region where the fields behave as $1/p'$, there may be no advantage to scanning on a larger area at least if only the pattern near the boresight direction is required.

It is shown in reference [20] that eqs. (32) and (36) slightly modified apply to broadbeam horn antennas as well as electrically large aperture antennas. For these broadbeam antennas the limiting value of η can be significant.

II the errors in gain function, sidelobe level, polarization ratio, and beamwidth are derived in terms of $\eta(\bar{r})$ and the far-field pattern.) In order to simplify the theoretical analysis, the errors will be evaluated as if the probe were a perfect electric dipole. The justification for choosing a perfect dipole in the analysis is similar to that stated in Section III.A. The dipole measures the electric field components at a point. All physically realizable probes respond to a weighted average of the fields near the probe. Thus any small error in position would be expected to change the output of a perfect dipole by as much or more than any other probe. As for instrumentation errors, they remain essentially independent of the particular measurement probe. Also, as in the previous sections, any uncertainty in probe receiving characteristics (S'_{01}) will be ignored for this part of the error analysis.

Under the above conditions the far-field error in $\Delta\bar{E}_t$ may be found with the help of eq. (10):

$$\Delta\bar{E}_t(\bar{r}) \underset{r \to \infty}{=} -\frac{ik\cos\theta}{2\pi r} e^{ik(r-d\cos\theta)} \int_{A'} \Delta\bar{E}_t(\bar{P},d) e^{-i\frac{k}{r}\bar{R}\cdot\bar{P}} d\bar{P}. \quad (37)$$

$\Delta\bar{E}_t(\bar{P},d)$ is the difference between the actual electric field at the point $(\bar{P},d)$ and the measured output of the hypothetical dipole probe (for two orientations in general) at the point $(\bar{P},d)$. For errors near the z-axis ($\theta < 2\lambda/L_o^{max}$, see footnote 5) eq. (37) becomes

$$\Delta\bar{E}(\bar{r}) \underset{r \to \infty}{=} -\frac{ik}{2\pi r} e^{ik(r-d)} \int_{A_o} \Delta\bar{E}_t(\bar{P},d)\, e^{-i\frac{k}{r}\bar{R}\cdot\bar{P}} d\bar{P}, \quad (38)$$

where A_o designates that part of the scan area over which the major variations in phase are relatively small. (For the position and instrumentation error analysis the scan plane is assumed to lie nearly parallel to the near-field planes of "uniform" phase, i.e., perpendicular to the center of the main beam of sum patterns or to the null axis of difference patterns.) For scan planes in the very near-field, A_o is approximately equal to $A\cos\theta_o$, i.e., the projected area of the antenna aperture. (Only electrically large aperture

antennas are being considered.) θ_o is the angle between the perpendicular to the aperture and the perpendicular ($\hat{e}_z$) to the scan plane. $\theta_o = 0$ for beams which are not steered off-axis electronically.

The scan area outside A_o can be neglected for this part of the error analysis because the rapidly changing phase in the region outside A_o contributes little when integrated to find the far-field and the errors in the far-field near the z-axis. It follows from footnote 5, or more rigorously from an asymptotic analysis like the one performed in Appendix A for a circular aperture of uniform distribution, that eq. (38) can be used as an upper bound expression for $\Delta\bar{E}$ in the region given approximately by $\theta < 2\lambda/L_o^{max}$ where L_o^{max} is the maximum breadth of the partial scan area A_o. This region is large enough to include the first sidelobe maximum of many electrically large aperture radiators. For example, a circular aperture of uniform distribution and radius $a \simeq L_o^{max}/2$ has its first sidelobe maximum at an angle $\theta \simeq 1.7\lambda/L_o^{max}$ radians.

Physically this $2\lambda/L_o^{max}$ condition says that for most electrically large aperture antennas, the part of the near-field (A_o) over which the phase is fairly uniform strongly influences the far-field within the angle $2\lambda/L_o^{max}$. Beyond this angle the edge diffracted fields dominate the far-fields to a greater and greater extent until in the far sidelobes the fields are determined essentially by the edge diffracted fields alone.

To find either the position or instrumentation errors, the integr

$$\bar{I}_o = \int_{A_o} \Delta\bar{E}_t(\bar{P},d)\, e^{-i\frac{k}{r}\bar{R}\cdot\bar{P}}\, d\bar{P} \qquad (39)$$

in eq. (38) must be evaluated. Of course, the integration can be performed only after $\Delta\bar{E}_t(\bar{P},d)$ is found. In Section 1 below, $\Delta\bar{E}_t$, $\bar{I}_o$, and thus $\eta(\bar{r})$ are evaluated for position errors, and in Section 2 for instrumentation errors.

The approach that is taken is quite straightforward. For position errors $\Delta\bar{E}_t$ is expanded in a Taylor series about (P,d) assuming the deviation in the position of the scanner is small compared to a wavelength. The Taylor series and the integral (39) into which it

is substituted divides naturally into a longitudinal or z-position part and a transverse or xy-position part. The upper-bound for each integral and thus for the z- and xy-position errors are then determined as a function of the measured near-field data and the computed far-field pattern.

For instrumentation errors, $\Delta\bar{E}_t$ is expressed in terms of the amplitude and phase errors introduced by the nonlinearities in the receivers which measure these quantities as the probe traverses the scan area. Mathematically, the integrals involving the receiver phase errors are handled in the same way as z-position errors, and thus the final upper-bound expressions have the same form. The integrals involving the amplitude errors have their upper-bound determined by characterizing the receiver nonlinearity in measuring amplitude in dB of error per dB down from the maximum amplitude of the probe output on the scan area.

1. Position Errors

Consider the scanner which moves the probe throughout the near-field scan area. Typically the scanner covers the area by traversing a grid or raster of lines while the probe output is recorded at given points along each line. Ideally, all the scan lines lie perfectly straight and parallel in a single plane, and the position of the data points along each line is recorded exactly. In reality, of course, none of these idealizations hold, basically because the scan lines will never be perfectly straight and the data must always be recorded over an interval rather than at a point.

Regardless of the reason for the position errors, they all effect the near-field data simply by positioning the probe at points $(\bar{P}+\Delta\bar{P},\ d+\Delta z)$ rather than (P,d). In other words, the difference $\Delta\bar{E}_t(\bar{P},d)$ in eq. (39) can be written for position errors as

$$\Delta\bar{E}_t(\bar{P},d) = \bar{E}_t(\bar{P}+\Delta\bar{P},d+\Delta z) - \bar{E}_t(\bar{P},d), \qquad (40)$$

where, as usual, $\bar{E}_t(\bar{P},z)$ is the electric field at the point $(\bar{P},z)$ in the near-field. In general, $\Delta\bar{P}$ and Δz, which will be referred to as displacement errors, are functions of the transverse position $\bar{P}$.

Before continuing with the analysis it should be pointed out that displacement errors caused by a small initial translation of the entire scanner with respect to the test antenna will not cause a change in the computed far-field amplitude, as eqs. (6) and (8) indicate. Also, an initial rotation of the entire scanner through a small angle will have no effect on the far-field pattern other than to rotate the entire pattern through that same angle.

Since the displacement errors must be much smaller in magnitude than a wavelength, the right hand side of eq. (40) can be expanded in a three dimensional Taylor series. By letting $\Delta\bar{r} = \Delta\bar{P}+\Delta z\hat{e}_z$ and keeping only the first two terms in the series, eq. (40) becomes

$$\Delta\bar{E}_t(\bar{P},d) = \Delta\bar{r}\cdot\Delta\bar{E}_t(\bar{P},d) + \frac{1}{2}\,\Delta\bar{r}\cdot[\Delta\bar{r}\cdot\nabla\nabla\bar{E}_t(\bar{P},d)], \tag{41}$$

$$\text{where } \nabla\nabla\bar{E}_t \equiv (\nabla\nabla E_x)\hat{e}_x + (\nabla\nabla E_y)\hat{e}_y$$

$$\text{and} \quad \nabla\bar{E}_t \equiv (\nabla E_x)\hat{e}_x + (\nabla E_y)\hat{e}_y.$$

Substitution of eq. (41) into eq. (39) yields a useful expression for $\bar{I}_o$,

$$\bar{I}_o = \int_{A_o} \Delta\bar{r}\cdot[\nabla\bar{E}_t+\tfrac{1}{2}\Delta r\cdot\nabla\nabla\bar{E}_t]\; e^{-i\frac{k}{r}\bar{R}\cdot\bar{P}}\; d\bar{P}. \tag{42}$$

Again it is emphasized that $\Delta\bar{r}$ is, in general, a function of $\bar{P}$, the transverse coordinates over which eq. (42) is integrated. Also, as we shall see shortly, it is necessary to retain the second term in the integrand of eq. (42) when on-axis errors for sum patterns are considered. As a check on eq. (42) let $\bar{R} = 0$ (on-axis) and $\Delta\bar{r}$ be constant over A_o so that $\Delta\bar{r}$ can be taken outside the integral. The terms containing the transverse part of the gradient operator convert to line integrals around the boundary of A_o. These line integrals must equal zero because in effect eq. (42) assumes negligible fields outside A_o. Only the "z" derivatives, which can also be taken outside the integral, are left, and eq. (42) may be written

$$\bar{I}_o = \Delta z\left(\frac{\partial}{\partial z} + \Delta z^2\,\frac{\partial^2}{\partial z^2}\right)\int_{A_o} \bar{E}_t\, d\bar{P}. \qquad (43)$$

With the aid of eq. (10), eq. (43) converts to

$$\bar{I}_o = -(\Delta z + ik\Delta z^2)2\pi r e^{-ik(r-d)}\,\bar{E}_t(\bar{r}). \qquad (44)$$
$$r \to \infty$$

Equations (38), (39), (42) and (44) combine to show that

$$|\bar{E}(\bar{r})+\Delta\bar{E}(\bar{r})|_{r\to\infty} \simeq \left(1 + \frac{(k\Delta z)^4}{8}\right)|\bar{E}(\bar{r})|_{r\to\infty},$$

i.e., the error in the far field amplitude calculated from eq. (42) is of higher order than $(\frac{|\Delta\bar{r}|}{\lambda})^2$, i.e., it is negligible when $\Delta\bar{r}$ is constant -- a result which must hold if eq. (42) is a valid expression for $\bar{I}_o$, because, as mentioned above, a translation of the entire scanner has a negligible effect on the far-field pattern. Equation (42) also checks in a similar way for $R \neq 0$, but the proof is more involved.

In order to evaluate $\bar{I}_o$ of eq. (42) exactly, both $\Delta\bar{r}$ and $\bar{E}_t(\bar{r})$ in the near-field would have to be known. Fortunately, an upper bound approximation can be found for $\bar{I}_o$ without detailed information about $\Delta\bar{r}$ or $\bar{E}_t(\bar{r})$.

Consider one component, say E_x, of the integrand of eq. (42). For an electrically large aperture antenna, we can express E_x within the area A_o as

$$E_x(\bar{P},z) \simeq (1+\Delta A_x(\bar{P},z))E_{ox}(\bar{P})\, e^{i(kz+\phi_{ox}+\Delta\phi_x(\bar{P},z))}, \qquad (45)$$

where ϕ_{ox} is a real arbitrary phase constant, and ΔA_x, $\Delta\phi_x$ and E_{ox} are real functions of the indicated near-field coordinates. The functions $\Delta A_x(\bar{P},z)$ and $\Delta\phi_x(\bar{P})$ typically oscillate over a distance equal to or greater than a wavelength, each with a magnitude usually much less than one. $E_{ox}(\bar{P})$ is the smoothly tapered amplitude function. In other words, eq. (45) simply states that the near-field across the area A_o of an electrically large aperture antenna has a phase equal essentially to kz and a smoothly tapered amplitude except for small variations which oscillate over distances equal to or

greater than a wavelength. (Recall that for the position and instrumentation error analysis we are assuming that the perpendicular to the scan area is approximately aligned with the boresight direction of the antenna.)

In Appendix A eq. (45) is verified for a circular aperture of radius "a" and uniform aperture distribution ($E_{ox} = E_o$). In that case ΔA_x and $\Delta\phi_x$ are on the order of $\frac{1}{\pi}\sqrt{\lambda/a}$ or less. Rusch and Potter report similar results for the circular aperture [14]. Equation (45) has been verified experimentally by the substantial near-field scan and extrapolation data taken at the NBS. The measured amplitude and phase on a near-field plane of a typical microwave antenna are plotted in figures 9a,b,d. This particular scan was taken 25 cm in front of the circular "constrained lens array" (see figure 9c) of radius 40 cm operating at 9.2 GHz (λ = 3.26 cm). This antenna is the same one described in the paragraph following eq. (34) and whose centerline amplitude envelope is plotted in figure 7a.

When eq. (45) is substituted into the integrand of eq. (42) and all terms higher than either second order in $|\Delta\bar{r}|/\lambda$ or first order in $|\Delta\bar{r}|/\sqrt{A_o}$ are discarded, the following expression for the x component of $\bar{I}_o$ remains:

$$I_{ox} \simeq \int_{A_o} \left([\Delta\bar{r}\cdot\nabla|E_x| - \frac{1}{2}\left(\frac{2\pi\Delta z}{\lambda}\right)^2 E_{ox} + i\left(\frac{2\pi\Delta z}{\lambda}\right)E_{ox}\right] e^{i\phi_x} e^{-i\frac{k}{r}\bar{R}\cdot\bar{P}}\, d\bar{P}, \tag{46}$$

where $E_x = |E_x|e^{i\phi_x}$, or from eq. (45)

$$|E_x| = (1+\Delta A_x)E_{ox}$$

$$\phi_x = kd + \phi_{ox} + \Delta\phi_x.$$

It has been assumed that the transverse ($\bar{P}$) and longitudinal (z) displacement errors are of the same order of magnitude. Eq. (46) can be simplified further by writing $e^{i\phi_x}$ as $e^{i(kd+\phi_{ox})}(\cos\Delta\phi_x + i\sin\Delta\phi_x)$, to put I_{ox} in the form

$$I_{ox} \simeq e^{i(kd+\phi_{ox})} \int_{A_o} (\Delta\bar{r}\cdot\nabla|E_x| - \frac{1}{2}\delta^2 E_{ox} + i\delta E_{ox})$$

$$\cdot (\cos\Delta\phi_x + i\sin\Delta\phi_x) e^{-i\frac{k}{r}\bar{R}\cdot\bar{P}} d\bar{P}. \qquad (47)$$

$$(\delta = 2\pi\Delta z/\lambda)$$

First consider on-axis errors for antennas operating in a sum mode, that is $\frac{k\bar{R}\cdot\bar{P}}{r} << 1$ or θ less than about $\lambda/(10\ L_o^{max})$. Then the exponential in eq. (47) can be approximated by unity. The arbitrary phase constant ϕ_{ox} can be chosen so that $\Delta\phi_x$ varies about zero throughout the area A_o. Furthermore, since the variations in $\Delta\phi_x$ are small, oscillate many times across the area A_o, and remain completely independent of the variations in the displacement errors $\Delta\bar{r}$ of the scanner, to a high probability, ϕ_{ox} can be chosen such that the integration in eq. (47) which is multiplied by $\sin\Delta\phi_x$ can be neglected compared to the maximum possible value of the $\cos\Delta\phi_x$ integration. In addition, since $E_{ox}\cos\Delta\phi_x$ remains positive throughout A_o for a sum pattern, the reference plane (z=d) for δ can be chosen to make

$$\int_{A_o} \delta E_{ox} \cos\Delta\phi_x\, d\bar{P} = 0. \qquad (48)$$

Thus, under the above conditions the $i\delta$ term of eq. (47) is eliminated entirely and eq. (47) simplifies to

$$I_{ox} \simeq e^{i(kd+\phi_{ox})} \int_{A_o} (\Delta\bar{P}\cdot\nabla_t E_{ox} - \frac{1}{2}\delta^2 E_{ox})\cos\Delta\phi_x\, d\bar{P}. \qquad (49)$$

$$(\Delta = \Delta_t + \hat{e}_z \frac{\partial}{\partial z})$$

E_{ox} in the first term of eq. (49) has replaced $|E_x| = (1+\Delta A_x)\ E_{ox}$ of eq. (47) because the many oscillations of ΔA_x would also (to a high probability) eliminate upon integration all but higher order contributions from the $\nabla(\Delta A_x)$ term.

It is interesting that eq. (48) expresses the same condition chosen by Ruze [15] in his well-known work on "antenna tolerance theory." Of course, in his work δ represented a small "arbitrary

phase error or aberration" (what we call $\Delta\phi_x$) rather than the displacement errors of a near-field scanner. It would be desirable that the reference planes of Δx and Δy ($\Delta\bar{P} = \Delta x\hat{e}_x + \Delta y\hat{e}_y$) be chosen such that $\int_{A_o} \Delta\bar{P}\cdot\nabla_t E_{ox} \cos\Delta\phi_x \, d\bar{P}$ became zero also. Unfortunately, such a choice is impossible (in general) because neither derivative, $\frac{\partial E_{ox}}{\partial x}$ or $\frac{\partial E_{ox}}{\partial y}$, stay the same sign throughout A_o.

From eqs. (38) and (39) it is seen that the fractional error η of eq. (1) can be written as

$$\eta(\bar{r}) = \frac{1}{\lambda r|\bar{E}(\bar{r})|_{r\to\infty}} \sqrt{|I_{ox}|^2 + |I_{oy}|^2}. \tag{50}$$

The amplitude of I_{ox} is found from eq. (49) to be

$$\begin{aligned} |I_{ox}| &= \left|\int_{A_o} (\Delta\bar{P}\cdot\nabla_t E_{ox} - \tfrac{1}{2}\delta^2 E_{ox})\cos\Delta\phi_x \, d\bar{P}\right| \\ &\le \Delta P_{max}\int_{A_o} |\nabla_t E_{ox}| d\bar{P} + \tfrac{1}{2}\delta^2_{max}\int_{A_o} E_{ox}\, d\bar{P}, \end{aligned} \tag{51}$$

where ΔP_{max} and $\frac{\lambda\delta_{max}}{2\pi}$ are the maximum magnitudes of the transverse ($\bar{P}$) and longitudinal (z) displacement errors, respectively, introduced by the near-field scanner.

The last integral in eq. (51) can be related to the maximum far-field $|E_{xo}|_{r\to\infty}$, i.e. from eq. (10) or (30b)

$$\int_{A_o} E_{ox}\, d\bar{P} \simeq \lambda r|E_{xo}|_{r\to\infty}. \tag{52}$$

The remaining integral,

$$\int_{A_o} |\nabla_t E_{ox}|\, d\bar{P}, \tag{53}$$

is a bit more troublesome. However, it can also be estimated by expressing the integral in polar coordinates (p,ϕ) as follows:

$$\int_{A_o} |\nabla_t E_{ox}|\, dP = \int_{A_o} \sqrt{\left(\frac{\partial E_{ox}}{\partial p}\right)^2 + \left(\frac{1}{p}\frac{\partial E_{ox}}{\partial\phi}\right)^2}\, pdpd\phi. \tag{54}$$

If we assume that the amplitude of the aperture distribution tapers with much greater slope in the radial direction (p) than in the azimuthal direction (ϕ), the second term under the radical sign of eq. (54) can be neglected, leaving

$$-\int_{A_o} \frac{\partial E_{ox}}{\partial p}\, pdpd\phi. \tag{55a}$$

The negative sign is present in eq. (55a) because $\frac{\partial E_{ox}}{\partial p}$ is negative for amplitude distributions which taper toward the boundary of A_o. (We are assuming $p = 0$ at the maximum of E_{ox}.) Integration of eq. (55a) by parts with respect to p yields

$$-\int_{A_o} \frac{\partial E_{ox}}{\partial p}\, pdpd\phi = \int_{A_o} E_{ox}\, dpd\phi \simeq \frac{\pi}{2} E_{xo} L_o^{max}, \tag{55b}$$

where E_{xo} and L_o^{max} denote the maximum amplitude of E_{ox} and the maximum breadth of the partial scan area A_o, respectively. With the aid of eq. (55b), eq. (54) becomes

$$\int_{A_o} |\nabla_t E_{ox}|\, d\bar{P} \leq \frac{\pi}{2} L_o^{max} E_{xo}. \tag{56}$$

Since the area A_o is in the very near-field of the aperture antenna, the maximum amplitude E_{xo} on A_o is approximately equal to the maximum amplitude on the aperture itself. Thus E_{xo} is related to the maximum far-field by (see eqs. (30b) and (31))

$$E_{xo} = \frac{\alpha\lambda r |E_{xo}|_{r\to\infty}}{A}, \tag{57}$$

and eq. (56) becomes

$$\int_{A_o} |\nabla_t E_{ox}| d\bar{P} \leq \frac{\pi\alpha\lambda r L_o^{max} |E_{xo}|_{r\to\infty}}{2\ A}. \tag{58}$$

Substitution of eqs. (52) and (58) into eq. (51) yields

$$|I_{ox}| \leq \lambda r |E_{xo}|_{r\to\infty} \left\{ \frac{\pi\alpha\Delta P_{max} L_o^{max}}{2\ A} - + \frac{1}{2}\delta_{max}^2 \right\}. \tag{59}$$

A corresponding inequality holds for $|I_{oy}|$ with $|E_{yo}|_{r\to\infty}$ replacing $|E_{xo}|_{r\to\infty}$. At first sight, one may raise the objection that the reference plane for δ cannot necessarily be chosen so that both eq. (48) and the corresponding equation with E_{oy} are satisfied simultaneously. It should be noted, however, that the two equations need not be satisfied simultaneously. It is only necessary that one reference plane can be found that allows eq. (48) to hold, and that a second reference plane can be found that allows the corresponding equation with E_{oy} to hold. If the two reference planes are a slight distance apart, the relative phase of the x and y components of the far-electric-field will be in slight error but not the Hermitian amplitude of the far-electric-field, i.e., the far-field pattern will remain unchanged even though the far-field polarization ratio will be shifted slightly.

Eq. (59) and the corresponding equation for $|I_{oy}|$ combine with eq. (50) to give an expression for the maximum position error η in the far-field:

$$\eta(\bar{r}) \leq \left[\frac{\pi\alpha\Delta P_{max} L_o^{max}}{2A} + \frac{1}{2}\delta_{max}^2\right] \qquad \theta < \frac{\lambda}{10 L_o^{max}} \quad \text{(sum patterns)}. \tag{60a}$$

Equation (60a) was derived assuming the antenna was operating in a sum pattern and does not apply to difference patterns since eq. (48) may not be satisfiable for difference patterns. However, in Appendix B it is shown that an error expression similar to eq. (60a) may be derived near the boresight direction (null axis) of difference patterns as well. Specifically,

$$\eta(\bar{r}) \leq \left[\frac{\pi\alpha\Delta P_{max} L_o^{max}}{2A} + 4\Delta F\delta_{max}\right] g(\bar{r}), \quad \theta < \frac{\lambda}{10 L_o^{max}} \quad \text{(difference pattern)} \tag{60b}$$

where ΔF and $g(\bar{r})$ are defined below after eq. (61).

Finally for the angular region $\theta > \lambda/10\, L_o^{max}$, but still less than $2\lambda/L_o^{max}$ (see eqs. (37) and (38)), we can derive an upper bound expression similar to eq. (60a). Specifically, the magnitude of I_{ox} in eq. (47) may be written

$$|I_{ox}| \leq \int_{A_o} |\Delta\bar{r}\cdot\nabla|E_x|| \, d\bar{P} + \frac{1}{2}\int_{A_o} |\delta E_{ox}| \, d\bar{P}.$$

The term second order in δ has been ignored since now the first order term in δ is the major contributor to the z-displacement error. When we carry the analysis through in a way similar to that described between eqs. (51) to (59), the following expression for the fractional error for both sum and difference patterns results:

$$\eta(\bar{r}) \leq \left[\frac{\pi\alpha\Delta P_{max} L_o^{max}}{A} + \delta_{max}\right]\frac{g(\bar{r})}{2} \qquad \frac{\lambda}{10L_o^{max}} < \theta < \frac{2\lambda}{L_o^{max}} \qquad (60c)$$

Although eq. (60c) was derived for $\theta < 2\lambda/L_o^{max}$, it remains valid as an upper-bound expression all the way to $\theta = \pi/2$. This result follows from the fact, which will not be proven here, that the contribution from the integration in eq. (37) outside the area A_o is negligible compared to the upper-bound contribution obtained from inside A_o and expressed by eq. (60c). (It is interesting to note that the maximum possible errors in even the far sidelobes are determined by the displacement errors across A_o, whereas the field itself in the far sidelobe region is determined by the near-field outside A_o.)

Thus, if we combine eqs. (60a), (60b), and (60c); insert the approximations, $L_o^{max} \simeq \ell^{max}$, $A \simeq (\ell^{max})^2$ into eqs. (60); and let $\Delta_{max} = \frac{2\pi\Delta P_{max}}{\lambda}$; an upper-bound expression for η valid over the entire far-field hemisphere emerges

$$\eta(\bar{r}) \leq \left[\frac{\alpha\lambda}{2\ell^{max}}\Delta_{max} + \eta_z\right]\frac{g(\bar{r})}{2} \qquad (61)$$

$$\eta_z = \begin{cases} \delta_{max}^2 & \text{(sum patterns)} \\ 8\Delta F\,\delta_{max} & \text{(difference patterns)} \\ \delta_{max} & \text{(sum and difference patterns)} \end{cases} \qquad \theta < \frac{\lambda}{10\ell^{max}} \quad \text{or} \quad \frac{\lambda}{10\ell^{max}} < \theta < \frac{\pi}{2}$$

where

λ = wavelength.

ℓ^{max} = maximum width of the antenna aperture.

Δ_{max} = $2\pi\Delta P_{max}/\lambda$, where ΔP_{max} is the maximum amplitude of the transverse displacement errors within the partial scan area A_o. (A_o is that part of the scan area over which the phase is fairly uniform. For near-field scans parallel to the aperture $A_o \approx A$, the aperture area.)

δ_{max} = $2\pi\Delta z_{max}/\lambda$, where Δz_{max} is the maximum amplitude of the longitudinal displacement errors within the partial scan area A_o.

ΔF = fractional difference between the amplitude of the two main far-field lobes of the difference pattern (see Appendix B).

α = a "taper" factor -- equal to a minimum of 1.0 (for apertures of uniform amplitude and phase) and less than 5 for most tapered distributions found in practice. (See eq. (31) for the precise definition of α; for a difference pattern one should still use the taper factor of the constituent sum patterns.)

$g(\bar{r})$ = ratio of the amplitude of the maximum far-electric-field to the far-electric-field at the given direction $\bar{r}$, i.e., the inverse of the normalized far-field pattern. ($g(\bar{r}) = 1$ for the center of the main beam, or beams if a difference pattern.)

(If desired, the errors in the gain function, sidelobe level, polarization ratio, and beamwidth may be calculated from eqs. (2)-(5) once η and the far-field pattern are known.)

The expression (61) represents an upper bound to the far-field error η caused by inaccuracies in the position of the near-field scanner. It applies to both sum and difference patterns in the entire forward hemisphere of all electrically large aperture antennas. Equation (61) was derived under the assumption that the scan plane is parallel or nearly parallel to the near-field planes of "uniform" phase, i.e., the plane perpendicular to the electrical boresight direction.

In addition, eq. (61) holds for arbitrary (random as well as systematic) errors in the positioning of the scanner, since only the

maximum magnitude of displacement errors Δ_{max} and δ_{max} are required to evaluate eq. (61). However, it proves useful to derive an expression similar to eq. (61) which separates the effects of the systematic and random errors in position.

To do this and also clarify what is meant by systematic and random errors, consider the motion of the scanner as it takes measurements along lines in the near-field plane. As the scanner moves along each line it will deviate from a perfectly straight-line by a gently varying curve that will contain at most a few oscillations from one end of the scan line to the other. These curves, which may also change gently from scan line to scan line, represent the systematic errors in position of the scanner. For example, a slight warp or deformation of the scanner frame would create a systematic error.

Superimposed upon the systematic deviations from the straight-line would be position errors which changed randomly (within limits) from measurement point to measurement point. These random errors in position have zero or nearly zero mean and could result, for example, from vibrations of the entire scanner or from a slight play in the drive mechanisms. The maximum magnitude of the random errors are often smaller than that of the systematic errors. However, it is possible that the scanner is aligned so precisely, that essentially all but the random errors are eliminated.

Return to eq. (47) and separate $\Delta\bar{P}$ and δ into systematic and random displacement errors, i.e.,

$$\Delta\bar{P} = \Delta\bar{P}^{s} + \Delta\bar{P}^{rn} \tag{63a}$$

$$\delta = \delta^{s} + \delta^{rn}. \tag{63b}$$

All the integrals in eq. (47) which contain linear terms in $\Delta\bar{P}^{rn}$ or δ^{rn} can be dropped. Since $\Delta\bar{P}^{rn}$ and δ^{rn} change randomly from measurement point to measurement point (over distances less than $\lambda/2$), the integrals actually summations -- see footnote 3a) containing these linear terms will be extremely small compared to the largest possible errors produced by the remaining integrals (summations). Thus, substituting eqs. (63) into eq. (47) and proceeding as we did before with eq. (47), yields the desired expression for η separated into

systematic and random errors,

$$\eta(\bar{r}) \leq \left(\frac{\alpha\lambda}{2\ell^{max}} \Delta^{s}_{max} + \eta_z^{s,rn} \right) \frac{g(\bar{r})}{2} \tag{64}$$

$$\eta_z^{s,rn} = \begin{cases} (\delta^{s}_{max})^2 + (\delta^{rn}_{max})^2 & \text{(sum patterns)} \\ 8\Delta F \, \delta^{s}_{max} & \text{(difference patterns)} \quad \theta < \dfrac{\lambda}{10\ell^{max}} \\ \delta^{s}_{max} & \text{(sum and difference patterns)} \quad \dfrac{\lambda}{10\ell^{max}} < \theta < \dfrac{\pi}{2} \end{cases}.$$

All symbols have the same definitions found after eq. (61). The superscripts "s" and "rn" refer to "systematic" and "random" errors respectively.

Note from eq. (64) that to the given order of approximation the longitudinal random errors (δ^{rn}), but not the transverse random errors (Δ^{rn}), cause an error in the on-axis far-field of sum patterns (provided, of course, that Δ^{rn} is of the same order of magnitude or less than δ^{rn}). In addition, eqs. (64) and (61) above show that the maximum possible transverse (xy) position errors do not depend upon wavelength for a given $g(\bar{r})$ since Δ_{max} behaves as $1/\lambda$. Also note that in expressions (64) and (61) above, the z-position error is not continuous across the angle $\theta = \lambda/10\ell^{max}$. There lies no contradiction in this fact since the expressions remain valid as inequalities. The jump between the two regions merely indicates that the upper-bound was determined by a different method in each region. Obviously expressions (61) and (64) do not represent a least upper-bound throughout the region $\theta > \lambda/10\ell^{max}$. This region will be discussed further at the end of the section.

One can get an idea of the magnitude of the position errors by plotting the on-axis gain from eqs. (64) and (2c) for the fixed-beam constrained lens array described in the paragraph following eq. (34) and shown in figure 9. In that case,

$$\lambda/\ell^{max} = .04$$

$$g(\bar{r}) = 1,$$

and with α equal to 3, eq. (64) combines with eq. (2c) to give

$$\eta_G^{dB} \leq \pm 8.7\left\{.03\ \Delta_{max}^{s} + \frac{1}{2}(\delta_{max}^{s})^2 + \frac{1}{2}(\delta_{max}^{rn})^2\right\}. \tag{65}$$

If we assume $\delta_{max}^{rn} = 0$ and let $\delta_o = \delta_{max}^{s} = \Delta_{max}^{s}$, eq. (65) may be written

$$\eta_G^{dB} \leq \pm 8.7\ \delta_o(.03 + \frac{1}{2}\ \delta_o). \tag{66}$$

The solid curve in figure 10 depicts the maximum value of η_G^{dB} in eq. (66) versus δ_o, i.e. when the random errors are negligible. The dashed line represents the maximum error η_G^{dB} when the $\Delta_{max}^{s} = \delta_{max}^{s} = 0$ and $\delta_o = \delta_{max}^{rn}$, i.e., when the systematic errors are negligible.

To insure that the on-axis gain is less than .01 dB for this particular antenna, δ_o must be less than about .027. That is, each component of systematic displacement error of the scanner must be less than .027 $\lambda/2\pi$, or less than about .004λ. For this constrained lens antenna λ = 3.26 cm, so the errors in each component of displacement must be less than about .14 mm for better than .01 dB accuracy in the on-axis far-field.

For random errors only (the dashed line) the z-displacement errors must be less than about .26 mm for .01 dB accuracy in the on-axis far-field for this particular wavelength. As a matter of fact, when the systematic errors are negligible, eq. (64) shows that the "random" error in gain $\eta_{G,rn}^{dB}$ for the sum-pattern main-beam of an arbitrary (electrically large aperture) antenna can be written simply as

$$\eta_{G,rn}^{dB} \leq \pm\frac{8.7}{2}\ (\delta_{max}^{rn})^2. \qquad (\delta_{max}^{rn} = 2\pi\Delta z_{max}^{rn}/\lambda) \tag{67}$$

For $\eta_{G,rn}^{dB} \leq \pm$ .01, δ_{max}^{rn} must be less than about .05 radians or Δz_{max}^{rn} less than .008 of a wavelength (3 degrees). That is, the random errors in z-position should be no greater than about $\pm$ .01λ to insure a .01 dB accuracy in the gain of the main beam. Equation (67) reveals that the random error in the on-axis far-field gain of sum patterns increases as the square of the random error in the

z-position of the near-field scanner. For example, a position error of $\pm .025\lambda \simeq 10°$ (@ 3.125 x .008λ) leads to a maximum $\eta^{dB}_{G,rn}$ of about ± .1 dB (@$(3.125)^2$ x .01) for the center of the main beam.

To date, little experimental data are available with which to compare the results of eqs. (61), (64) or (67). However, a comparison can be made between eq. (67) and the computations performed by Rodgrigue, Joy, and Burns [16]. They introduced errors into a hypothetical near-field distribution in order to compute the effects of the errors on the far-field. The results of their computations for the effect of random phase errors (or equivalently z-position errors) on on-axis gain are plotted in figure 3-14 or A-21 of [16], and are reproduced here by the dashed line in figure 11 below. The solid line is $\eta^{dB}_{G,rn}$ plotted from eq. (67). One can see from figure 11 that the two curves are in close agreement. The solid line lies slightly above the computed dashed line as indeed it should if eq. (67) represents an upper bound.

Figure 12, which will be explained in greater detail below under instrumentation errors, shows a comparison between the effects on the on-axis gain of a sum pattern from systematic (quadratic in this case) phase errors introduced into actual near-field data by Newell [17,21] and the corresponding upper-bound results calculated from eq. (64). Again agreement is close, with the upper-bound curve lying just above the actual curve for small deviations in phase.

Next, let's calculate the effect of systematic z-displacement errors on the depth of the null for an antenna operaing in a difference pattern. From eq. (64)

$$\eta^{dB}_{G,s} \leq \pm\ 35\ \Delta F\ \delta^{s}_{max}\ g(\bar{r}),$$

where $g(\bar{r})$ is no longer equal to unity because $\bar{r}$ is in the direction of the boresight null. Typically, ΔF is about .01 and the depth of the null is 25 dB down from the main beams of the difference pattern. Thus

$$g(\bar{r}) \simeq 10^{5/4} \simeq 18,$$

and

$$\eta^{dB}_{G,s} \leq \pm 6.3\ \delta^{s}_{max}$$

for the null depth. For example, if $\Delta z^{rn}_{max} = .01\lambda$ (which would correspond to an accuracy of about .27 dB for the main beams) eq. (68) insures that the null depth would be accurate to within .40 dB. This surprisingly high insensitivity of the null depth to z-displacement errors (or, equivalently, phase errors) has been observed by Newell [21] upon introducing phase errors into the measured near-field data of a number of antennas operating in the difference mode. To understand the reasons for this high accuracy in null depth, one must refer to the derivation in Appendix B. There appears to be no simple way to explain this result heuristically.

It is also found in Appendix B that the maximum shift θ_{shift} in the direction of the far-field null of a difference pattern caused by z-position errors is given by the simple expression which is not a function of wavelength:

$$\theta_{shift} \leq \frac{4\Delta z^{s}_{max}}{\ell^{max}} = \frac{2\lambda}{\pi \ell^{max}} \delta^{s}_{max} \text{ radians.} \qquad (68)$$

In general, the shift in the null caused by all other sources of error are negligible compared to this shift caused by the z-position error or, equivalently, the phase errors.

Table 2 lists the upper-bound position errors in a number of far-field parameters for a typical X-band and K-band antenna. The values in the table were calculated from expressions (61) and (68). As eqs. (61) and (64) show, the maximum possible transverse (xy) position errors do not depend upon frequency for a given $g(\bar{r})$. Table 2 also shows quite dramatically that the z-position or phase errors everywhere except in the boresight direction can be extremely large compared to all other representative sources of error -- compare Tables 1-4. (This is also true of the shift in the difference pattern null.) Especially note that the error in a -25 dB sidelobe can be several dB for phase errors ($2\pi\Delta z_{max}/\lambda$) of just a few degrees. Whether or not these maximum possible far-field errors are actually experienced in practice depend strongly upon the shape of the near-field z-position or phase error throughout the scan area. For example, we shall find in the next section that receiver phase distortion usually has a functional dependence which introduces

negligible errors into the sidelobe fields. It is important to know exactly what effect various distributions of near-field phase errors have on the far-field in order to avoid experimentally, if possible, the distributions which produce large far-field errors in the directions of interest. Such a detailed study of the dependence of the far-field errors on the functional form of the near-field z-position or phase errors will not be included as part of this report but will be contained in a forthcoming report by Newell [21].

2. Instrumentation Errors

The amplitude and phase of the probe output are measured at discrete points as the probe moves back and forth across the near-field scan area. The receivers are capable of sampling and recording the amplitude and phase to within a certain accuracy only. The errors in the near-field data, caused by the inaccuracies in the receivers or instrumentation used to measure the probe output, produce errors in the computed far-field. This section estimates the far-field errors under given limits of accuracy of the instrumentation which measures the amplitude and phase of the probe output. It is emphasized that the errors produced by the imperfect positioning of the scanner were determined in the previous section and are not considered as part of the instrumentation error analysis of this section. Also the instrumentation errors associated with converting analogue to digital information is assumed negligible.

Under the conditions explained in Section III.B, the far-field errors can be found in the region

$$\theta < \lambda/(10\ell^{max})$$

by evaluating the integral (39)

$$\bar{I}_o = \int_{A_o} \Delta\bar{E}_t(\bar{P},d)\, d\bar{P}.$$

Here, $\Delta\bar{E}_t(\bar{P},d)$ represents the difference between the measured ($\bar{E}_t^{meas}$) and "actual" ($\bar{E}_t$) output of the probe at the point ($\bar{P}$,d), i.e.

$$\Delta\bar{E}_t(\bar{P},d) = \bar{E}_t^{meas}(\bar{P},d) - \bar{E}_t(\bar{P},d). \qquad (69)$$

If we look at just the x-component first, the integral $\bar{I}_o$ and eq. (69) combine to give

$$I_{ox} = \int_{A_o} (E_x^{meas} - E_x)\, d\bar{P}. \tag{70}$$

By writing

$$E_x = |E_x| e^{i\phi_x} \tag{71a}$$

and

$$E_x^{meas} = [|E_x| + \Delta A_x^I] e^{i(\phi_x + \Delta\phi_x^I)}, \tag{71b}$$

where ΔA_x^I and $\Delta\phi_x^I$ are the errors in amplitude and phase respectively introduced by the measuring instrumentation, eq. (70) becomes

$$I_{ox} = \int_{A_o} [(|E_x| + \Delta A_x^I) e^{i\Delta\phi_x^I} - |E_x|] e^{i\phi_x}\, d\bar{P}. \tag{72}$$

In general, both ΔA_x^I and $\Delta\phi_x^I$ are functions of the transverse coordinates $\bar{P}$. For small errors $\Delta\phi_x^I << 1$, so that

$$e^{i\Delta\phi_x^I} \simeq 1 + i\Delta\phi_x^I - \frac{(\Delta\phi_x^I)^2}{2} + \cdots$$

and

$$I_{ox} = \int_{A_o} [\Delta A_x^I + i(|E_x| + \Delta A_x^I)\Delta\phi_x^I - \frac{|E_x|}{2}(\Delta\phi_x^I)^2] e^{i\phi_x}\, d\bar{P}. \tag{73}$$

All terms higher than second order have been neglected in eq. (73). If a sum pattern is assumed and the exponential $e^{i\phi_x}$ is written as in eq. (47),

$$e^{i\phi_x} = e^{i(kd + \phi_{ox})} (\cos\Delta\phi_x + i \sin\Delta\phi_x),$$

with the arbitrary phase constant ϕ_{ox} chosen as in eq. (47), then to a high probability, the integration in eq. (73) which is multiplied by the oscillating quantity $\sin\Delta\phi_x$ can be neglected compared to the

maximum possible value of the $\cos\Delta\phi_x$ integration. (Note the distinction between $\Delta\phi_x$ and $\Delta\phi_x^I$. $\Delta\phi_x$ is the actual variation in phase of the x-component of electric field within A_o, whereas $\Delta\phi_x^I$ is the error in phase introduced by the phase measuring instruments.) In addition, since $(|E_x|+\Delta A_x^I)\cos\Delta\phi_x$ is always greater than zero for sum patterns, the reference phase for the instrumentation phase error $\Delta\phi_x^I$ can be chosen to make

$$\int_{A_o} (|E_x|+\Delta A_x^I)\Delta\phi_x^I \cos\Delta\phi_x = 0, \tag{74}$$

which again expresses essentially the same condition as that chosen by Ruze [15] in his work on antenna tolerance theory. Under the above conditions, the imaginary term within the brackets of eq. (73) is eliminated and the magnitude of I_{ox} reduces to

$$\begin{aligned} |I_{ox}| &= \left|\int_{A_o} [\Delta A_x^I - \frac{|E_x|}{2}(\Delta\phi_x^I)^2]\cos\Delta\phi_x \, d\bar{P}\right| \\ &\leq \int_{A_o} |\Delta A_x^I| \, d\bar{P} + \frac{1}{2}(\Delta\phi_{xmax}^I)^2 \int_{A_o} |E_x| \, d\bar{P}. \end{aligned} \tag{75}$$

$\Delta\phi_{xmax}^I$ is the maximum value (in absolute value) of the instrumentation phase error within the partial scan area A_o.[10]

Since it can be shown that (see eq. (10), (30b) or (52))

$$\int_{A_o} |E_x| \, d\bar{P} \simeq \lambda r |E_{xo}|_{r\to\infty} \tag{76}$$

where $|E_{xo}|_{r\to\infty}$ is the magnitude of the maximum x-component of far-field, $|I_{ox}|$ may be rewritten

[10] Because the errors in measuring phase are usually greatest at points in the scan area where the amplitude is least, it is desirable to choose the partial scan area A_o as small as possible when estimating $\Delta\phi_{xmax}^I$. The far-field within $\theta < 2\lambda/\ell^{max}$ is hardly effected by the near-field outside that part of the scan area where the amplitude of electric field is equal to the edge taper down from the maximum amplitude. Thus for the sake of designating maximum errors in phase measurement on a near-field scan plane, the area A_o need be chosen no larger than this effective "edge taper" scan area.

$$|I_{ox}| \leq \int_{A_o} |\Delta A_x^I| \, d\bar{P} + \frac{1}{2}(\Delta\phi_{xmax}^I)^2 \lambda r |E_{xo}|_{r\to\infty}. \qquad (77)$$

It is usually possible to express the errors in amplitude in dB per dB change of amplitude. That is, the receivers are assumed to read the correct (zero error) amplitude of the probe output at its maximum value point on the area A_o. At all other points the amplitude lies a certain number of dB down from its maximum value. Typically the dB errors in measuring the amplitude are linearly related to this number of dB down from the maximum amplitude, and thus the errors can be expressed in dB per dB down. Even if the actual amplitude error curve is not linear, for the sake of the upper bound expression (77), it can be replaced by a straight line (linear curve) which is equal to or greater than the actual error curve.

Specifically, if N_{dB}^I designates the amplitude error in the number of dB per dB down, and A_{dB} the amplitude in dB down from the maximum amplitude, ΔA_x^I can be expressed as (for small errors)

$$|\Delta A_x^I| = |E_x| \, N_{dB}^I \, A_{dB}/8.7 \quad . \qquad (78)$$

By definition

$$A_{dB} = 20 \log \frac{E_{xo}}{|E_x|} \leq 8.7 \left(\frac{E_{xo}}{|E_x|} - 1 \right), \qquad (79)$$

where E_{xo} denotes the maximum of $|E_x|$ on the scan area. Substitution of eq. (79) into eq. (78) and the result into eq. (77) yields

$$|I_{ox}| \leq N_{dB}^I \int_{A_o} (E_{xo} - |E_x|) \, d\bar{P} + \frac{1}{2}(\Delta\phi_{xmax}^I)^2 \lambda r |E_{xo}|_{r\to\infty}. \qquad (80a)$$

With the help of eqs. (57) and (76), eq. (80a) becomes

$$|I_{ox}| \leq \left(N_{dB}^I \left(\frac{\alpha A_o}{A} - 1 \right) + \frac{1}{2}(\Delta\phi_{xmax}^I)^2 \right) \lambda r |E_{xo}|_{r\to\infty}. \qquad (80b)$$

By combining eq. (80b) and the corresponding equation for $|I_{oy}|$ with eq. (50), assuming $E_{yo} \approx E_{xo}$, and approximating $\frac{A_o}{A}$ by 1, the upper-bound expression for the fractional far-field error η caused by the

instrumentation is obtained:[11]

$$\eta(\bar{r}) \leq [N_{dB}^{I}(\alpha-1) + \tfrac{1}{2}(\Delta\phi_{max}^{I})^2] \qquad \theta < \frac{\lambda}{10\ell^{max}} \text{ (sum patterns).} \quad (81)$$

Equation (81), which is analagous to the position error equation (60a), holds only for sum patterns within an angle $\lambda/(10\ell^{max})$ of the boresight direction. For difference patterns as well, and for $\theta > \lambda/(10\ell^{max})$, the following upper bound expression analagous to the position error equation (61) applies:

$$\eta(\bar{r}) \leq [2N_{dB}^{I}(\beta^{I}) + \eta_z^{I}]\,\frac{g(\bar{r})}{2} \quad (82)$$

$$\eta_z^{I} = \begin{cases} (\Delta\phi_{max}^{I})^2 & \text{(sum patterns)} \\ 8\Delta F\ \Delta\phi_{max}^{I} & \text{(difference patterns)} \\ \Delta\phi_{max}^{I} & \text{(sum and difference patterns)} \end{cases} \qquad \theta < \frac{\lambda}{10\ell^{max}} \quad \frac{\lambda}{10\ell^{max}} < \theta < \frac{\pi}{2}$$

$$\beta^{I} = \begin{cases} (\alpha-1) & \text{(sum patterns)} \\ 2/g(\bar{r}) & \text{(difference patterns)} \\ (\alpha-1)/2 & \text{(sum and difference patterns)} \\ \dfrac{\alpha\lambda L^{max}}{3A} & \end{cases} \qquad \theta < \frac{\lambda}{10\ell^{max}} \quad \frac{\lambda}{10\ell^{max}} < \theta < \frac{2\lambda}{\ell^{max}} \quad \frac{10\lambda}{\ell^{max}} < \theta < \frac{\pi}{2}$$

where

λ = wavelength.

N_{dB}^{I} = the maximum instrumentation errors involved in measuring the amplitude of the probe output -- N_{dB}^{I} is expressed in dB error per dB amplitude down from the maximum amplitude on the scan area. (For the present purposes, the amplitude error is designated as zero at the maximum amplitude.)

[11] When the maximum value of the probe output on the scan area for the x-orientation is very different from that of the y-orientation ($E_{yo} \neq E_{xo}$), it can be shown that eq. (81) remains valid as an upper bound for the errors in magnitude of the far-field. But for errors in polarization ratio an extra term, $N_{dB}^{I}|x_p|/8.7$, must be added to eq. (81), where x_p is the difference between the maximum probe outputs measured in dB for the two orientations.

$\Delta\phi^{I}_{max}$ = the maximum instrumentation errors (expressed in radians) involved in measuring the phase of the probe output on the effective scan area A_o (see footnotes 10 and 13).

ΔF = fractional difference between the amplitude of the two main far-field lobes of the difference pattern (see Appendix B).

α = a "taper" factor -- equal to a minimum of 1.0 (for apertures of uniform amplitude and phase) and less than 5 for most tapered distributions found in practice. (See eq. (31) for the precise definition of α; for a difference pattern one should still use the taper factor of the constituent sum patterns.)

$g(\bar{r})$ = ratio of the amplitude of the maximum far-electri -field to the far-electric-field at the given direction $\bar{r}$, i.e., the inverse of the normalized far-field pattern. ($g(\bar{r})$ = 1 for the center of the main beam, or beams if a difference pattern.)

ℓ^{max} = maximum width of the antenna aperture.

L^{max} = maximum width of scan area.

A = area of antenna aperture.

The derivation of η^{I}_{z} is identical to that done for z-position errors in Section III.B.1. The derivation of β^{I} for $\frac{\lambda}{10\ell^{max}} < \theta < \frac{2\lambda}{\ell^{max}}$ is accomplished by the same procedure used above for $\theta < \lambda/(10\ell^{max})$. In the far sidelobe region, $\theta > 10\lambda/\ell^{max}$, the far-field errors become approximately equal to the corresponding errors in the near-field amplitude, and after using eqs. (30b), (31), and (79) β^{I} in this region can be written as shown in eq. (82). Between θ equal to $2\lambda/\ell^{max}$ and $10\lambda/\ell^{max}$ the value of β^{I} can be estimated by connecting a straight line from its value at $2\lambda/\ell^{max}$ to its value at $10\lambda/\ell^{max}$. β^{I} near the boresight direction $\theta < \lambda/(10\ell^{max})$ of difference patterns is derived in Appendix B. (Note that the error factor β^{I} is generally much smaller near the boresight direction or null axis of difference patterns than near the center of the main beam of sum patterns. This result occurs, as Appendix B shows, because the instrumentation distorts the amplitude on the "positive" and "negative" sides of a difference pattern by approximately the same amount.) Appendix B also shows that we can write an upper-bound expression for the null shift of difference patterns caused by the instrumentation errors:

$$\theta_{shift} \leq \frac{2\Delta\phi^{I}_{max}\lambda}{\pi\ell^{max}} \text{ radians.} \tag{83}$$

Equation (83) is identical to eq. (68) with the instrumentation phase error replacing the z-position error.

Equation (82) represents an upper bound to the far-field errors produced by the instrumentation which measures the amplitude and phase of the probe output. It applies to either sum or difference patterns in the forward hemisphere of all electrically large aperture antennas. As with eq. (61), eq. (82) was derived for scan planes which are parallel or nearly parallel to the plane perpendicular to the electrical boresight direction. (If desired, the errors in the gain function, sidelobe level, polarization ratio, and beamwidth may be calculated from eqs. (2)-(5) once η and the far-field pattern are known.)

A comparison of eq. (82) with eq. (61) shows that the instrumentation phase error $\Delta\phi^{I}_{max}$ in eq. (82) has taken the place of δ_{max} in eq. (61). This result acts as a check on eqs. (61) and (82) because δ_{max} simply represents a phase error caused by a z-displacement error in the position of the scanner.[12] Also, $\Delta\phi^{I}_{max}$ can be separated into a random and systematic part to get a result analagous to eq. (64). However, the random phase errors introduced by the instrumentation are usually much smaller than the systematic phase errors, and thus can usually be neglected.

Figure 11 reveals that the phase ($\Delta\phi^{I}_{max}$) part of eq. (82) for the on-axis gain of a sum pattern is in good agreement (as an upper bound) with the computer error analysis performed by Rodrigue, Joy and Burns [16] on a hypothetical near-field distribution with random phase errors. Newell [17,21] has introduced phase errors which are quadratic with respect to the xy coordinates, into the actual near-field data of the 60 GHz, 46 cm (18 inch) reflector antenna whose

[12] Note that the "phase error terms" in eqs. (61) and (82) for sum patterns and $\theta < \lambda/(10\ell^{max})$ depend on the square of δ_{max} and $\Delta\phi_{max}$ respectively. Thus, these two squared terms should not be added directly when estimating the total error in the far-field. Instead, δ_{max} should be added to $\Delta\phi^{I}_{max}$ before the square is taken.

near-field amplitude envelope is shown in figure 7b. The resulting errors in η_G^{dB} for on-axis gain computed by Newell are shown with the dashed line in figure 12. The solid line represents the maximum phase error plotted from eqs. (82) and (2c). Again it appears that the expression (82) represents a useful upper bound estimate for the instrumentation phase errors in on-axis gain, especially when the measured phase is accurate to within a few degrees across the effective scan area A_o (as is usually the case in practice).

The accuracy with which the receiver can measure the phase of the probe output is related to the amplitude of the probe output. Specifically, the smaller the amplitude the larger the phase errors usually become (see footnote 10). For example, a typical receiver used at the NBS near-field range measures phase to within ± .001 radians (± .05°) at the maximum amplitude on the near-field scan plane, and ± .01 radians (.5°) at an amplitude 20 dB down from the maximum. Thus, for an edge taper 20 dB down, $\Delta\phi^I_{max}$=.01, and eq. (82) shows that the error in the main beam of a sum pattern caused by the errors in measuring the phase of the probe output are negligible ($\eta_G^{dB} = \frac{\pm 8.7}{2}(.01)^2 < \pm .001$ dB).[13] The same is true for the null depth and shift of difference patterns. Of course, the errors in sidelobe level could be affected to a greater extent by the phase errors, depending on the shape and distribution of the phase errors across the scan area. However, since receiver phase errors usually increase monotonically with decreasing amplitude, it can be shown as a consequence [21] that the upper-bound off-axis or sidelobe phase errors ($\Delta\phi^I_{max}/2\ g(\bar{r})$) given in eq. (82) represents a much larger error in far-field than would usually occur in practice. Thus, in general, receiver phase errors have a relatively small effect over the entire far-field of sum or difference patterns. In fact, compared to the maximum possible effect that typical z-position errors can have on the off-axis far-fields, instrumentation phase errors can be ignored completely in the off-axis region.

[13] Even for aperture antennas with edge tapers greater than 20 dB down, it is unlikely that the near-fields outside these -20 dB points (or even the -15 dB points) have a significant effect on the maximum possible far-field errors. In other words, regardless of how large the edge taper, the effective scan area A_o need not extend beyond about the -15 or -20 dB points.

For receivers which measure phase with high accuracy, the phase part of the instrumentation error can be neglected and only the amplitude error remains in eq. (82), i.e.

$$\eta(\bar{r}) \leq N_{dB}^{I}(\beta^{I})\ g(\bar{r}).$$

Amplitude errors for $\theta < 2\lambda/\ell^{max}$ do not depend directly on frequency or the size of the antenna, only on the taper factor α of the near-field beam, the receiver inaccuracy N_{dB}^{I}, and the inverse of the normalized far-field pattern $g(\bar{r})$. (For null depth of a difference pattern the amplitude errors are extremely small and do not even involve $g(\bar{r})$. These results are proven in Appendix B.) Also, in the far sidelobe region, $\theta > 10\lambda/\ell^{max}$, the instrumentation amplitude errors are relatively small, usually less than a few tenths of a dB for N_{dB}^{I} less than a few thousands of a dB per dB. The far-field error in the on-axis ($g(\bar{r}) = 1$) gain for sum patterns is found from the above equation and (2c) to be

$$\eta_{G}^{dB} \leq \pm\ 8.7\ N_{dB}^{I}(\alpha-1). \tag{84}$$

Note that for $\alpha=1$ (uniform amplitude distribution) the far-field error, caused by the instrumentation errors in measuring near-field amplitude, equals zero--as it should since the receivers measure essentially at a constant amplitude across the effective scan area.

The maximum error in on-axis gain (eq. (84)), which is linear with respect to N_{dB}^{I}, is plotted with the solid lines in figure 13 for different values of α. Rodrigue et al. [16] have also computed linear amplitude errors for their hypothetical near-field distribution, which has an α exactly equal to 3.0. Their results (see figures 3-5 or A-5 of [16]) are reproduced by the dotted line in figure 13. The errors computed by Rodrigue et al. and the maximum errors predicted by the analytically derived expression (84) are in good agreement. The solid line for $\alpha=3$ lies above the dotted line -- as it must if eq. (84) represents a valid upper bound expression for the errors.

To insure an on-axis gain error less than ± .01 dB, the error in measuring the near-field amplitude should be kept less than about ± .001 dB per dB down. Unfortunately, the accuracy of most receiver

systems is of the order of ± .01 dB per dB down (rather than ± .001) which, according to figure 13, can lead to errors in the on-axis gain of about ± .1 dB. This value of far-field error can be larger than the errors from all other sources combined. Thus, if high accuracy is desired, special effort should be devoted to designing a receiver system which can measure the amplitude of the probe output to better than ± .001 dB per dB down. Alternatively, the amplitude calibration curve for the receivers could be determined to within ± .001 dB per dB down and the errors in amplitude compensated for by including the calibration curve as part of the computer program that deconvolutes the near-field data.

This latter correction procedure has been adopted by A.C. Newell et al. at the National Bureau of Standards. The difference between the on-axis gain computed by Newell [17,21] with and without the amplitude calibration curve is shown by the dashed line in figure 13 for the 46 cm (18 in) reflector antenna operating at 60 GHz. (Actually, Newell found a .112 dB on-axis gain difference for an amplitude calibration curve that deviated by at most .02 dB per dB down over the effective scan area. The dashed line in figure 13 assumes linearity and simply connects the origin to the point .112 dB at .02 dB per dB.) The value of α for this antenna was estimated at 2 from the measured near-field data shown in figure 7b. Again it is seen from figure 13 that the computed errors for this particular antenna correspond quite well with the maximum possible errors predicted by the general expression (84) for $\alpha = 2$.

In brief, the computations of both Rodrigue et al. and Newell indicate that eq. (82) yields reasonable values for the maximum far-field errors expected from instrumentation errors in measuring the amplitude and phase of the probe output.

Table 3 lists some representative far-field amplitude errors calculated from eq. (82) for an antenna with taper factor α equal to 3, and a receiver nonlinearity in measuring amplitude (N^{I}_{dB}) equal to .002 dB per dB. Note the extremely small effect that amplitude errors have on the null depth of difference patterns. As Appendix B shows, this small effect on the null depth is due to the fact that the receiver which measures the amplitude of the probe output distorts the opposite sides of the near-field difference pattern by approximately the same amount.

C. Multiple Reflections

Consider a probe which scans on a plane in the near-field of a radiating test antenna. The radiation that the probe receives can be described by an infinite series of rapidly decreasing terms, with the first term equal to the unperturbed field of the test antenna. This unperturbed field scatters from the probe, reflects from the test antenna and other nearby objects, and returns to the probe to give the second term in the series. The return radiation again scatters from the probe, reflects, and returns to the probe to yield the third term. The process repeats ad infinitum.

In order to determine the far-field of the test antenna by "deconvoluting" the measured near-field data (without knowing the detailed scattering properties of the probe or test antenna), the multiple reflections must be neglected. That is, the second and higher order terms in the infinite series just described are assumed negligible when applying the planar near-field scanning techniques [3].

Multiple reflections can be reduced by decreasing the size of the probe antenna, by increasing the distance between the probe and test antenna, and by appropriately covering the scanning range with efficient absorber material. These measures will not, however, eliminate the multiple reflections entirely.[14] It is the purpose of this section to estimate the effects of the multiple reflections on the far-field which is computed from the near-field scan data under the assumption of zero multiple reflections.

As we shall see shortly, it is a fairly simple matter to estimate maximum and minimum values expected for the far-field errors produced by the multiple reflections. However, it is impossible to derive an accurate estimate of the far-field errors analytically without knowing the phase of the multiply reflected fields throughout the scan area. Thus, the only reliable way to get an accurate estimate of the far-field errors caused by multiple reflections is through measurement. Specifically, a number of near-field scans could be

[14] In principle, the effect of multiple reflections could be eliminated at microwave frequencies by the use of gated sinewaves instead of CW. Unfortunately, the speed of electromagnetic propagation (c) is so great that the necessary gating times are too short for the present-day electronics to handle. It is possible, however, in the analagous measurement of electroacoustic transducers to eliminate the problem of multiple reflections by the use of gated sinewaves because the speed of sound is much smaller than that of light [18].

taken on parallel planes separated by about 1/4 wavelength and the far-field computed from each scan. Any differences observed in the far-fields computed from the separate near-field scans would indicate the extent of the effect of multiple reflections (assuming the scan area is large enough so that changes in finite scan errors are negligible). In this way the far-field errors can be determined straightforwardly and accurately. Of course, the main disadvantage of this "straightforward method" of determining errors lies in the time and effort it takes to record data and compute far-fields from several near-field scan planes for every antenna that has to be measured. Because of this disadvantage it may prove worthwhile, particularly when the multiple reflections are very small, to derive the following very approximate, yet general, upper and lower bound expressions for the far-field errors caused by the multiple reflections. In addition to the upper and lower limits of errors, the far-field errors will be derived for multiply reflected fields which satisfy a certain class of hypothetical near-field distributions.

Consider a probe antenna scanning en a plane in the near-field of an electrically large, aperture antenna. Assume once again, for the sake of simplifying the mathematics, that the probe behaves as an electric dipole, i.e. its output in one orientation is proportional to E_x and in a second orientation proportional to E_y. Then the error $(\Delta\bar{E})_{r\to\infty}$ in the computed far-electric-field can be expressed with the aid of eqs. (37) and (12d),

$$\Delta\bar{E} \underset{r\to\infty}{\leq} \frac{-ik}{2\pi r} e^{ik(r-d\cos\theta)} \int_{A'} \Delta\bar{E}_t^{mr}(\bar{P},d) e^{-i\frac{k}{r}\bar{R}\cdot\bar{P}} d\bar{P}. \tag{85a}$$

The superscript "mr" on $\Delta\bar{E}_t^{mr}$ denotes that part of the transverse near-electric-field caused by multiple reflections, and A' refers to the scan area.

The determination of $(\Delta\bar{E})_{r\to\infty}$ requires the evaluation of the integral

$$\bar{I} = \int_{A'} \Delta\bar{E}_t^{mr}(\bar{P},d) e^{-i\frac{k}{r}\bar{R}\cdot\bar{P}} d\bar{P}, \tag{85b}$$

or if the x-component is concentrated on first

$$I_x = \int_{A'} \Delta E_x^{mr}(\bar{P},d) e^{-i\frac{k}{r}\bar{R}\cdot\bar{P}} \, d\bar{P}. \tag{85c}$$

The amplitude and phase of ΔE_x^{mr} can be written explicitly as

$$\Delta E_x^{mr} = \Delta A_x^{mr} \, e^{i\phi_x^{mr}}$$

to recast eq. (85c) in the form

$$I_x = \int_{A'} \Delta A_x^{mr} \, e^{i(\phi_x^{mr} - \frac{k}{r}\bar{R}\cdot\bar{P})} \, d\bar{P}. \tag{86}$$

The maximum value of the integral in eq. (86) occurs when $\phi_x^{mr} = \frac{k}{r}\bar{R}\cdot\bar{P}$, i.e.

$$I_x \leq \int_{A'} \Delta A_x^{mr} \, d\bar{P}. \tag{87}$$

If polarization is not changed drastically upon reflection from the probe and test antenna, ΔA_x^{mr} will be roughly proportional to the magnitude of the x-component of electric field at the probe. That is,

$$\Delta A_x^{mr} \simeq \epsilon_x^{mr} |E_x|, \tag{88}$$

where ϵ_x^{mr} is an average proportionality constant between the amplitude of the multiply reflected x-component of electric field and the amplitude of the total x-component of electric field as the probe traverses the scan area. Substitution of eqs. (88) and (52) into eq. (87) yields

$$I_x \leq \epsilon_x^{mr} \, \lambda \, r \, |E_{xo}|_{r\to\infty}. \tag{89a}$$

In the same manner, the expression for I_y is found to be

$$I_y \leq \epsilon_y^{mr} \, \lambda \, r \, |E_{yo}|_{r\to\infty}. \tag{89b}$$

An upper bound expression for the fractional error η emerges when eqs. (89) and (85) are combined with eq. (1):

$$\eta(\bar{r}) \leq \epsilon^{mr} \, g(\bar{r}), \tag{90}$$

where ϵ^{mr} is the average proportionality constant between the amplitude of the multiply reflected electric field (probe output) and the amplitude of the total electric field (probe output) as the probe traverses the scan area. The value of ϵ^{mr} can be estimated experimentally by changing the distance between the probe and test antenna by a few wavelengths at various locations within the scan area. Periodic variations in the amplitude of the probe output which repeated about every $\lambda/2$ would be caused primarily by the multiple reflections. As usual, $g(\bar{r})$ is the ratio of the amplitude of the maximum far-electric-field to the far-electric-field at the given direction $\bar{r}$.

Equation (90) represents an upper bound expression for the errors in the far-field caused by multiple reflections. It applies to the entire far-field of electrically large aperture antennas. However, for nearly all antenna-probe interactions it will give much too large an estimate of the far-field errors because it was derived under the unrealistic assumption that the multiply reflected fields possessed just the right phase across the scan area to maximize the far-field errors. In reality, as the probe traverses the scan area it will usually experience large variations in the phase of the multiply reflected fields throughout the scan area that will greatly reduce their effect on the far field. We emphasize the word "usually" because there exist some antennas (like the constrained lens, fixed-beam array shown in figure 9) which present a rather flat reflective surface to the radiation scattered from the probe, and thus a rather constant effective path length and phase for the multiply reflected fields as the probe scans on a plane parallel to the aperture. In that case the maximum error could be experienced at the center of the main beam.

The multiple reflections would have a minimum effect on the far-field when their phase varied radically over the scan area, or more precisely, when $\phi_x^{mr} - \frac{k}{r}\bar{R}\cdot\bar{P}$ in eq. (86) has no critical points and varies rapidly with position $\bar{P}$ on the scan area. Then eq. (86) written in polar coordinates (p, ϕ_p) can be integrated by parts with respect to p to give

$$I_x \simeq \frac{\lambda}{2\pi i}\int_0^{2\pi} \frac{\Delta A_x^{mr}(p',\phi_p)}{\partial f/dp'} e^{ikf(p',\phi_p)} p'd\phi_p, \qquad (91)$$

where p' refers to the distance from the origin within the scan area to the point on the boundary of the scan area at the angle ϕ_p. The function $f(p',\phi_p)$, which is assumed to possess no stationary points with respect to p, is defined by

$$kf = \phi_x^{mr} - \frac{k}{r}\,\bar{R}\cdot\bar{P}. \tag{92}$$

As mentioned above, the smallest values of I_x occur, in general, when the phase function f varies rapidly with p and ϕ_p. Experience at the NBS [17] indicates that it is unlikely that the average phase variations in multiple reflections which occur in practice ever exceed 360° per wavelength across the scan area. Thus it is also unlikely that $|I_x|$ will be smaller than its value when f is chosen as a function which changes an average of about 360° per wavelength of motion in any direction across the scan area. For example, one such function is

$$f = p(1+\cos^2\theta_p). \tag{93}$$

Substitution of the function (93) into eq. (91) shows that the magnitude of I_x may be expressed as

$$|I_x| \geq \frac{\lambda}{2\pi}\left|\int_0^{2\pi} \frac{\Delta A_x^{mr}(p',\phi_p)}{1+\cos^2\theta_p}\, p'\, e^{ikp'(1+\cos^2\theta_p)}\, d\phi_p\right|. \tag{94}$$

Equation (94) is written as an inequality to emphasize that for nearly all antennas $|I_x|$ would be larger than the right side of eq. (94).

In order to get an idea of the value of eq. (94), assume that $\frac{\partial p'}{\partial \phi_p} \ll p'$ so that the points of stationary phase of $p'(1+\cos^2\phi_p)$ with respect to ϕ_p occur near $\phi_p = 0,\ \pi/2,\ \pi$ and $3\pi/2$. Then integration by the method of stationary phase shows that eq. (94) may be written approximately as

$$|I_x| \geq \frac{\lambda}{2\pi}\sqrt{\lambda\, L^{ave}}\;\Delta A_x^{ave}, \tag{95a}$$

with L^{ave} equal to the average of the width of the scan area, and ΔA_x^{ave} equal to the average amplitude of the x-component of the multiply reflected electric field at the four points $\phi_p = 0,\ \pi/2,\ \pi$ and $3\pi/2$

on the boundary of the scan area. If we approximate ΔA_x^{ave} by $\epsilon_x^{mr}|E_x|^{ave}$, where $|E_x|^{ave}$ refers to the average amplitude of the x-component of electric field on the boundary of the scan area, eq. (95a) becomes

$$|I_x| \geq \frac{\lambda}{2\pi}\sqrt{\lambda\, L^{ave}}\;\epsilon_x^{mr}|E_x|^{ave}. \tag{95b}$$

Since $|\bar{I}| = \sqrt{|I_x|^2 + |I_y|^2}$, eq. (95b) combines with the corresponding equation for $|I_y|$ to give

$$|\bar{I}| \geq \frac{\lambda}{2\pi}\sqrt{\lambda\, L^{ave}}\;\epsilon^{mr}|\bar{E}_t|^{ave}. \tag{96}$$

The average amplitude $|\bar{E}_t|^{ave}$ of the transverse electric field may be expressed in terms of the maximum transverse electric field (E_{to}) on the scan plane,

$$|\bar{E}_t|^{ave} = 10^{\frac{-X^{ave}}{20}}\,E_{to}, \tag{97}$$

with X^{ave} denoting the number of dB down from that maximum (see footnote 7).

Equations (30b) and (31) can be utilized in conjunction with eqs. (97) and (96) to give the final expression for the minimum value of $|\bar{I}|$,

$$|\bar{I}| \geq \sqrt{\lambda\, L^{ave}}\;\frac{10^{\frac{-X^{ave}}{20}}\;\epsilon^{mr}\;\alpha\;\lambda^2 r|\bar{E}_o|_{r\to\infty}}{2\pi A}. \tag{98}$$

From eqs. (98), (85) and (1) we find the minimum value expected for the fractional error η in the far-field caused by multiple reflections:

$$\eta(\bar{r}) \geq \left(\frac{\lambda}{L^{ave}}\right)^{3/2}\frac{10^{\frac{-X^{ave}}{20}}\;\alpha\;\epsilon^{mr}\;g(\bar{r})}{\pi}. \tag{99}$$

(The aperture area A has been taken as $.5(L^{ave})^2$.) The inequality (99) represents a lower bound expression for η in the sense that the actual far-field errors caused by multiple reflections would, to a high probability, be greater than but could lie reasonably close to

the value of the right side of eq. (99). Of course, there remains the possibility that for some points in the far-field the effects of the multiple reflections will cancel to such a degree that η would actually be less than the right side of eq. (99). These exceptional points must be ignored if eq. (99) is accepted as a valid lower bound.

Between eqs. (90) and (99) we have approximate upper and lower limits to the value of η,

$$\left(\frac{\lambda}{L^{ave}}\right)^{3/2} \frac{\alpha\, 10^{\frac{-X^{ave}}{20}}}{\pi}\, \varepsilon^{mr} g(\bar{r}) \leq \eta(\bar{r}) \leq \varepsilon^{mr}\, g(\bar{r}), \qquad (100)$$

where

λ = wavelength.

ε^{mr} = the average ratio of the amplitude of the multiply reflected probe output to the amplitude of the total probe output as the probe traverses the scan area. (Its value can be estimated experimentally by changing the distance between the probe and test antenna at various locations within the scan area, and calculating one-half the fractional peak to peak height of the variations in amplitude that repeat about every $\lambda/2$.)

L^{ave} = average width of the scan area.

X^{ave} = the average amplitude of the probe output at the boundary of the scan area measured in dB down from the maximum amplitude of probe output in the scan plane.

α = a "taper" factor -- equal to a minimum of 1.0 (for apertures of uniform amplitude and phase) and less than 5 for most tapered distributions found in practice (see eq. (31) for the precise definition of α; for a difference pattern one should still use the taper factor of the constituent sum patterns).

$g(\bar{r})$ = ratio of the amplitude of the maximum far-electric-field to the far-electric-field at the given direction $\bar{r}$, i.e., the inverse of the normalized far-field pattern. ($g(\bar{r}) = 1$ for the center of the main beam, or beams if a difference pattern.)

(If desired, upper and lower limits for the errors in the gain function, sidelobe level, polarization ratio, and beamwidth may be found by combining eq. (100) with eqs. (2)-(5) and the far-field pattern.)

The value of the factor

$$\left(\frac{\lambda}{L^{ave}}\right)^{3/2} \frac{\alpha\ 10^{\frac{-\chi^{ave}}{20}}}{\pi}$$

for a typical microwave antenna and scan area is on the order of .001; in which case eq. (100) becomes

$$.001\ \varepsilon^{mr} g(\bar{r}) \leq \eta(\bar{r}) \leq \varepsilon^{mr} g(\bar{r}). \qquad (101)$$

It is clear from eq. (101) that the errors in the far-field produced by multiply reflected fields of a given relative amplitude, i.e. a given ε^{mr}, can span an extremely wide range of values depending on the variation in phase of the multiply reflected fields across the scan area. (For example, if the multiple reflections are down 40 dB ($\varepsilon^{mr} = .01$), eqs. (101) and (2c) show that the multiple reflection error in the on-axis gain of the main beam lies between about ± .0001 and ± .1 dB.) Essentially, the right side of eq. (101) gives the far-field errors when the effective phase of the multiply reflected fields is uniform, and the left side when the phase varies an average of 360° every wavelength across the scan area. Because of the extremely large range in the possible value of η, it appears unlikely that a precise value of the far-field errors produced by the multiple reflections can be obtained by any method other than direct measurement. As was mentioned at the beginning of this section, data could be taken on a number of parallel scan planes separated by about $\lambda/4$, and the far-fields computed for each plane. Any differences noted in the computed far-fields for the separate scan planes would be caused primarily by the multiple reflections. In addition, it appears likely that the effect of multiple reflections could be reduced appreciably by averaging the far-fields obtained from a number of different scan planes separated by a small fraction of a wavelength over a distance of one wavelength.

Finally, we shall evaluate the far-field errors for multiply reflected fields which are described by a class of hypothetical

near-field distributions. In particular, assume that the fields are linearly polarized and that ϕ_x^{mr} in eq. (86) has the functional dependence,

$$\phi_x^{mr} = 2\pi\left(\frac{x}{\lambda_1} + \frac{y}{\lambda_2}\right), \tag{102}$$

where λ_1 and λ_2 are arbitrary real constants. Also, assume that the test antenna has a circular aperture of radius "a" and uniform amplitude distribution. Then for scans in the very near-field, ΔA_x^{mr} in eq. (86) can be approximated by a constant (ΔE_o^{mr}) inside the aperture area and zero outside. Under these conditions, the integral (85b) may be written in polar coordinates as

$$I = \Delta E_o^{mr} \int_0^{2\pi}\int_0^{a} e^{\frac{i2\pi p}{\lambda}\left[\frac{\lambda}{\lambda_1}\cos\theta_p + \frac{\lambda}{\lambda_2}\sin\phi_p - \sin\theta\cos(\phi_p-\phi)\right]} p\,dp\,d\phi_p. \tag{103}$$

The ϕ_p integration can be performed after writing the bracketed expression in the exponential of eq. (103) in the form

$$\frac{\lambda}{\lambda_1}\cos\phi_p + \frac{\lambda}{\lambda_2}\sin\phi_p - \sin\theta\cos(\phi_p-\phi) = B\cos(\phi_p-b). \tag{104}$$

where

$$B = \sqrt{(\lambda/\lambda_1 - \sin\theta\cos\phi)^2 + (\lambda/\lambda_2 - \sin\theta\sin\phi)^2} \tag{105a}$$

and

$$b = \tan^{-1}\left(\frac{\frac{\lambda}{\lambda_2} - \sin\theta\,\sin\phi}{\frac{\lambda}{\lambda_1} - \sin\theta\,\cos\phi}\right). \tag{105b}$$

Using the integral representation of the Bessel function,

$$J_o(z) = \frac{1}{2\pi}\int_0^{2\pi} e^{iz\cos\psi}\,d\psi,$$

eq. (103) reduces to

$$I = 2\pi\Delta E_o^{mr}\int_0^{a} J_o\left(\frac{2\pi pB}{\lambda}\right)p\,dp, \tag{106}$$

and eq. (106) becomes

$$I = \lambda a \Delta E_o^{mr} \frac{J_1\left(\frac{2\pi aB}{\lambda}\right)}{B}. \tag{107}$$

By combining eqs. (107), (85), and (1), the fractional error η in the far-field takes the form

$$\eta(\bar{r}) = \frac{a\Delta E_o^{mr}\left|J_1\left(\frac{2\pi aB}{\lambda}\right)\right|}{Br\left|E(\bar{r})\right|_{r\to\infty}}. \tag{108}$$

For a circular aperture with uniform amplitude distribution E_o, eq. (10) can be integrated to yield the far-field,

$$\left|E(\bar{r})\right|_{r\to\infty} = E_o \frac{a}{r}(\cos^2\theta+\sin^2\theta\cos^2\phi)\frac{\left|J_1\left(\frac{2\pi a}{\lambda}\sin\theta\right)\right|}{\cos\theta}. \tag{109}$$

The definition of $\eta(\bar{r})$ loses significance when its value becomes larger than 1, i.e. when the far-field amplitude $\left|E(\bar{r})\right|_{r\to\infty}$ becomes less than the amplitude of the far-field error. To avoid this situation, $J_1(\frac{2\pi a}{\lambda}\sin\theta)$ in eq. (109) can be approximated by its envelope,

$$\left|J_1(z)\right| \simeq J_1^e(z) \equiv \begin{cases} (\frac{1}{2}z - \frac{1}{8}z^2) & z < 2 \\ \sqrt{\frac{2}{\pi z}} & z > 2. \end{cases} \tag{110}$$

Substitution of eq. (110) into eq. (109) and the result into eq. (108) transforms the expression for η into

$$\eta(\bar{r}) = \frac{\varepsilon^{mr}\sin\theta\left|J_1\left(\frac{2\pi aB}{\lambda}\right)\right|}{B(\cos^2\theta+\sin^2\theta\cos^2\phi)\,J_1^e\left(\frac{2\pi a}{\lambda}\sin\theta\right)}. \tag{111}$$

$$(\varepsilon^{mr} = \Delta E_o^{mr}/E_o)$$

If λ_1 and λ_2 (see eq. (102)) are chosen such that $\lambda_1 = \lambda_2 = \lambda_0$, and ϕ is set equal to zero, B can be written from eq. (105a) as

$$B = \sqrt{2\frac{\lambda}{\lambda_o}\left(\frac{\lambda}{\lambda_o} - \sin\theta\right) + \sin^2\theta},$$

and η becomes

$$\eta(\theta) = \frac{\varepsilon^{mr}\sin\theta\left|J_1\left(\frac{2\pi a}{\lambda}\sqrt{2\frac{\lambda}{\lambda_o}\left(\frac{\lambda}{\lambda_o}-\sin\theta\right)+\sin^2\theta}\right)\right|}{\sqrt{2\frac{\lambda}{\lambda_o}\left(\frac{\lambda}{\lambda_o}-\sin\theta\right)+\sin^2\theta}\; J_1^e\left(\frac{2\pi a}{\lambda}\sin\theta\right)}. \qquad (112)$$

We can compare this result with the previous maximum and "minimum" values estimated for η in eq. (100) when $g(\bar{r}) = \alpha = 1$, and $X^{ave} = 0$. For $\lambda_o = \infty$ (uniform phase for the multiply reflected fields) eq. (112) should equal the right side of eq. (100). For $\lambda_o = \lambda$ eq. (112) should be of the same order of magnitude as the left side of eq. (100). Indeed, when $\lambda_o = \infty$, eq. (112) becomes ε^{mr} (the right side of eq. (100)), and when $\lambda_o = \lambda$ it reduces to approximately $.06\,(\lambda/a)^{3/2}$, which is nearly equal to the left side of eq. (100) since $A = \pi a^2$ was taken as $.5(L^{ave})^2$ in eq. (100). This agreement between eqs. (112) and (110) supports the validity of both expressions.

Equation (112) reveals that the on-axis far-field error $\eta(o)$ can be expressed in the especially simple form,

$$\eta(o) = \varepsilon^{mr}\left|J_1\left(\frac{2\sqrt{2}\pi a}{\lambda_o}\right)\right| \Big/ \frac{\sqrt{2}\pi a}{\lambda_o}. \qquad (113)$$

Figure 14 shows the on-axis error $\eta(o)$ plotted against the variable $\sqrt{2}\pi a/\lambda_o$. Note that for $\lambda_o < 2a$, $\eta(o)$ is given approximately by

$$.06\left(\frac{\lambda_o}{a}\right)^{3/2}\left|\cos\left(8.9\,\frac{a}{\lambda_o} - \frac{3}{4}\,\pi\right)\right|\varepsilon^{mr},$$

and never gets larger than about $.1\ \varepsilon^{mr}$. That is, if the phase of the multiply reflected fields changes 360° or more across the diameter of the aperture area, the error in the on-axis far-electric-field is less than one-tenth ε^{mr}, where ε^{mr} is the ratio of the amplitude of the multiply reflected electric field (probe output) to the total electric field (probe output) as the probe traverses the effective scan area. Only when the phase of the multiply reflected fields is uniform ($\lambda_o = \infty$) across the scan area does the on-axis far-field error equal ε^{mr}.

In figure 15, $\eta(\theta)$ is plotted for different values of a/λ_o from eq. (112) for $a/\lambda = 12$. When λ_o is greater than a couple of aperture

diameters, the envelope of the errors from multiple reflections are on the order of ε^{mr} throughout the far-field. As λ_o becomes less than a couple of diameters, the near-axis errors grow much smaller than ε^{mr} but the envelope of errors in the far sidelobes remains at about ε^{mr}. Finally, when λ_o gets as small as the free-space wavelength λ, the far-field errors are much smaller than ε^{mr} all the way to $\theta = 30°$ in the far-field.

IV. Summary

The far-field characteristics of a radiating test antenna can be determined throughout the forward hemisphere by scanning on a near-field plane of the test antenna with a probe antenna of arbitrary but known receiving characteristics. The amplitude and phase of the probe output are recorded on the near-field scan plane and the far-field pattern is computed by "deconvolving" the near-field data. The accuracy of the computed far-field depends upon the size of the scan area, the accuracy with which the scanner positions the probe, the accuracy with which the instrumentation measures the amplitude and phase of the probe output, the extent of the multiple reflections, the computation errors involved with deconvoluting the near-field data, and, of course, the accuracy with which the probe is calibrated and the input power to the test antenna is measured. Essentially, this report derives upper bound expressions for the errors in the far-field pattern produced by these sources of error in the near-field measurements. The upper-bound expressions are written in a form that can be used to stipulate design criteria for the construction of near-field scanning facilities. In particular, the limits of accuracy in a given far-field parameter are expressed in terms of the measured near-field data and/or the computed far-field, the frequency and dimensions of the antenna-probe system, the systematic and random variation in the positioning of the scanner, and the precision of the instrumentation which measures the probe output. In order to simplify the mathematics, the probe was usually assumed to be an electric dipole, although the resulting upper bound expressions hold for arbitrary probes.

The analysis and resulting upper-bound expressions are not restricted to a particular antenna as previous computer studies [11,16] and direct far-field comparisons have been, but apply generally to electrically large aperture antennas which can be operating in either a sum or difference pattern. The results for position and instrumentation errors apply only to nonscanning antennas in the sense that the analysis for these two sources of error assumed that the scan plane lay perpendicular or nearly perpendicular to the boresight direction of the antenna pattern. Position and instrumentation errors for beams which are steered away from the perpendicular to the scan plane will be included in a subsequent report by Newell [21]. Except for the position and instrumentation errors, however, the results of the present report, and in particular the error expressions pertaining to the truncation of the scan plane, apply to arbitrarily steered antennas.

Broadbeam antennas where the wavelength is on the same order of magnitude as the dimensions of the aperture are not examined in this report. But it is shown in a report by Crawford et al. [20] that many of the conclusions and upper bound expressions derived here apply directly or in slightly modified form to broadbeam antennas.

It is emphasized that the upper-bound expressions derived in this report determine the limits of accuracy of the far-field computed from the planar near-field scanning technique without resorting to comparisons with direct far-field measurements. This is probably the foremost purpose of the report along with the report acting as an aid in deciding design criteria and tolerances for the construction of new near-field scanning facilities. It has been the feeling of those involved with near-field measurement techniques at the NBS that often the near-field techniques determine the far-field more accurately than conventional far-field measurements with a standard antenna. Thus comparison with measurements made on conventional far-field ranges would not be a reliable method, even if it were feasible, for estimating the accuracy of the near-field techniques, which do not have the problems of proximity corrections, ground reflections, or the need of a standard far-field antenna. A brief summary of the major conclusions and results of the report follows:

Errors in computation can be ignored immediately. A simple exercise in Section I showed that their effect on the far-field is extremely small compared to the effects of the other sources of error. Far-field errors from the approximation involved in applying the sampling theorem are also negligible (see footnote 1).

In Section II it was demonstrated that errors in various far-field parameters could be expressed conveniently in terms of the fractional far-electric-field error ($\eta = |\Delta\bar{E}|/|\bar{E}|_{r\to\infty}$) and the approximate far-field pattern. In particular, the errors in gain function, sidelobe level, polarization ratio, and beamwidth were expressed in terms of η (see eqs. (1)-(5)).

In Section III.A the far-field errors associated with neglecting the near-fields outside the finite scan area were investigated. First it was shown analytically that no reliable information about the far-field pattern could be obtained by the planar near-field scan method outside the "solid angle" formed by the edge of the antenna aperture and the boundary of the scan area. Well within this solid angle ($\theta \lesssim \frac{1}{2}\theta_{max}$, see eq. (33) and following), reasonable upper bound expressions for the finite scan errors were found that could be applied to center-line data (eq. (32)) as well as full-scan data (eq. (36) or (32)). As part of the finite scan analysis, asymptotic expres sions for the near-fields in front of a circular antenna of uniform aperture distribution were derived in Appendix A and plotted in figures A3 and A4. A comparison was made between the empirical analysis of finite scan errors performed by Newell and Crawford [11] with centerline data and the maximum errors calculated from the upper bound expression (32). Agreement is quite reasonable, as figures 8a and 8b indicate. Table 1 shows the finite scan error for various far-field parameters of a typical X-band antenna. The finite scan errors are proportional to wavelength, so changing the wavelength while holding the other antenna dimensions the same merely changes the values in Table 1 proportionately. Of course, such an isolated change is rather unrealistic.

Deviations in the position of the probe from its assumed position in the scan area will produce errors in the near-field data which show up as errors in the computed far-field pattern. Section

III.B.1 derives an upper bound expression throughout the forward hemisphere for the far-field errors produced by both systematic and random errors in the positioning of the probe (see eqs. (61), (64), (68) and figures 10, 11, and 12). (Of course, a uniform displacement of the scanner does not alter the far-field pattern, and a uniform rotation of the scanner simply rotates the entire far-field pattern through the same angle.) The contribution from the inaccuracies in the position of the scanner divides naturally into a transverse or xy (parallel to the scan area) and longitudinal or z (perpendicular to the scan area) part.

For sum patterns, the on-axis far-field errors were found proportional to the xy-displacement errors of the scanner but proportional to the square of the z-displacement errors (normalized to wavelength). This latter result is analogous to that obtained by Ruze [15] in his classical work on "antenna tolerance theory" for a small arbitrary phase error or aberration in the surface of an antenna. This result does <u>not</u> imply that the z-displacement errors generally have a much smaller effect on the main beam than the xy errors, because the multiplying factor is, in general, much larger for the z term. It does imply, however, that random and systematic displacement errors in the longitudinal or z direction weigh equally in their contribution to errors near the center of the main beam of sum far-field patterns. Unlike the z errors, random errors in the transverse or xy-displacement of the scanner have a negligible effect throughout the far-field compared to systematic transverse errors of the same order of magnitude, and the xy-position errors do not depend on wavelength. The xy-position errors also differ from the z-position errors in that the same xy error expression applies throughout the far-field hemisphere whereas the z errors are given by one expression close to the main beam, i.e., near the boresight direction, and another expression for the errors off-axis. Specifically, the maximum possible off-axis (or sidelobe) z-position errors depend linearly upon the systematic z-displacement errors of the scanner and are much larger than the on-axis errors, which are proportional to the square of the z-displacement errors. In fact, as Tables 2 and 4 indicate, these off-axis errors caused by displacements in the

z-position of the scanner can be much larger than the total off-axis errors from all other sources combined. The present report does not examine in detail the relationship between the distribution of z-displacement errors and the off-axis or sidelobe errors, but such an analysis will be included as part of the subsequent report by Newell [21].

For difference patterns, the effect of the near-field displacement errors on the far-field were given by the same upper-bound expressions derived for sum patterns, except for the effect of z-displacement errors on the null depth. This error in null depth for difference patterns was shown in Appendix B to be independent of the value of the null depth itself and proportional to the z-displacement errors, but, in general, proportional by a very small proportionality constant. In fact, for most antennas and reasonably accurate scanning systems, the z-displacement errors do not affect the null depth by more than a few tenths of a dB. This rather surprising result, which is rather difficult to explain without going through the mathematics of Appendix B, has been confirmed by an empirical error analysis performed by Newell [21] on the measured near-field data of a number of antennas operating in the difference mode. Although the z-displacement errors do not have a strong influence on the depth of the null of difference patterns, eq. (68), which was also derived in Appendix B, shows that they do have a strong influence on the direction of this null. In fact, the effect of all other sources of errors combined on the null direction of difference patterns is generally negligible compared to the effect of z-position errors, although instrumentation phase errors can sometimes shift the null an appreciable amount as well.

Table 2 shows the xy- and z-position error in various far-field parameters for a typical X-band and K-band antenna. Again, note the strong influence that z-position or phase errors can have on the off-axis far-field parameters (sidelobe level, beamwidth, mainlobes of difference patterns) and on the null shift of the difference pattern. Note also that the maximum possible null shift caused by z-position errors is independent of frequency.

The far-field errors caused by the inaccuracies of the receivers in measuring the phase and amplitude of the probe output are estimated in Section III.B.2 (see eqs. (82), (83) and figures 11-13). (It should be mentioned that instrumentation errors associated with converting analog to digital information is assumed negligible.) As would be expected, the instrumentation errors in measuring phase contribute to the far-field errors in exactly the same way as longitudinal or z-position errors of the scanner. However, since the errors which a typical receiver introduces into the phase are small and increase monotonically with decreasing amplitude of the probe output, calculations show that their effect is often negligible throughout the far-field.

Although typical instrumentation errors in measuring phase are small and often introduce insignificant errors into the far-field, typical instrumentation errors in measuring amplitude can have a pronounced effect on the far-field (see figure 13), except for the far sidelobe region and in the null depth of difference patterns. In general, if high accuracy is desired, the receiving system which measures the amplitude of the probe output should be calibrated and the calibration curves included as part of the computer program which deconvolutes the near-field data to get the far-field. It is significant, however, that the instrumentation errors in measuring near-field amplitude have a relatively small affect on the null depth of difference patterns, as eq. (82) and Table 3 demonstrate. The reason for this is that the receiver distorts the opposite lobes of the near-field amplitude by approximately the same amount (see Appendix B). Table 3 also displays the amplitude error in various other far-field parameters for a typical microwave antenna. The instrumentation amplitude errors for $\theta < 2\lambda/\ell^{max}$ do not depend directly upon frequency or the size of the test antenna, only upon the taper factor α of the near-field amplitude, the receiver inaccuracy N^I_{dB}, and, except for the null depth of difference patterns, the inverse of the normalized far-field pattern $g(\bar{r})$. It should also be pointed out that the instrumentation amplitude errors in the far sidelobe region, $\theta > 10\lambda/\ell^{max}$, are relatively small, usually less than a few tenths of a dB for N^I_{dB} less than a few thousands of a dB per dB.

Whenever comparisons were possible, the expressions for both position and instrumentation errors (eqs. (61), (64), (68), (82), and (83)) agreed well as an upper-bound with the results of the empirical error analysis of Newell et al. [11,17,21] at the National Bureau of Standards, and with the error analysis performed by Rodrigue et al. [16] at the Georgia Institute of Technology with a hypothetical near-field distribution (see figures 11-13).

In Section III.C upper and "lower" bound expressions were derived for the far-field errors caused by multiple reflections (see eq. (100)). The upper and lower bounds were extremely far apart because the phase of the multiply reflected fields has a strong influence on the far-field errors. Since the phase of the multiply reflected fields for a given test and probe antenna interaction would, in general, be difficult to measure or estimate, it was concluded that the only reliable way to get an accurate estimate of the far-field errors from multiple reflections would be to use the following straightforward but tedious procedure. Take several near-field scans on parallel planes separated by about 1/4 wavelength or less. Any deviations in the far-field patterns computed from the data on the separate scan planes would be caused primarily by the multiple reflections (assuming the scan area is large enough so that changes in finite scan errors are negligible). If necessary, the effect of multiple reflections could probably be reduced appreciably by averaging the amplitude of the far-fields obtained from these different scan planes separated by a small fraction of a wavelength and covering a total change in separation distance of one wavelength In addition to the upper and lower limits of error, the far-field errors were derived for multiply reflected fields which satisfy a certain class of hypothetical near-field distributions (see eq. (112) and figures 14 and 15).

The major analytical results of this error analysis study can be combined into one long upper-bound expression for the fractional far-electric-field error $\eta(\theta,\phi)$. (θ and ϕ specify the angular spherical coordinates of the far-field pattern.)

$$\eta(\theta,\phi) \leq \left[\frac{\alpha\lambda L^{max} 10^{\frac{-X}{20}}}{A \sin\theta_{max}} + \frac{\alpha\lambda\Delta^{s}_{max}}{2\ell^{max}} + \eta'_z + 2N^{I}_{dB}(\beta^{I}) + 2\boxed{\varepsilon^{mr}}\right] \frac{g(\theta,\phi)}{2}$$

$$+ \eta_{probe}(\theta,\phi) + \eta_{input}. \qquad (114a)$$

$$\theta_{shift} = \begin{matrix}\text{null shift of} \\ \text{difference pattern}\end{matrix} \leq \frac{2\lambda}{\pi\ell^{max}} \left(\delta^{s}_{max}+\Delta\phi^{I}_{max}\right) \text{radians} \qquad (114b)$$

$$\eta'_z = \begin{cases} (\delta^{s}_{max}+\Delta\phi^{I}_{max})^2 + (\delta^{rn}_{max})^2 & \text{(sum patterns)} \\ 8\Delta F(\delta^{s}_{max}+\Delta\phi^{I}_{max}) & \text{(difference patterns)} \\ \delta^{s}_{max} & \text{(sum and difference patterns)} \end{cases} \quad \theta < \frac{\lambda}{10\ell^{max}}, \quad \frac{\lambda}{10\ell^{max}} < \theta < \frac{\pi}{2}$$

$$\beta^{I} = \begin{cases} (\alpha-1) & \text{(sum patterns)} \\ 2/g(\theta,\phi) & \text{(difference patterns)} \\ (\alpha-1)/2 & \text{(sum and difference patterns)} \\ \frac{\alpha\lambda L^{max}}{3A} & \end{cases} \quad \theta < \frac{\lambda}{10\ell^{max}}, \quad \frac{\lambda}{10\ell^{max}} < \theta < \frac{2\lambda}{\ell^{max}}, \quad \frac{10\lambda}{\ell^{max}} < \theta < \frac{\pi}{2}$$

Equations (114) represent essentially an amalgamation of eqs. (32), (64), (68), (82), (83) and (100), under the extreme condition that the various near-field errors combine in such a way as to create the maximum possible far-field errors. If desired, the tighter upper-bound, eq. (36), for the finite scan error could be used for the first term in eq. (114a) instead of eq. (32). Recall from Section III.A.3 that the finite scan error term represents a valid upper-bound halfway or more within the "solid angle" formed by the edges of the aperture and the boundary of the scan area ($\theta \leq \frac{1}{2}\theta_{max} = \frac{1}{2}(90-\gamma_{max})$; and outside this solid angle region the planar near-field scanning technique cannot be relied upon with any confidence to yield accurate far-fields. The instrumentation amplitude factor β^{I} is not given explicitly by eqs. (114) in the region between θ equal to $2\lambda/\ell^{max}$ and $10\lambda/\ell^{max}$. However β^{I} can be estimated in this region by connecting a straight line from its value at $2\lambda/\ell^{max}$ to its value at $10\lambda/\ell^{max}$. The detailed derivation of each of the terms in eq. (114), except

η_{probe} and η_{input}, can be found in the part of the main text from which each particular term came. The extra terms η_{probe} and η_{input} will be explained below. The definition of the various parameters in eqs. (114) can also be found from the preceeding main text:

λ = wavelength.

A = area of the antenna aperture.

ℓ^{max} = maximum width of the antenna aperture.

L^{max} = maximum width of the scan area.

γ_{max} = maximum acute angle between the plane of the scan area and any line connecting the edges of the aperture and scan area ($\theta_{max} = 90-\gamma_{max}$).

X = the largest amplitude of the probe output at the edge of the scan area, measured in dB down from the maximum amplitude of probe output in the scan plane.

α = a "taper" factor--equal to a minimum of 1.0 (for apertures of uniform amplitude and phase) and less than 5 for most tapered distributions found in practice. (See eq. (31) for the precise definition of α; for a difference pattern one should still use the taper factor of the constituent sum patterns.)

$\Delta_{max} = 2\pi\Delta P_{max}/\lambda$, where ΔP_{max} is the maximum amplitude of the transverse (xy) displacement errors within the effective scan area A_o. (A_o is that part of the scan area over which the phase is fairly uniform. For near-field scans parallel to the aperture $A_o \simeq A$.)

$\delta_{max} = 2\pi\Delta z_{max}/\lambda$, where Δz_{max} is the maximum amplitude of the longitudinal (z) displacement errors within the effective scan area A_o.

$\Delta\phi^{I}_{max}$ = the maximum instrumentation errors (expressed in radians) involved in measuring the phase of the probe output on the effective scan area A_o (see footnotes 10 and 13).

ΔF = fractional difference between the amplitude of the two main far-field lobes of the difference pattern (see Appendix B).

N^{I}_{dB} = the maximum instrumentation errors involved in measuring the amplitude of the probe output--N^{I}_{dB} is expressed in dB error per dB amplitude down from the maximum amplitude

on the scan area. (The amplitude error is designated as zero at the maximum amplitude; see footnote 11.)

ε^{mr} = the average ratio of the amplitude of the multiply reflected probe output to the amplitude of the total probe output as the probe traverses the scan area. (Its value can be estimated experimentally by changing the distance between the probe and test antenna at various locations within the scan area, and calculating one-half the fractional peak to peak height of the variations in amplitude which repeat about every $\lambda/2$.)

$g(\theta,\phi)$= the ratio of the amplitude of the maximum far-electric field to the far-electric-field at the given direction (θ,ϕ), i.e., the inverse of the normalized far-field pattern. ($g(\theta,\phi) = 1$ for the center of the main beam, or beams if a difference pattern.)

The superscripts "s" and "rn" refer to the "systematic" and "random" parts of the displacement errors respectively. The instrumentation phase and amplitude errors ($\Delta\phi^{I}_{max}$, N^{I}_{dB}) are assumed systematic in nature. The phase error $\Delta\phi^{I}_{max}$ does not show up in η'_z for $\theta > \lambda/(10\ell^{max})$ because, as explained in Section III.B.2, the shape of the near-field instrumentation phase error is such that it has negligible effect in this off-axis region compared to the maximum effect of typical systematic z-position errors δ^{s}_{max}. Random position errors have non-negligible effect only near the boresight direction of sum patterns.

The multiple reflection ratio ε^{mr} is enclosed in a box in eq. (114a) to emphasize that for most antennas it represents an unrealistically large upper bound.

The error $\eta_{probe}(\theta,\phi)$ simply represents the uncertainty in the receiving characteristics of the probe in the direction corresponding to (θ,ϕ). For example, if the receiving characteristic S'_{01} of the

probe (see reference [3]) was known to an accuracy of 1% for the direction (θ,ϕ), then η_{probe} would be .01 for that direction.

The error η_{input} arises in normalizing the amplitude of the probe output to the input power or amplitude $|a_o|$ of the input mode to the test antenna. Such a measurement is necessary whenever absolute values of the gain function are required. Probably the simplest and most accurate method of performing this normalization is to connect the input waveguide of the test antenna directly to the output waveguide of the probe through a variable attenuator. If, as explained in Section III.B.2, the receiver which measures the amplitude of the probe output is specified arbitrarily to have zero error when the probe output is at its maximum amplitude on the scan area, then the normalization can be accomplished by measuring the attenuation needed to reduce the amplitude of the direct input from the transmitter to the level of the maximum amplitude of the probe output on the scan area. Of course, "mismatch factors" of any consequence must also be measured. The quantity η_{input} merely denotes the combined fractional error of the variable attenuator and of the devices used to measure the necessary mismatch factors. By using a high precision attenuator, the fractional error η_{input} can usually be kept below a few thousandths.

Table 4 shows the total maximum possible error in a number of far-field parameters for a typical X-band and K-band antenna and a reasonably accurate scanning facility. The table was computed from eqs. (114) for the representative values of the near- and far-field parameters listed above the table. It is emphasized that the values shown in Table 4 are the maximum possible upper-bounds to the far-field errors computed under the extreme condition that each of the sources of near-field error produce its maximum possible change in the far-field and then all these maximum changes in the far-field add in phase. The z-position errors have been separated and underlined when they represent the dominant contribution to the upper-bound errors, because whether or not these maximum possible z-position errors actually occur depends strongly on the far-field direction of interest and on the shape of the deviation in z-position throughout the scan area. As mentioned above, a detailed analysis of this dependence will be included as part of a subsequent report by Newell [21].

The error ($\eta^{dB}_{probe} + \eta^{dB}_{input}$) in the receiving characteristic of the probe and in normalizing to the input power of the test antenna was chosen as .1 dB in Table 4. For the error in on-axis gain of the sum patterns, Table 4 shows that this contribution of .1 dB is about as large as all the other errors combined. The same is true for the gain of the mainlobes of the difference pattern if the z-position part of the errors is ignored. Thus, for the situation described by Table 4, greater accuracy in the calibration of the probe and in the measuring of the input power to the test antenna could be a first step in significantly reducing the errors in the direction of maximum gain.

It is interesting to compare the maximum equivalent reflected signal [24] allowable in a conventional "far-field" range or anechoic chamber to get accuracies comparable to those shown in Table 4 for the near-field scanning technique. It is a simple matter to show that the maximum equivalent reflected signal (ERS) measured in dB down from the direct signal is related to the values of η_{dB} by

$$\text{ERS} = 20 \log \frac{\eta_{dB}}{8.7} \text{ (assuming small } \eta_{dB}).$$

For example, near the boresight direction the ERS would have to be 33 dB down for the sum pattern and 15 dB down for the difference pattern to give the corresponding errors shown in Table 4. Of course, there would also be errors on conventional ranges due to proximity effects, uncertainties in the calibration of the standard antenna, and instrumentation errors.

In conclusion, it can be seen from Tables 1-4 that for a reasonably accurate scanning system no one source of error dominates over all the others in the boresight direction of both sum and difference patterns. However, in the far-field region away from the boresight direction, but well within the solid angle region formed by the edge of the aperture and boundary of the scan area, the deviation in z-position of the scanner can, in principle, cause far-field errors which are much larger than the combined errors of all other sources. In practice, however, these maximum possible errors seldom occur. Moreover, it will be shown in the subsequent report by Newell [21]

that the scanner can be designed and utilized to keep the off-axis, z-position errors far below the upper-bound values given by eqs. (114) and shown in Tables 2 and 4. Of course, beyond the solid ang region formed by the edge of the aperture and boundary of the scan area, it was shown in Section III.A that the far-field computed fro the near-field data cannot be relied upon with any confidence.

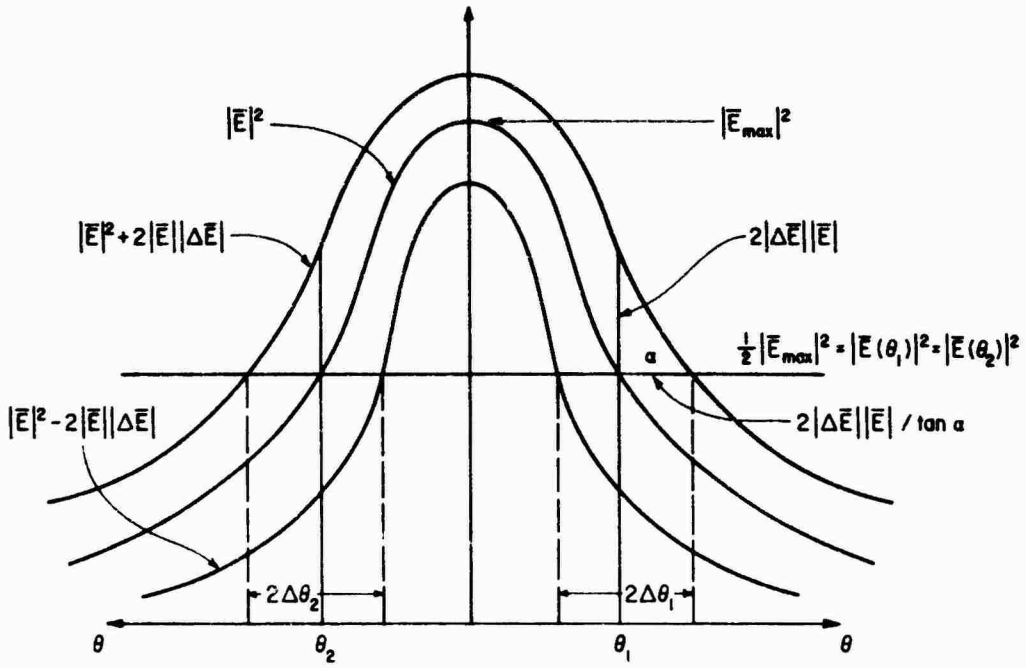

Figure 1. Main beam of a hypothetical test antenna.

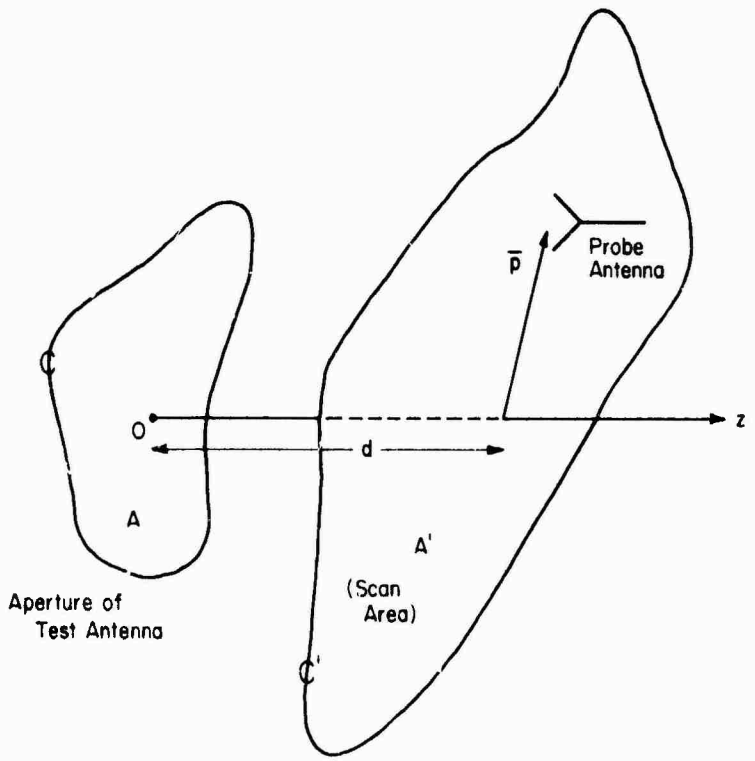

Figure 2. Schematic of scanning geometry.

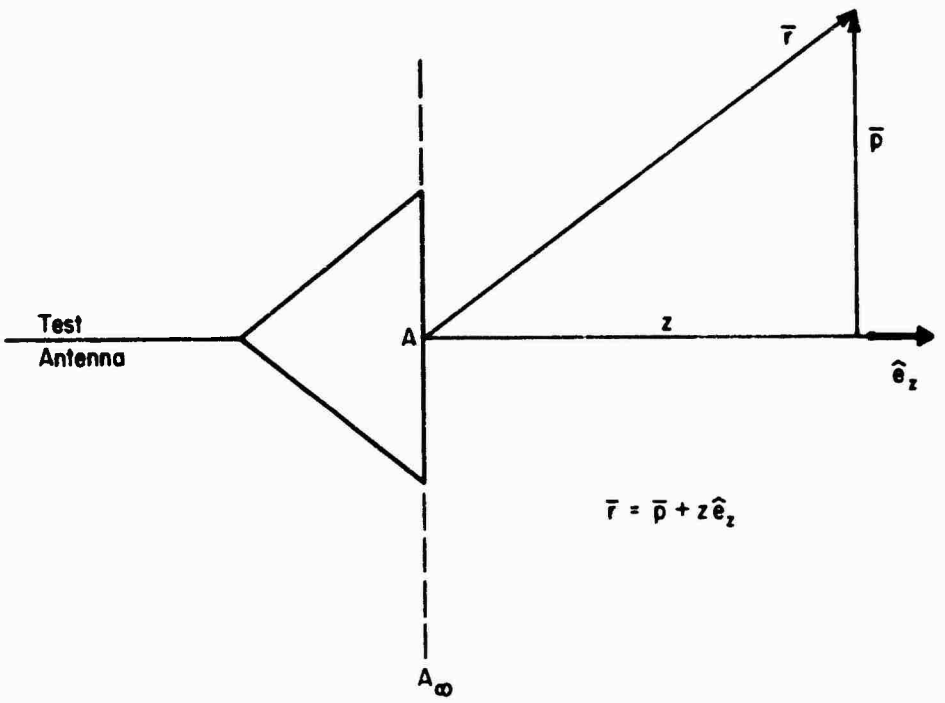

Figure 3. Schematic of aperture antenna.

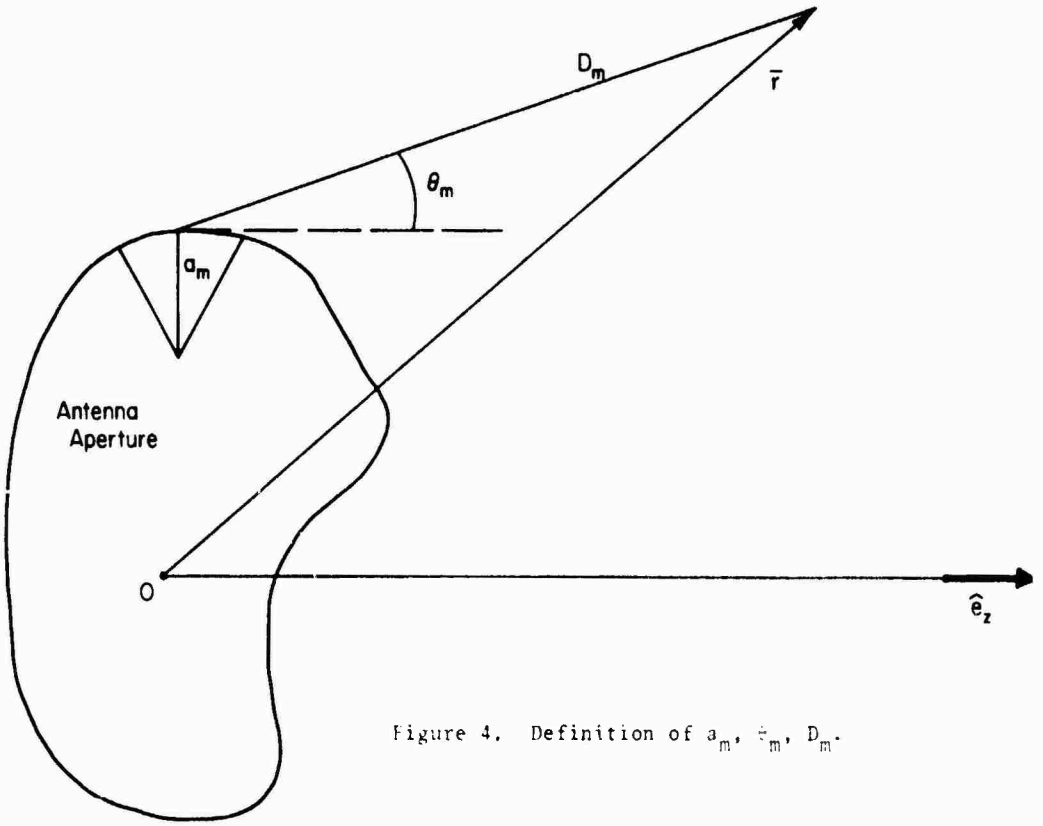

Figure 4. Definition of a_m, θ_m, D_m.

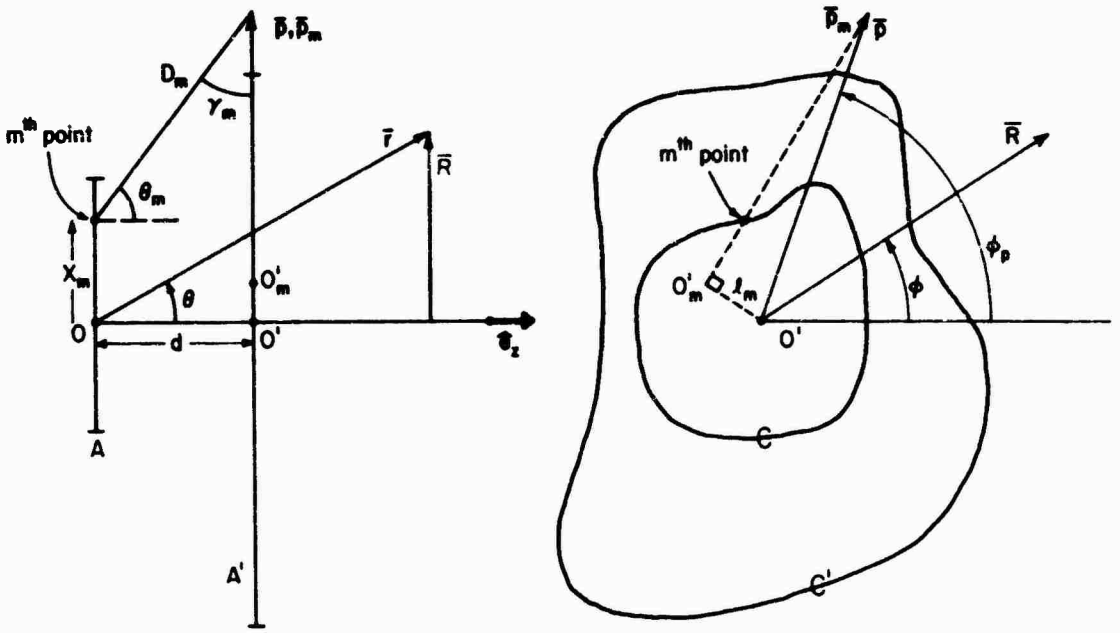

Figure 5. Schematic of aperture and scan areas. (Although A and A' are drawn parallel, it is not a necessary requirement of the theory.)

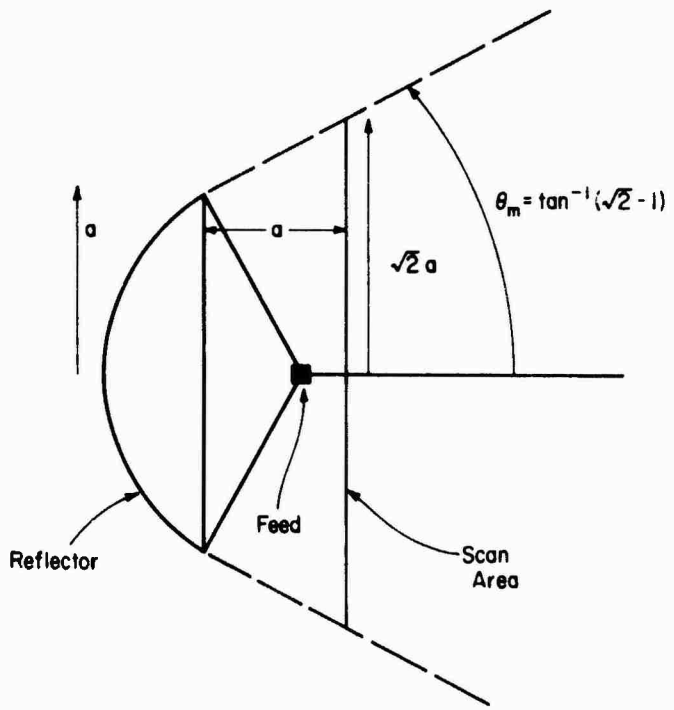

Figure 6. Circular reflector antenna.

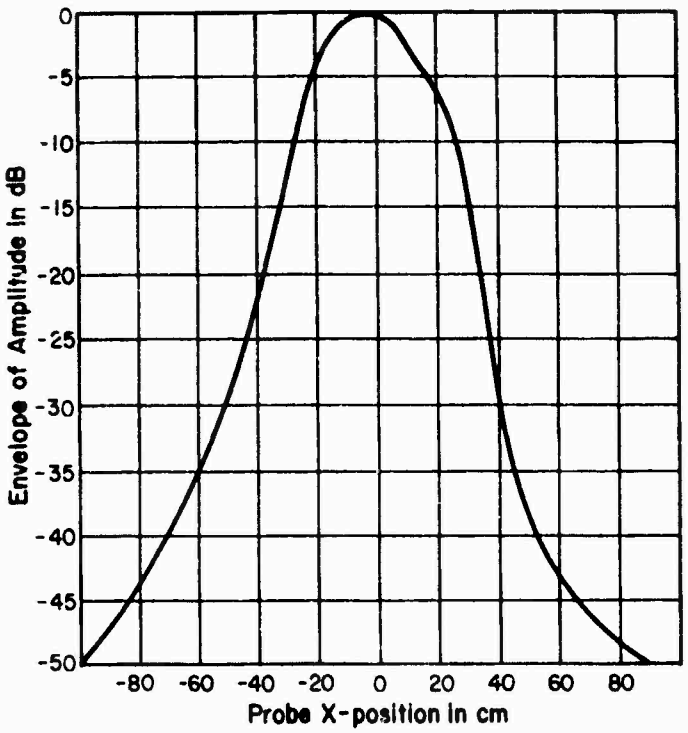

Figure 7a. Near-field centerline data (constrained lens) (z = 25 cm).

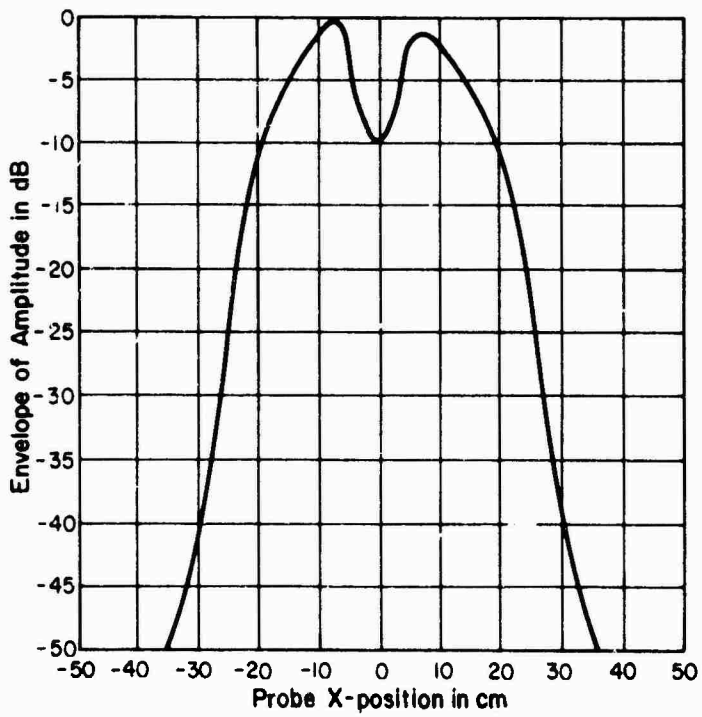

Figure 7b. Near-field centerline data (reflector antenna) (z = 43.18 cm).

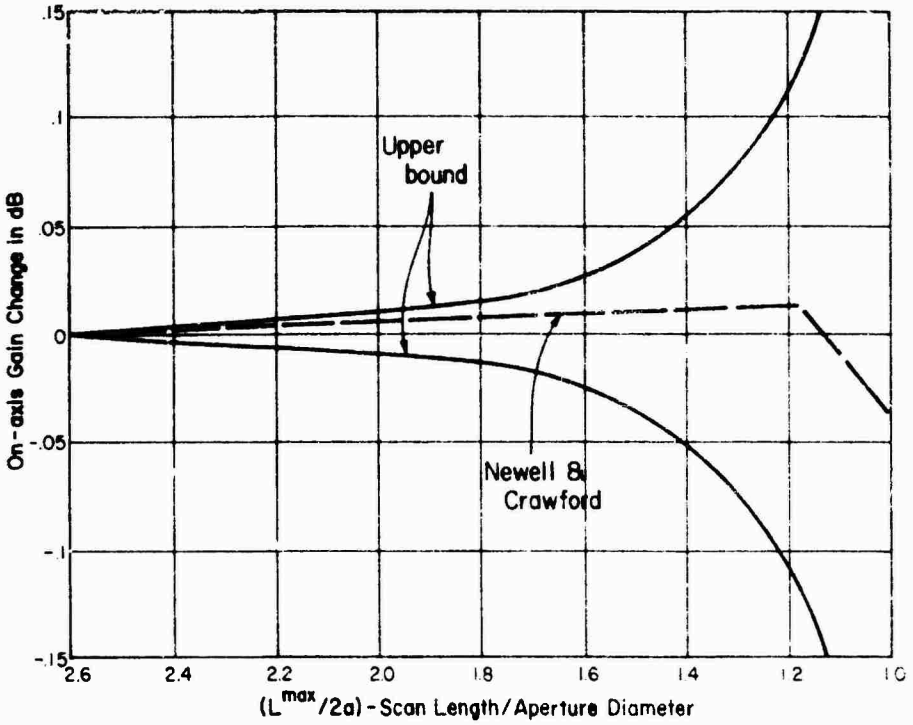

Figure 8a. Change in gain vs. decreasing scan length (constrained lens).

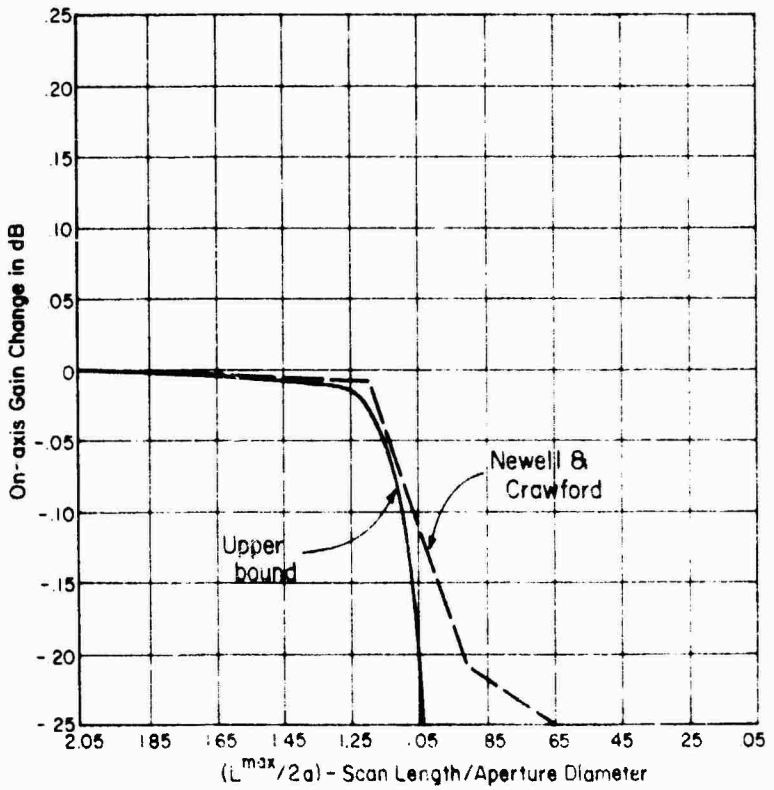

Figure 8b. Change in gain vs. decreasing scan length (reflector antenna).

Figure 9a. Constrained lens sum port near-field log amplitude, f=9.2 GHz, z=25.0 cm, no radome.

Figure 9b. Near-field phase, constrained lens sum port, f = 9.2 GHz, z = 25 cm.

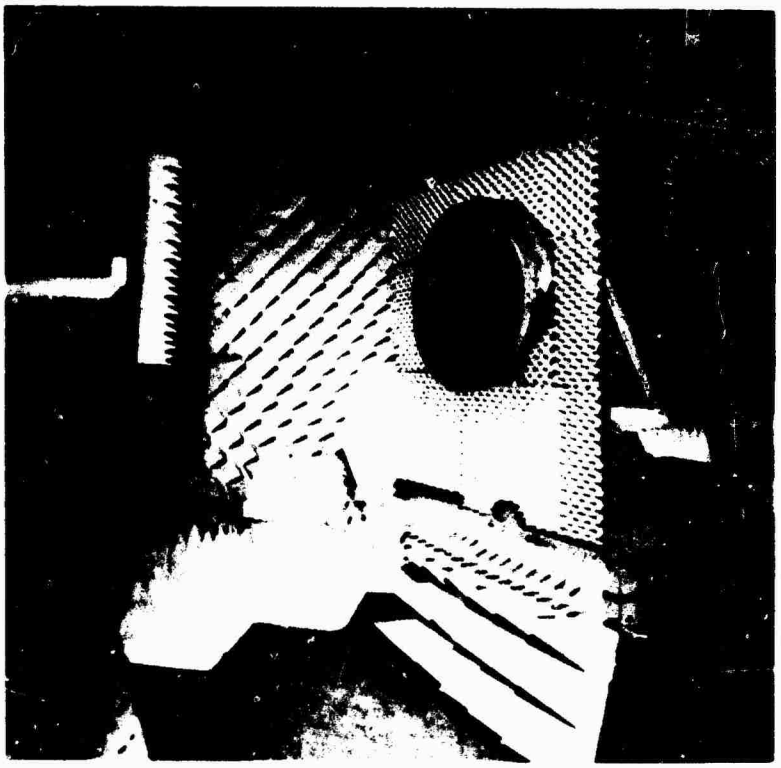

Figure 9c. Constrained lens antenna and probe.

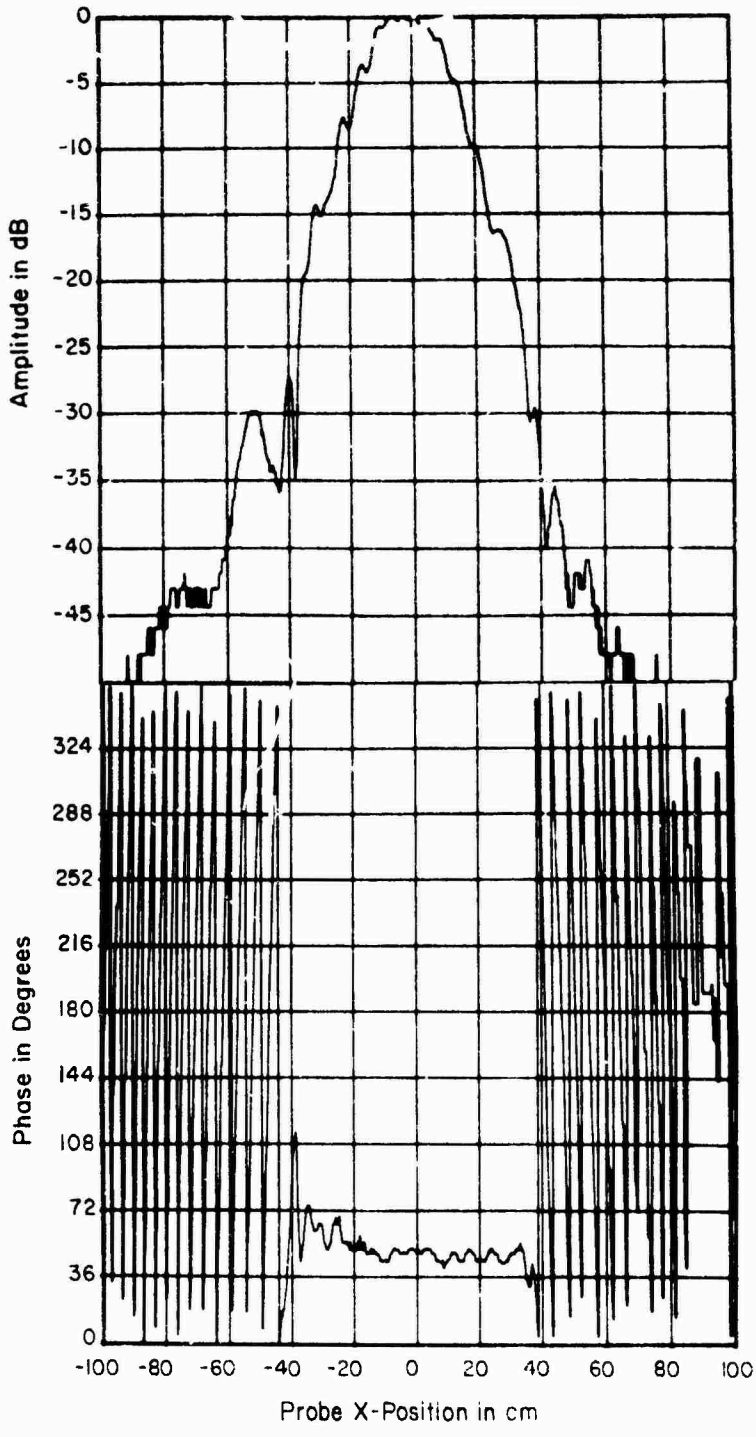

Figure 9d. Near-Field Centerline Data, z = 25 cm.

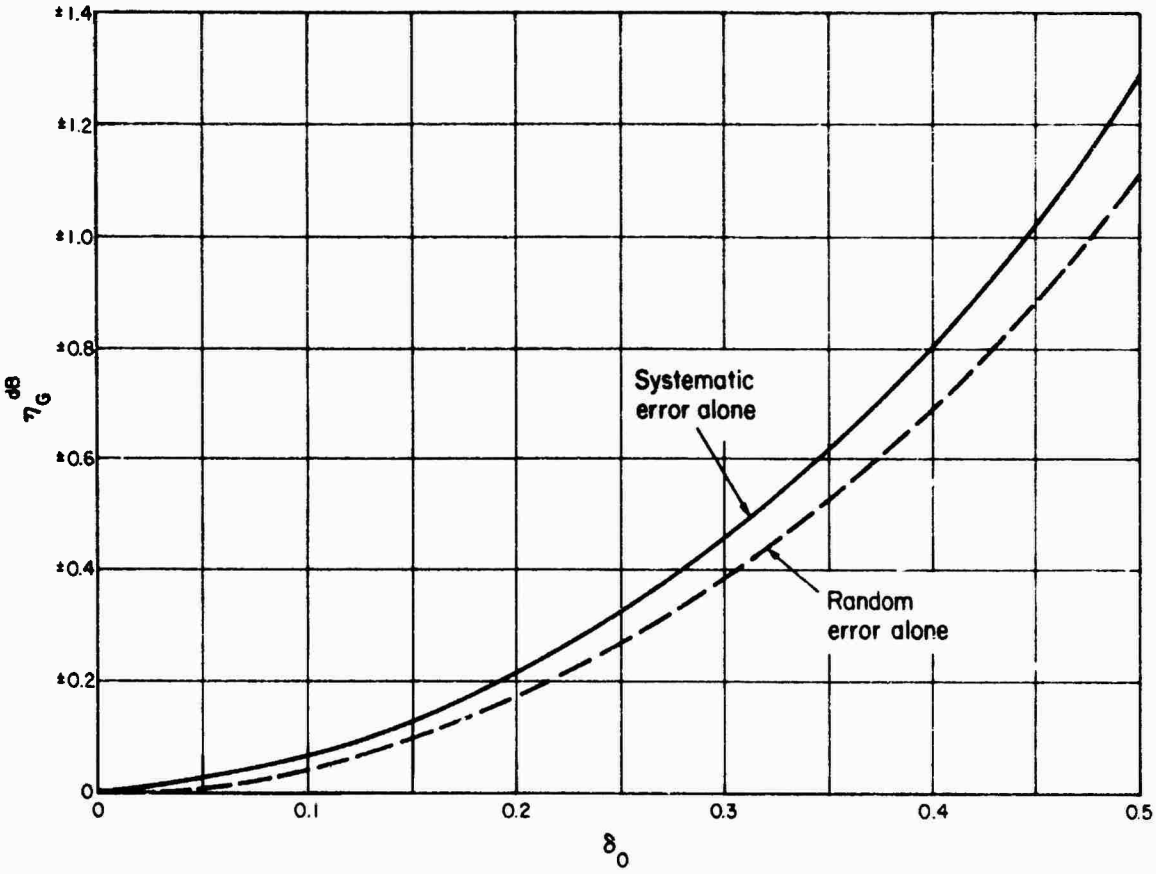

Figure 10. Position errors in on-axis gain.

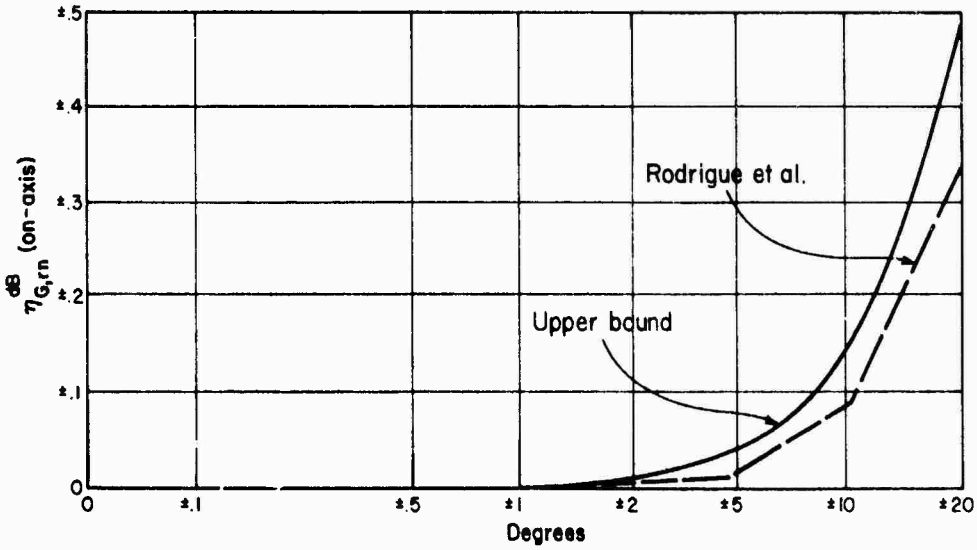

Figure 11. Comparison with Rodrigue et al. for random phase errors.

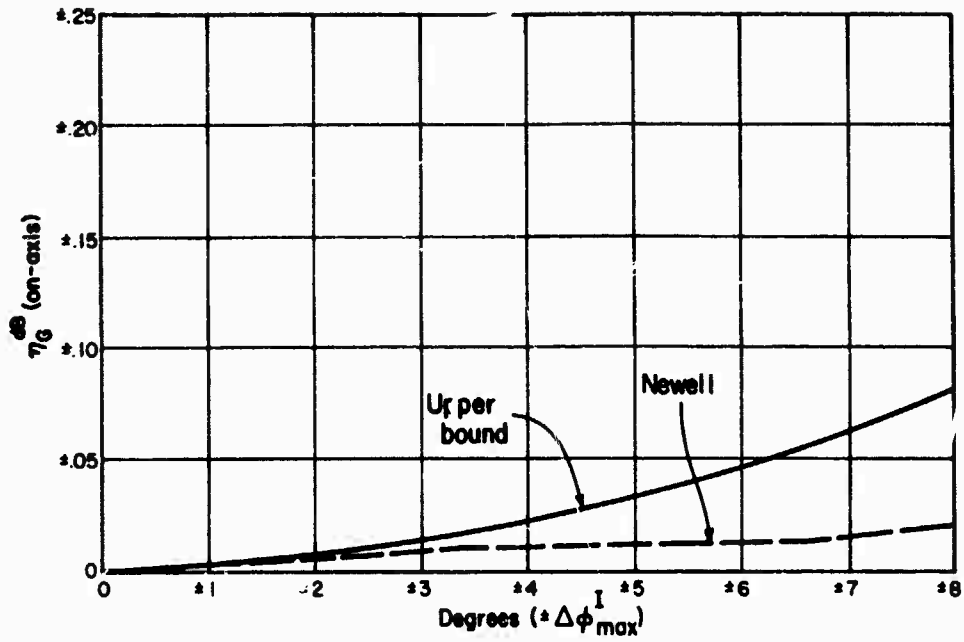

Figure 12. Comparison with Newell for quadratic phase errors.

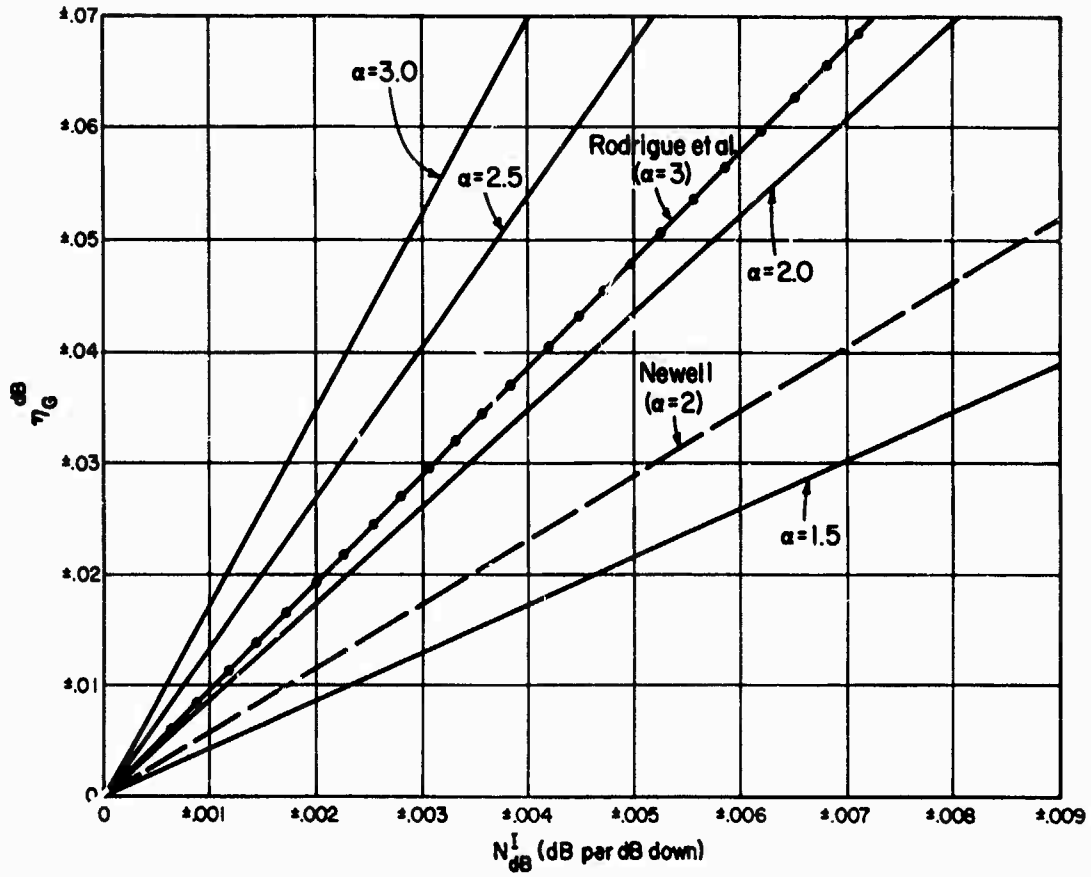

Figure 13. Amplitude errors in on-axis gain.

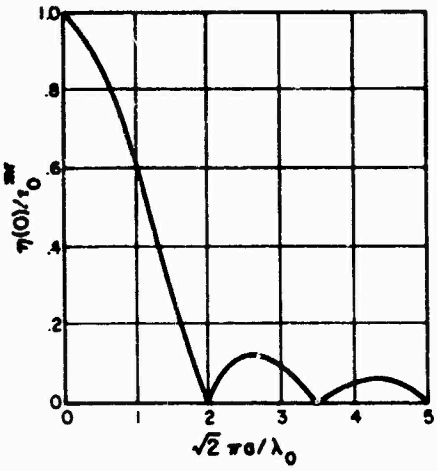

Figure 14. On-axis error in far-field from multiple reflections.

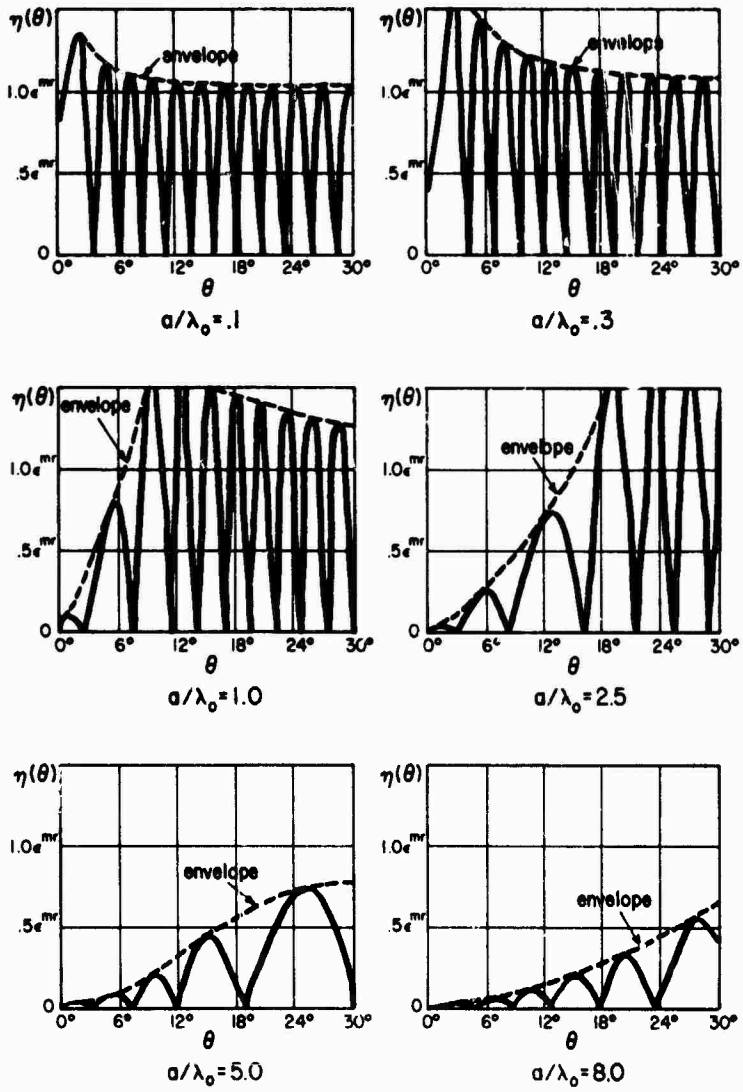

Figure 15. Far-field errors from multiple reflections ($a/\lambda = 12$).

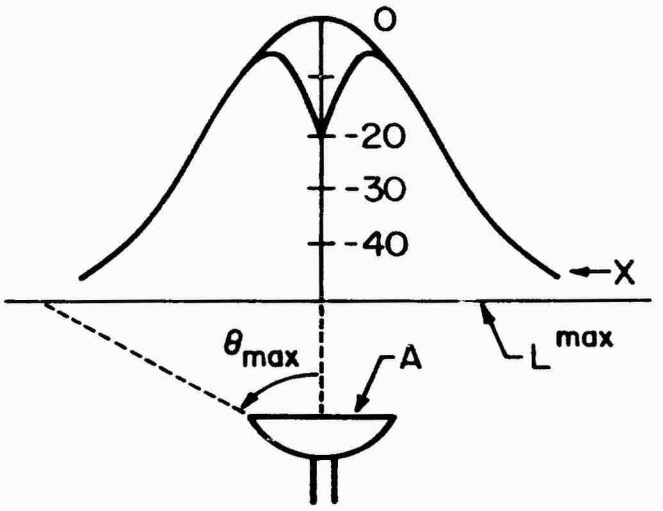

$\alpha = 3$

$\lambda = 3.26$ cm

$L^{max} = 160$ cm

$A = 5000$ cm^2

$\theta_{max} = 60°$

$X = 45$ dB

Sidelobe Level = -25 dB

Null Depth = -30 dB

	Far-Field Parameter	Finite Scan Error
sum pattern	On-Axis Gain	± .01 dB
	Sidelobe Level	± .16 dB
	Beamwidth ϕ_o	± .002 ϕ_o
	On-Axis Polarization Ratio	± .001
difference pattern	Null Depth	± .28 dB
	Null Shift	Negligible
	Main Lobes	± .01 dB

Table 1. Finite Scan Errors from Centerline Data of a Typical X-Band Antenna.

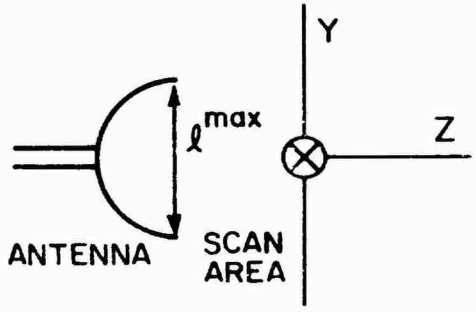

$\alpha = 3$

$\Delta Z_{max} = \Delta P_{max} = .2$ mm

$\ell^{max} = 80$ cm

$\Delta F = .01$

Sidelobe Level = -25 dB

Null Depth = -30 dB

		XY-Position Error		Z-Position (or Phase) Error	
	Far-Field Parameter	λ = 3.26 cm	λ = 1.63 cm	λ = 3.26 cm	λ = 1.63 cm
sum pattern	On-axis gain (dB)	± .01	± .01	± .006	± .026
	Sidelobe level (dB)	± .18	± .18	±2.5	±4.5
	Beamwidth ϕ_o	± .002ϕ_o	± .002ϕ_o	± .04ϕ_o	± .08ϕ_o
	On-axis polarization ratio	± .002	± .002	± .001	± .004
difference pattern	Null depth (dB)	± .32	± .32	± .42	± .34
	Null shift (degrees)	negligible	negligible	± .06	± .06
	Main lobes (dB)	± .01	± .01	± .17	± .33

Table 2. XY- and Z-Position Errors for a Typical X- and K-Band Antenna.

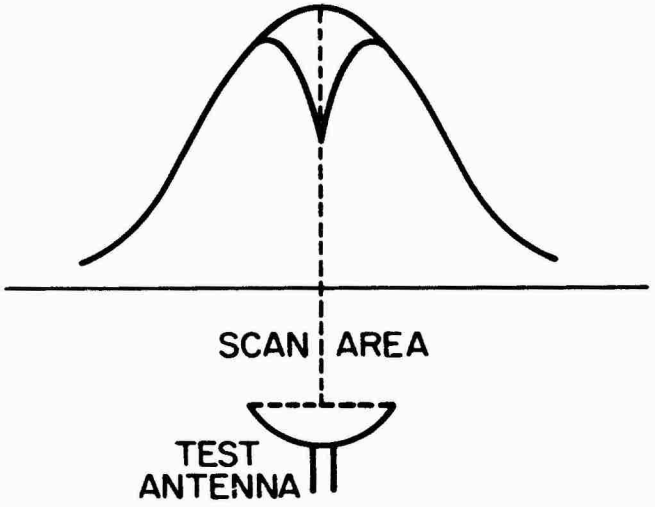

$\alpha = 3$

$N^{I}_{dB} = .002$ dB per dB

Sidelobe Level = -25 dB

	Far-Field Parameter	Amplitude Error
sum pattern	On-Axis Gain	± .035 dB
	Sidelobe Level	± .31 dB
	Beamwidth ϕ_o	± .004 ϕ_o
	On-Axis Polarization Ratio	± .006
difference pattern	Null Depth	± .035 dB
	Null Shift	Negligible
	Main Lobes	± .018 dB

Table 3. Instrumentation Errors in Measuring Amplitude.

$\alpha = 3$ $\quad x = 45$ dB $\quad$ Sidelobe Level = -25 dB

$L^{max} = 160$ cm $\quad \Delta Z^{s}_{max} = \Delta P^{s}_{max} = .2$ mm $\quad$ Null Depth = -30 dB

$\ell^{max} = 80$ cm $\quad \Delta Z^{rn}_{max} = .1$ mm $\quad \Delta F = .01$

$A = 5000\ cm^2$ $\quad \Delta\phi^{I}_{max} = 1°$ $\quad \boxed{\varepsilon^{mr}} = .001$

$\theta_{max} = 60°$ $\quad N^{I}_{dB} = .002$ dB per dB $\quad \eta^{dB}_{probe} + \eta^{dB}_{input} = .1$ dB

		Total Error	
	Far-Field Parameter	$\lambda = 3.26$ cm	$\lambda = 1.63$ cm
sum pattern	On-axis gain (dB)	± .18	± .20
	Sidelobe level (dB)	± (.86+2.5)	± (.80+4.5)
	Beamwidth ϕ_o	± (.01 +.038)ϕ_o	± (.01 +.077)ϕ_o
	On-axis polarization ratio	± .029	± .032
difference pattern	Null depth (dB)	± 1.50	± 1.74
	Null shift (degrees)	± (02+.06)	± (01+.06)
	Mainlobes (dB)	± (.14+.17)	± (.14+.33)

Table 4. Total Far-Field Errors for a Typical X- and K-Band Antenna.

Appendix A

Near-Fields of a Circular Antenna with Uniform Aperture Distribution

The purpose of this Appendix is to derive expressions for the near-field of a circular antenna of uniform aperture distribution. Specifically, the amplitude and phase are constant within the aperture and zero outside. The antenna is electrically large in the sense that the diameter of the aperture is many wavelengths across.

The transverse electric field to the right of the aperture is given exactly by eq. (16). If we assume that the aperture fields are linearly polarized in the x-direction, eq. (16) becomes

$$E_x(\bar{r}) = \frac{-E_o}{2\pi} \frac{\partial}{\partial z} \int_0^{2\pi} \int_0^a \frac{e^{ik|\bar{r}-\bar{R}'|}}{|\bar{r}-\bar{R}'|} R'dR'd\phi' \qquad (A1)$$

for the circular aperture of radius a and uniform amplitude E_o. The element of area has been written in terms of the polar coordinates (R',ϕ') of the vector $\bar{R}'$. In addition it can be proven from eq. (15) that if the aperture fields have longitudinal components which are small compared to the transverse components, then the longitudinal components remain relatively small in the near-field ($z << a^2/\lambda$), provided $a/\lambda >> 1$.

The change of variable $\bar{t} = \bar{R}'-\bar{R}$, where $\bar{R}$ is the transverse part of $\bar{r}$, converts eq. (A1) to

$$E_x(\bar{r}) = -2iE_o \frac{\partial}{\partial z}\left[e^{ikz} - \int_0^{\pi} e^{ik\sqrt{t_o^2(\alpha)+z^2}} d\alpha\right] \quad R<a \qquad (A2a)$$

$$E_x(\bar{r}) = -2iE_o \frac{\partial}{\partial z} \int_0^{\alpha_1} \left[e^{ik\sqrt{t_1^2(\alpha)+z^2}} - e^{ik\sqrt{t_2^2(\alpha)+z^2}}\right] d\alpha \quad R>a. \qquad (A2b)$$

The variables t_o, t_1 and t_2 and the limit of integration α_1 are defined in figures A1a and A1b. Apparently, eqs. (A2) were first derived by Schoch [19].

For large k, the integrals in eqs. (A2) can be evaluated by the method of stationary phase. The integrand of eq. (A2a) has two stationary points, one at $\alpha = 0$ and one at $\alpha = \pi$. The two terms in

the integrand of eq. (A2b) each have a single stationary point at $\alpha = 0$. After carrying through the details of the method of stationary phase, eqs. (A2) become

$$E_x(\bar{r}) = E_0[e^{ikz+\Delta I}] \quad R<a \tag{A3a}$$

$$E_x(\bar{r}) = E_0 \Delta I \qquad R>a, \tag{A3b}$$

where ΔI is given by

$$\Delta I = \frac{-z}{2\pi}\sqrt{\frac{\lambda a}{R}}\left[\frac{e^{i\left[k\sqrt{z^2+(R+a)^2}-\frac{\pi}{4}\right]}}{(R+a)\sqrt[4]{z^2+(R+a)^2}} - \frac{e^{i\left[k\sqrt{z^2+(R-a)^2}+\frac{\pi}{4}\right]}}{(R-a)\sqrt[4]{z^2+(R-a)^2}}\right]. \tag{A3c}$$

Equation (A3b) is identical to eq. (17) of the main text when the following substitutions are made:

$$D_1 = \sqrt{z^2+(R+a)^2} \qquad D_2 = \sqrt{z^2+(R-a)^2}$$

$$a_1 = -a \qquad a_2 = a$$

$$\cos\theta_1 = z/(R+a) \qquad \cos\theta_2 = z/(R-a)$$

Strictly speaking, eqs. (A3) are valid only as $k = 2\pi/\lambda$ approaches infinity. For finite k they represent first term approximations to an infinite asymptotic series, and the first term approximations are valid only in certain regions of the near-field. These regions of validity can be estimated by returning to eqs. (A2). First concentrate on eq. (A2a). In eq. (A2a) t_o ranges from (a-R) to (a+R). Thus if the rate of change of t_o is somewhat uniform with α on the interval $\alpha = 0$ to π, the method of stationary phase will yield a good approximation when

$$\frac{1}{\lambda}\left[\sqrt{(R+a)^2+z^2} - \sqrt{(a-R)^2+z^2}\right] >> 1. \tag{A4}$$

Unfortunately t_o does not change uniformly with α from $\alpha = 0$ to π, but it does so in the separate intervals 0 to $\frac{\pi}{2}$ and $\frac{\pi}{2}$ to π. Since $t^2 = a^2-R^2$ at $\alpha = \frac{\pi}{2}$, the condition (A4) must be replaced by the two conditions,

$$\frac{1}{\lambda}\left(\sqrt{(R+a)^2+z^2} - \sqrt{a^2-R^2+z^2}\right) > 3 \tag{A5a}$$

$$\frac{1}{\lambda}\left(\sqrt{a^2-R^2+z^2} - \sqrt{(a-R)^2+z^2}\right) > 3. \tag{A5b}$$

(Actually the right side of eqs. (A5) should be >> 1 but experience with the method of stationary phase indicates it remains a good approximation down to where the quantities in brackets in eqs. (A5) are just a few wavelengths--specifically 3λ is chosen in eqs. (A5).)

Manipulation of eqs. (A5) shows that they are satisfied for large a/λ if

$$3\lambda < R < [a-(12\lambda/a)\lambda] \tag{A6a}$$

$$z < \frac{a-R}{3\lambda}\sqrt{R^2-(3\lambda)^2}. \tag{A6b}$$

That is, eq. (A3a) approximates eq. (A2a) in the region defined by eqs. (A6). A similar analysis with eq. (A2b) shows that it is approximated by eq. (A3b) in the region defined by

$$R > [a+(12\lambda/a)\lambda] \tag{A7a}$$

$$z < (R-a)\frac{a}{3\lambda}. \tag{A7b}$$

The regions of validity defined by eqs. (A6) and (A7) are shown in figure A2 for an a/λ equal to 12. Each region is labeled by the equation which approximates the field in that region. In addition to the regions defined by eqs. (A6) and (A7) two other regions--one near the z-axis,

$$R < \frac{1}{2}a \tag{A8a}$$

$$R < \text{the larger of } \left\{\frac{\lambda}{2a}z \text{ or } .3\left(\frac{a}{\lambda}\right)^{2/3}\lambda\right\}, \tag{A8b}$$

and one near the edge of the aperture

$$z > \frac{1}{2}\left(\pi\frac{a}{\lambda}\right)^{\frac{1}{3}}a \tag{A9a}$$

$$z > \frac{\pi a}{\lambda}|a-R| \tag{A9b}$$

$$|R-a| < \frac{1}{4}a \tag{A9c}$$

are shown in figure A2.

In the axis region defined by eqs. (A8), the exponent in the integrand of eq. (A2a) can be approximated by the first two terms of its expansion in R/a, and integrated to give

$$E_x(\bar{r}) = E_o\left[e^{ikz} - \frac{ze^{ik\sqrt{z^2+a^2}}}{\sqrt{z^2+a^2}} J_1\left(\frac{ka}{\sqrt{z^2+a^2}} R\right)\right]. \tag{A10}$$

Similarly, in the edge region defined by eqs. (A9), the eq. (A2b) can be integrated approximately to give

$$E_x(\bar{r}) = \frac{E_o}{2}\left[e^{ikz} - \frac{ze^{ik\sqrt{z^2+2a^2}}}{\sqrt{z^2+2a^2}} J_o\left(\frac{ka^2}{\sqrt{z^2+2a^2}}\right)\right]. \tag{A11}$$

In the near-field in front of the aperture (z less than about $\frac{1}{12} a^2/\lambda$), eqs. (A3a) and (A10) reveal that the electric field can be approximated by a single equation,

$$E_x(\bar{r}) = E_o[e^{ikz} + \Delta I'], \tag{A12a}$$

with

$$\Delta I' = -\frac{za}{\sqrt{2}}\left[\frac{e^{i[k\sqrt{z^2+(R+a)^2} - \frac{\pi}{4}]}}{(R+a)\sqrt{z^2+(R+a)^2}} J_o^e\left(\frac{ka}{\sqrt{z^2+(R+a)^2}} R\right)\right. \tag{A12b}$$

$$\left. - \frac{e^{i[k\sqrt{z^2+(R-a)^2} + \frac{\pi}{4}]}}{(R-a)\sqrt{z^2+(R-a)^2}} J_o^e\left(\frac{ka}{\sqrt{z^2+(R-a)^2}} R\right)\right],$$

and J_o^e defined as

$$J_o^e(z) \equiv \begin{cases} (1 - \frac{1}{4} z^2) & z < 1.46 \\ \sqrt{\frac{1}{\pi z}} & z > 1.46. \end{cases} \tag{A12c}$$

Essentially, eqs. (A12) represent the total electric field for the linearly polarized circular aperture in the region

$$R < a - \lambda \tag{A13a}$$

$$z < \frac{1}{12} \frac{a^2}{\lambda}. \tag{A13b}$$

The amplitude $|E_x|$ and phase ϕ_x of E_x may be found from eqs. (A12),

$$|E_x| \simeq E_o\left[1-\frac{za}{\sqrt{2}}\left(Q_1 \cos\left(k\sqrt{z^2+(R+a)^2}-kz-\frac{\pi}{4}\right) - Q_2 \cos\left(k\sqrt{z^2+(R-a)^2}-kz+\frac{\pi}{4}\right)\right)\right] \tag{A14a}$$

$$\phi_x \simeq kz-\frac{za}{\sqrt{2}}\left[\cos kz\left(Q_1 \sin\left(k\sqrt{z^2+(R+a)^2}-\frac{\pi}{4}\right) - Q_2 \sin\left(k\sqrt{z^2+(R-a)^2}-\frac{\pi}{4}\right)\right)\right.$$

$$\left.-\sin kz\left(Q_1 \cos\left(k\sqrt{z^2+(R+a)^2}-\frac{\pi}{4}\right) - Q_2 \cos\left(k\sqrt{z^2+(R-a)^2}+\frac{\pi}{4}\right)\right)\right], \tag{A14b}$$

with

$$Q_1 = \frac{J_o^e\left(\frac{ka}{\sqrt{z^2+(R+a)^2}}R\right)}{(R+a)\sqrt{z^2+(R+a)^2}} \tag{A14c}$$

$$Q_2 = \frac{J_o^e\left(\frac{ka}{\sqrt{z^2+(R-a)^2}}R\right)}{(R-a)\sqrt{z^2+(R-a)^2}} \tag{A14d}$$

Equations (A14) hold (to a first order approximation) everywhere in the near-field region defined by eqs. (A13). Except within a wavelength or so of the z-axis, eqs. (A14) reveal that in this region the maximum amplitude fluctuations are about $\pm \frac{1}{\pi}\sqrt{\frac{\lambda}{a}}$, and the phase varies slightly from kz. The amplitude of the electric field given by eq. (A14a) is plotted in figure A3 for $a/\lambda = 12$ and 15, and for increments of z/a from 0 to $\frac{1}{12}\, a/\lambda$. The amplitude curves show large fluctuations within a wavelength of the points of maxima and minima along the z-axis. These z-axis maxima and minima, which are a well-known phenomenon for the circular aperture of uniform distribution, are less pronounced for noncircular apertures, or for apertures with a tapered distribution (see reference [13], Section 1-F).

Figure A3 also shows that the amplitude variations across the aperture repeat about every wavelength in the very near-field ($z < a/4$), but spread out as the distance from the aperture gets larger. This behavior has been observed for tapered distributions as well, by the many near-field measurements on microwave antennas performed at the National Bureau of Standards [17].

The phase in the near-field of a circular antenna with $a/\lambda = 12$ is plotted in figure A4. Except near the zeros in on-axis amplitude, the phase across the beam is uniform to within a few degrees of oscillation which repeat about every wavelength in the very near-field.

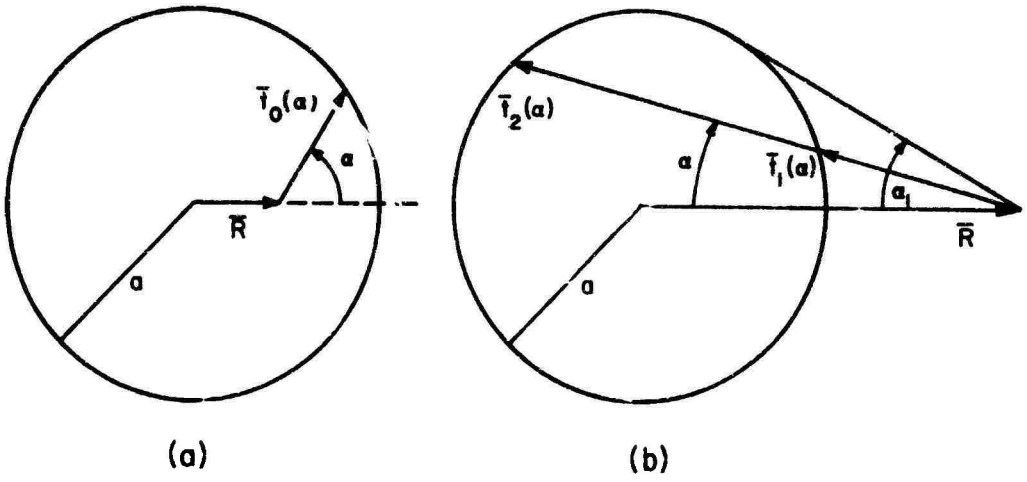

Figure A1. Definition of $\bar{t}$ and α.

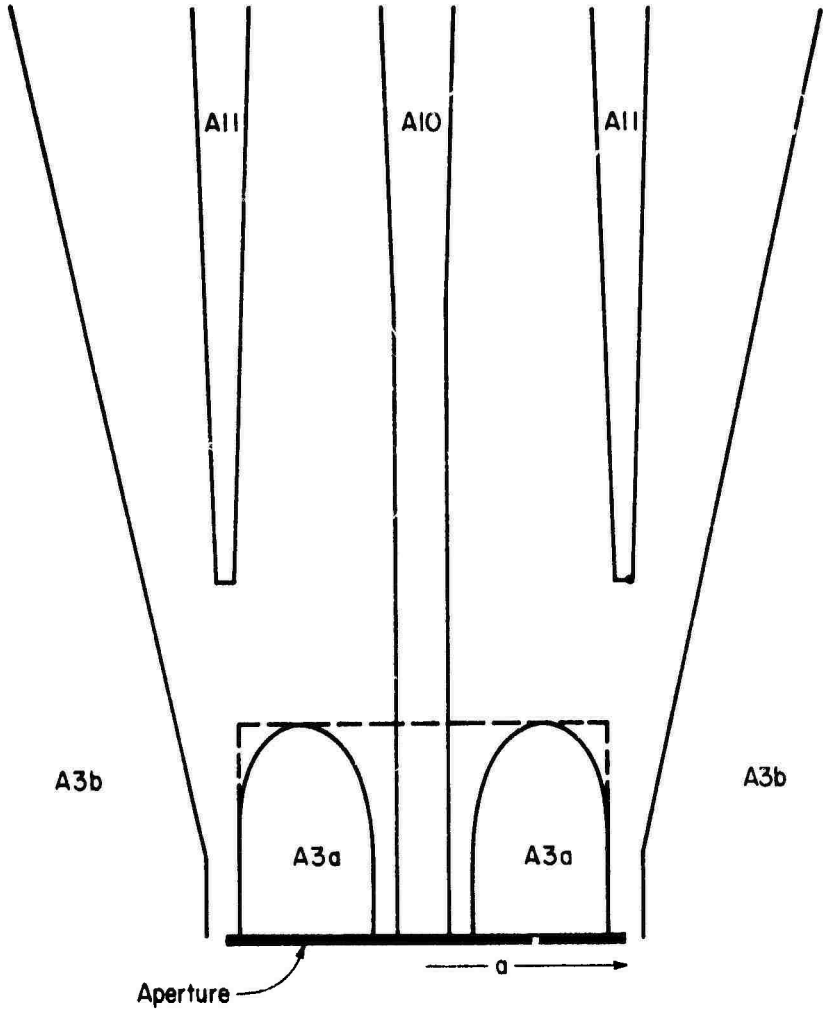

Figure A2. Dotted line shows region in which eq. (A12a) holds.

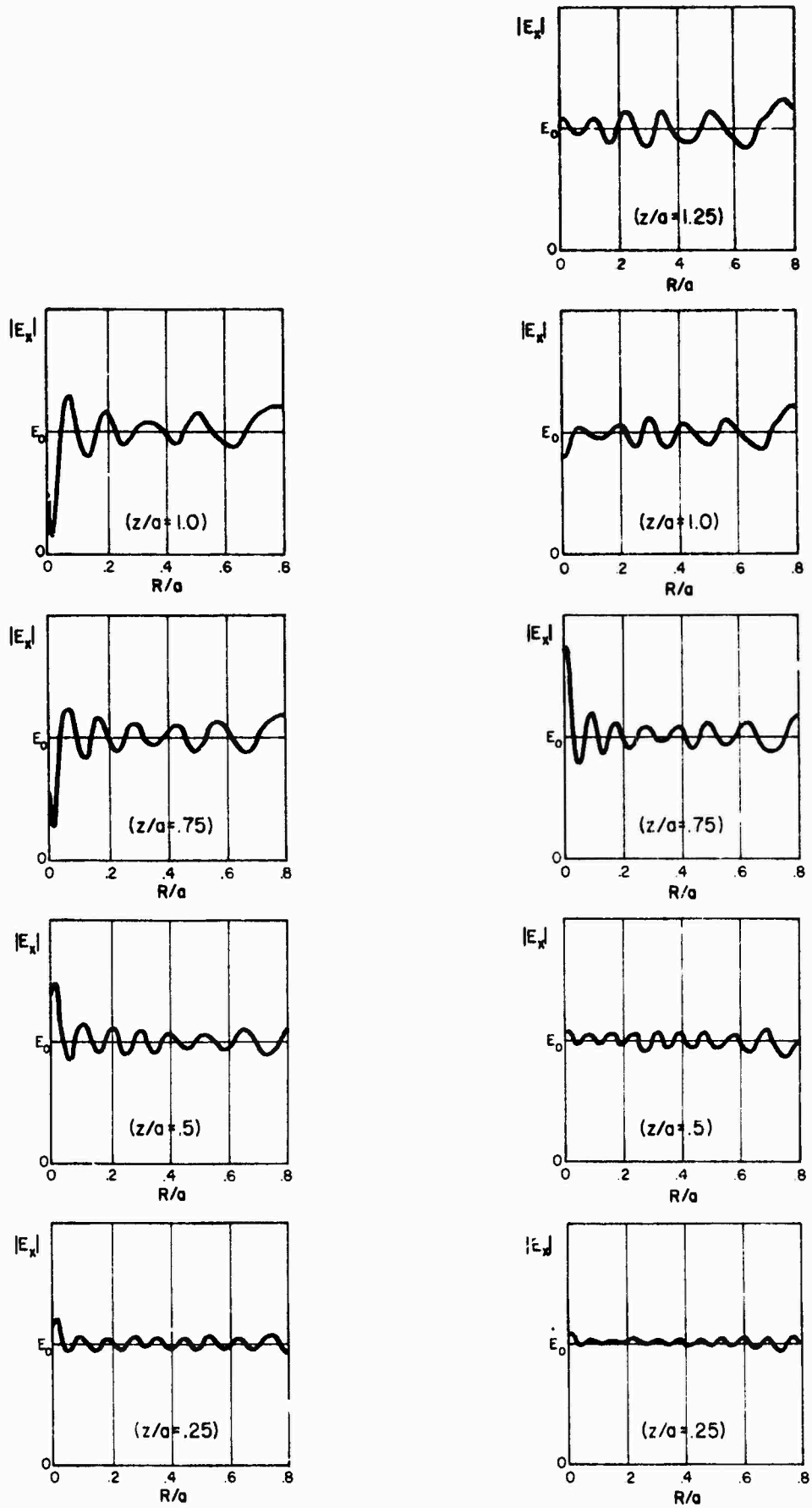

(a) $a/\lambda = 12$ (b) $a/\lambda = 15$

Figure A3. Near-field amplitude of circular antenna.

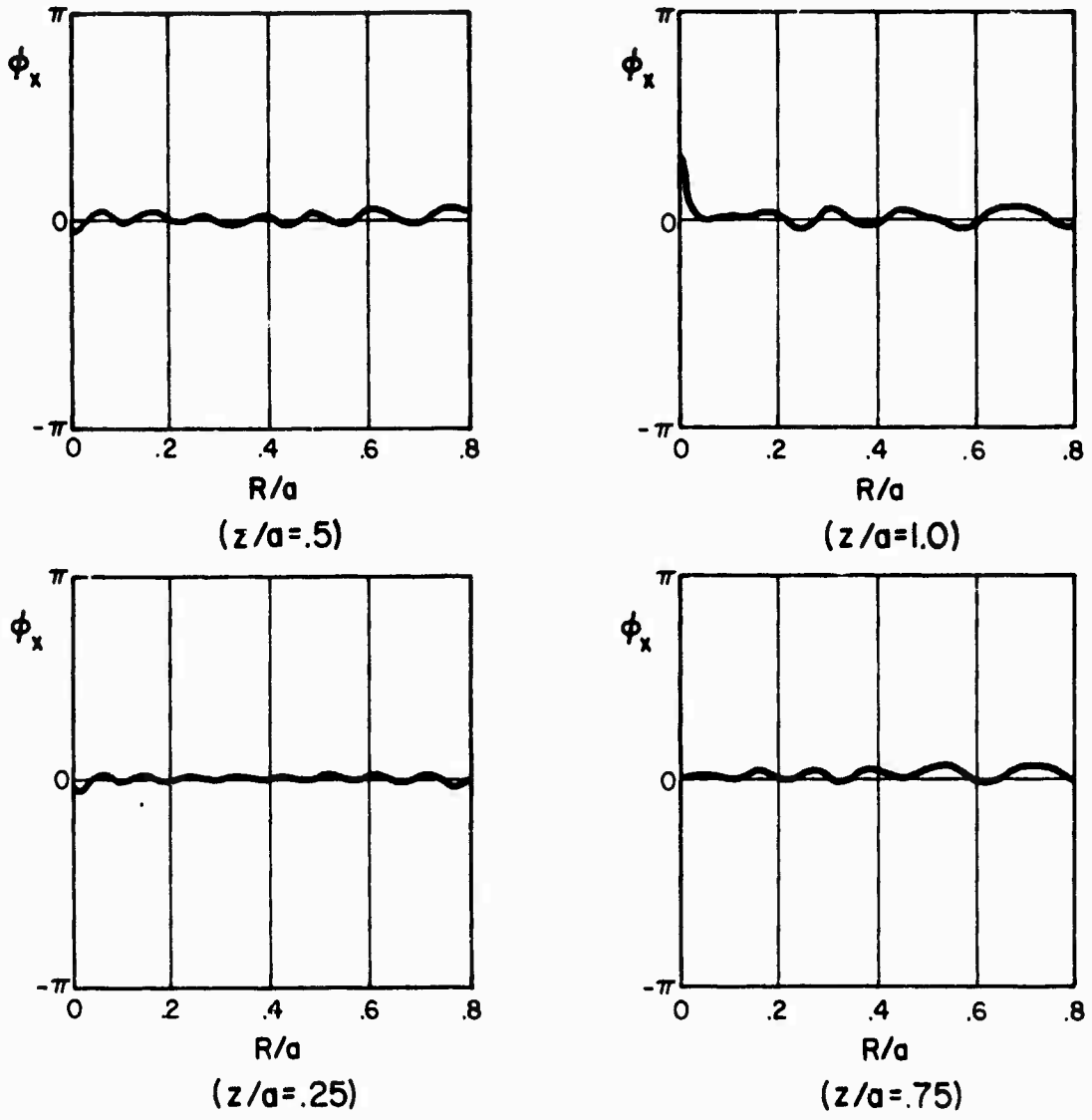

Figure A4. Near-field phase of circular antenna ($a/\lambda = 12$).

Appendix B
Position and Instrumentation Errors for the Null Depth of Difference Patterns

1. Position Errors

The errors in null depth of a difference pattern caused by transverse displacement errors ($\Delta\bar{P}$) of the near-field scanner can be derived in the same way and are given by the same upper bound expression as that of the transverse errors for sum patterns (eq. (60a)). However, the sum pattern derivation of Section III.B.1 for longitudinal displacement errors cannot be applied to finding errors in the null depth of difference patterns. The main reasons for this are twofold. The first and most obvious is that the equation for difference patterns analogous to eq. (48) may not be satisfiable because the near-field of a difference pattern changes phase by 180° across the aperture. Secondly, as the analysis below shows, the greatest effect of a longitudinal displacement error is a slight shift in the position of the null rather than a change in the depth of the null.

If the longitudinal position errors were zero and the perpendicular ($\hat{e}_z$) to the scan plane were parallel to the null axis, the far-field in the direction of the "null" is given in terms of the near-field by eq. (10):

$$E_x^{null} = \frac{1}{\lambda r} e^{ik(r-d)} \int_{A_o} E_x(\bar{P},d)\, d\bar{P}, \qquad (B1)$$

where, as usual, A_o refers essentially to that part of the scan area that covers the antenna aperture, and just the x-component of electric-field will be considered first.

Now if the amplitude of $E_x(\bar{P},d)$ on opposite halves of the aperture (and thus A_o) were equal and the phase difference exactly 180°, the field in the direction of the null axis would actually be zero. In reality the amplitudes are not exactly equal and the phase difference, even on the average, is not exactly 180°. Specifically, we can write $E_x(\bar{P},d)$ as

$$E_x(\bar{P},d) = \begin{cases} (A_x+\Delta A_x)\, e^{i(\phi_{ox}+kd)} & \text{(over one half, } A_{o1}\text{)} \\ -A_x\, e^{i(\phi_{ox}+kd+\Delta\psi_x)} & \text{(over second half, } A_{o2}\text{)} \end{cases} \qquad \text{(B2)}$$

with $\Delta A_x/A_x$ and $\Delta\psi_x$ both << 1. For simplicity ϕ_{ox} has been chosen constant, although it can be shown that the results do not change significantly if ϕ_{ox} is allowed to vary slightly across A_o. Substitution of eq. (B2) into (B1) and approximating $e^{i\Delta\psi_x}$ by $(1+i\Delta\psi_x)$ yields

$$E_x^{null} = \frac{e^{i(kr+\phi_{ox})}}{\lambda r}\left[\int_{A_{o1}} \Delta A_x d\bar{P} - \int_{A_{o2}} iA_x\Delta\psi_x\, d\bar{P}\right] \qquad \text{(B3)}$$

for the field in the null direction. Experimentally, it has been found at the NBS that for many if not all antennas operating in a difference mode the first integral in (B3) predominates [17], but for the sake of the error analysis we must retain both integrals.

When longitudinal displacement errors (Δz) are introduced, eq. (10) shows that eq. (B1) must be replaced by

$$E_x^{null'} = \frac{1}{\lambda r}\, e^{i(kr+\phi_{ox})} \int_{A_o} E_x(\bar{P},d)\, e^{ik(\Delta z - \sin\theta \hat{e}_R\cdot\bar{P})}\, d\bar{P}, \qquad \text{(B4)}$$

where $E_x^{null'}$ represents the null field computed from the actual near-field data containing errors in the z-position of the scanner. θ can no longer be set equal to zero because the error Δz may shift the angular position of the null axis. After substituting eq. (B2) into (B4), expanding the exponential in a power series, and discarding error terms higher than second order, eq. (B4) becomes,

$$|E_x^{null'}| = \frac{e^{i(kr+\phi_{ox})}}{\lambda r}\left[\int_{A_{o1}} \Delta A_x d\bar{P} - \int_{A_{o2}} iA_x\Delta\psi_x \, d\bar{P}\right. \tag{B5}$$

$$+ \int_{A_o} (\pm A_x+\Delta A_x^+)\left[ik(\Delta z-\theta\hat{e}_R\cdot\bar{P}) + k^2\Delta z\theta\hat{e}_R\cdot\bar{P}\right.$$

$$\left. - \frac{(k\Delta z)^2}{2} - \frac{(k\theta\hat{e}_R\cdot\bar{P})^2}{2}\right] d\bar{P}$$

$$\left. + k\int_{A_{o2}} A_x\Delta\psi_x(\Delta z-\theta\hat{e}_R\cdot\bar{P})\, d\bar{P}\right],$$

with

$$\Delta A_x^+ \equiv \begin{matrix} \Delta A_x \text{ in } A_{o1} \\ 0 \text{ in } A_{o2} \end{matrix}$$

and the + and - sign before A_x being used in the areas A_{o1} and A_{o2} respectively.

The first order error term in eq. (B5) can be made zero by choosing $\theta = \theta_s$ such that

$$\int_{A_o} (\pm A_x+\Delta A_x^+)\, \Delta z \, d\bar{P} = \theta_s \int_{A_o} (\pm A_x+\Delta A_x^+)(\hat{e}_R\cdot\bar{P})\, d\bar{P}. \tag{B6}$$

θ_s corresponds essentially to the shift in the direction of the null caused by longitudinal position errors. If we take the weighted average value of $|\hat{e}_R\cdot\bar{P}|$ at about $\ell^{max}/4$, eq. (B6) implies that for most antennas

$$\frac{\theta_s \, \ell^{max}}{4} \leq \Delta z_{max}, \tag{B7}$$

where ℓ^{max} denotes the maximum width of the antenna aperture. By defining $\delta_{max} = 2\pi\Delta z_{max}/\lambda$, eq. (B7) becomes approximately,

$$\boxed{\theta_s \leq \frac{2\delta_{max}}{\pi}\frac{\lambda}{\ell^{max}} = \frac{4\Delta z_{max}}{\ell^{max}}} \tag{B8}$$

With the choice of θ given by eq. (B6) the amplitude, $|E_x^{null'}-E_x^{null}|$, of the error field in the null direction may be written by subtracting eq. (B3) from eq. (B5),

$$|E_x^{null'} - E_x^{null}| \leq \frac{1}{\lambda r}\left| k^2 \int_{A_o} \pm A_x \left[\Delta z \theta_s \hat{e}_R \cdot \bar{\rho} - \frac{(\Delta z)^2}{2} - \frac{(\theta_s \hat{e}_R \cdot \bar{\rho})^2}{2} \right] d\bar{\rho} \right.$$

$$\left. + k \int_{A_{o2}} A_x \Delta\psi_x (\Delta z - \theta_s \hat{e}_R \cdot \bar{\rho})\, d\bar{\rho} \right|. \qquad \text{(B9)}$$

The first term in the first integral of eq. (B9) can be made zero by merely shifting the reference plane from which Δz is measured. The third term in the first integral is identically zero because it is an odd function over the scan area A_o. Thus eq. (B9) reduces to

$$|E_x^{null'} - E_x^{null}| \leq \frac{k}{\lambda r}\left| \int_{A_{o2}} A_x \Delta\psi_x (\Delta z - \theta_s |\bar{\rho}|)\, d\bar{\rho} + \frac{k}{2} \int_{A_o} \pm A_x (\Delta z)^2\, d\bar{\rho} \right|. \qquad \text{(B10)}$$

The second integral in eq. (B10) is also negligible if we assume the rms value of (Δz) is approximately equal on the "positive" and "negative" sides of A_o. Finally, since the maximum value of θ_s is $\delta_{max}\, \lambda/\ell^{max}$, eq. (B10) becomes

$$|E_x^{null''} - E_x^{null}| \leq \frac{k\, \delta_{max} \lambda}{\lambda r\, \ell^{max}} \left| \int_{A_{o2}} A_x \Delta\psi_x |\bar{\rho}|\, d\bar{\rho} \right| \simeq \frac{\delta_{max} \Delta\psi_x^{ave}}{\lambda r} \int_{A_{o2}} A_x\, d\bar{\rho}, \qquad \text{(B11)}$$

with $\Delta\psi_x^{ave}$ denoting the average phase difference from π radians of the probe output between the positive and negative sides of the partial scan area which is perpendicular to the null axis.

The factor $\frac{1}{\lambda r} \int_{A_{o2}} A_x\, d\bar{\rho}$ is approximately equal to the maximum field in the mainbeams of the difference pattern. And since an expression analagous to eq. (B11) holds for the y-component of the field, we can write the fractional error $\eta(\bar{r})$ near the null of a difference pattern as

$$\boxed{\eta(\bar{r}) \leq \delta_{max}\, \Delta\psi_{ave}\, g(\bar{r}),} \qquad \text{(B12a)}$$

where, as in the main text, $g(\bar{r})$ is the ratio of the amplitude of the maximum far-electric-field to the far-electric-field at the given direction $\bar{r}$. Here $\bar{r}$ is essentially the direction of the null axis and thus $g(\bar{r})$ the ratio of maximum far-field to null axis far-field.

Now eq. (B12) is a very simple expression. However, the average phase difference $\Delta\psi_{ave}$ of the probe output may be a difficult

quantity to estimate accurately from the near-field phase data. Fortunately, it can be shown that $\Delta\psi_{ave}$ is related to the relative size of the two mainlobes in the far-field of the difference pattern. Specifically, a straightforward but rather lengthy manipulation (which will not be shown here) of the near-field of a difference pattern reveals that $\Delta\psi_{ave}$ can be approximated by

$$\Delta\psi_{ave} \simeq 4\Delta F$$

where ΔF is the fractional difference between the amplitude of the two main far-field lobes of the difference pattern. For example, if the amplitude of one mainlobe is 10 on some linear scale and the amplitude of the other mainlobe is 10.1 then ΔF would equal (10.1-10)/ or .01. Equation (B12a) can now be written in the alternative form

$$\boxed{\eta(\bar{r}) \leq 4\delta_{max}\ \Delta F\ g(\bar{r}).} \qquad \text{(B12b)}$$

2. Instrumentation Errors

The inaccuracies in measuring near-field phase have the same effect on the null-depth as the longitudinal position errors. That is, $\Delta\phi^{I}_{max}$, the maximum instrumentation error in measuring phase, simply replaces δ_{max} in eqs. (B8) and (B12).

The inaccuracies in measuring amplitude affect the null depth differently, however, than the transverse position errors because the nonlinearities in the instrumentation distort the amplitude on each side of the difference pattern in nearly the same way and thus their effect on the null depth is much smaller than might first be expected. Specifically, errors in measuring amplitude show up in the null depth through distortion of only the ΔA part (see eq. (B2)) of the near field. Carrying through an analysis similar to that performed above for z-position errors yields the following expression for the maximum change ΔE^{null}_{A} in null electric field caused by amplitude errors:

$$|\Delta E^{null}_{A}| \leq \frac{N^{I}_{dB}}{\lambda r} \int_{A_{ol}} (\Delta A_{max} - |\Delta A|)\ dP \leq \frac{N^{I}_{dB} \Delta A_{max} A_{ol}}{\lambda r}, \qquad \text{(B13)}$$

where ΔA_{max} is the maximum of ΔA across A_{ol} and N^I_{dB} is the maximum instrumentation error in measuring the amplitude of the probe output (see Section III.B.2). If we approximate $|E_A^{null}|$, the x-component of which is given in eq. (B3), by $\frac{\Delta A_{max} A_{ol}}{2\lambda r}$, then the fractional error in null depth caused by instrumentation errors in measuring amplitude can be written

$$\boxed{\eta = \frac{|\Delta E|}{|E^{null}|} \leq 2N^I_{dB}.} \qquad \text{(B14)}$$

Note that the instrumentation amplitude error in null depth does not depend on the null depth itself. In addition, it can be shown that, unlike phase errors, the instrumentation amplitude errors have negligible effect on the angular position of the null direction.

References

[1] IEEE Standard Definitions of Terms for Antennas, IEEE Transactions on Antennas and Propagation, AP-22, 1 (January 1974).

[2] DeSize, L.K. and J.F. Ramsay, in Microwave Scanning Antennas, Ed. R.C. Hansen, Academic Press--New York, London (1964), Vol. 1, Ch. 2-II.B.

[3] Kerns, D.M., "Correction of Near-Field Antenna Measurements Made with an Arbitrary But Known Measuring Antenna," Electronics Letters, 6, 11, pp. 346-347 (28th May 1970).

[4] See e.g. Jackson, J.D., Classical Electrodynamics, John Wiley & Sons Inc., New York, London (1962), Section 9.6.

[5]a Braunbek, W., "Zur Beugung an der Kreisscheibe," Zeitschrift Für Physik, 127, pp. 405-415 (1950).

b Ufimtsev, P.Ia., "Approximate Computation of the Diffraction of Plane Electromagnetic Waves at Certain Metal Bodies," Soviet Physics--Technical Physics, 2, 8, pp. 1708-1718 (August 1957).

[6]a Keller, J.B., "Diffraction by an Aperture," Journal of Applied Physics, 28, 4, pp. 426-444 (April 1957).

b Keller, J.B., "Geometrical Theory of Diffraction," Journal of the Optical Society of America, 52, 2, pp. 116-130 (February 1962).

[7] Van Kampen, N.G., "An Asymptotic Treatment of Diffraction Problems," Physica, 14, 9, pp. 575-589 (January 1949).

[8] Keller, J.B., R.M. Lewis, and B.D. Seckler, "Diffraction by an Aperture II," Journal of Applied Physics, 28, 5, pp. 570-579 (May 1957).

[9]a Kouyoumjian, R.G., and P.H. Pathak, "A Uniform Geometrical Theory of Diffraction for an Edge in a Perfectly Conducting Surface," Proceedings of the IEEE, 62, 11, pp. 1448-1461 (November 1974).

b Hwang, Y.M. and R. G. Kouyoumjian, "A Dyadic Coefficient for an Electromagnetic Wave Which is Rapidly-Varying at an Edge," URSI 1974 Annual Meeting, Boulder, Colorado.

[10] See e.g., Born M., and E. Wolf, Principles of Optics, Pergamon Press, Oxford, New York (1970), 4th Ed., Appendix III.

[11] Newell, A.C. and M.L. Crawford, "Planar Near-Field Measurements on High Performance Array Antennas," NBSIR 74-380, National Bureau of Standards, Boulder, Colorado (July 1974).

[12] Kraus, J.D., Antennas, McGraw-Hill, Inc., New York, Toronto, London (1950), Chs. 3 and 12.

[13] Hansen, R.C., (Ch. 1, Sect. 2-I in ref [2]): $A_e/A = G/G_o$ in Table IX, p. 66.

[14] Rusch, W.V.T. and P.D. Potter, Analysis of Reflector Antennas, Academic Press, New York - London (1970), Section 2.52.

[15] Ruze, John, "Antenna Tolerance Theory -- A Review," Proceedings IEEE, 54, 4, pp. 633-640 (April 1966).

[16] Rodrigue, G.P., E.B. Joy, and C.P. Burns, An Investigation of the Accuracy of Far-Field Radiation Patterns Determined from Near-Field Measurements, Report -- Georgia Institute of Technology, Atlanta, Georgia (August 1973).

[17] Newell, A.C., private communication, National Bureau of Standards, Boulder, Colorado.

[18] Kerns, D.M., "Scattering-Matrix Description and Near-Field Measurements of Electroacoustic Transducers," The Journal of the Acoustical Society of America, 57, 2, pp. 497-507 (February 1975).

[19] Schoch, V.A., "Betrachtungen über das Schallfeld einer Kolbenmembran," Akustische Zeitschrift, 6, pp. 318-326 (1941).

[20] Crawford, M.L., A.C. Newell, J.W. Greene, and A.D. Yaghjian, "Planar Near-Field Measurements for Evaluation and Calibration of PPMS Antennas On-Board Sac RC-135 Aircraft," NBSIR 75-815, National Bureau of Standards, Boulder, Colorado (June 1975).

[21] Newell, A.C., "Planar Near-Field Measurement Techniques on High Performance Arrays -- Part II," Air Force Technical Report, Air Force Avionics Laboratory -- Wright Patterson Air Force Base, Ohio (to be published).

[22] Newell, A.C., R.C. Baird, and P.F. Wacker, "Accurate Measurement of Antenna Gain and Polarization at Reduced Distances by an Extrapolation Technique," IEEE Transactions on Antenna and Propagation, AP-21, 4, pp. 418-431 (July 1973).

[23] Kanda, M., "Accuracy Considerations in the Measurement of the Power Gain of a Large Microwave Antenna," IEEE Transactions on Antennas and Propagation, AP-23, 3, pp. 407-411 (May 1975).

[24] Appel-Hansen, J., "Reflectivity Level of Radio Anechoic Chambers," IEEE Transactions on Antennas and Propagation, AP-21, pp. 490-498 (July 1973).

☆ U. S GOVERNMENT PRINTING OFFICE 1975—657-630/36